

AD-A089 651

SPERRY RESEARCH CENTER SUDBURY MA
TIME-DOMAIN SONAR TARGET RESPONSE MODELING. (U)
OCT 79 H MIERAS, C L BENNETT
SRC-CR-79-74

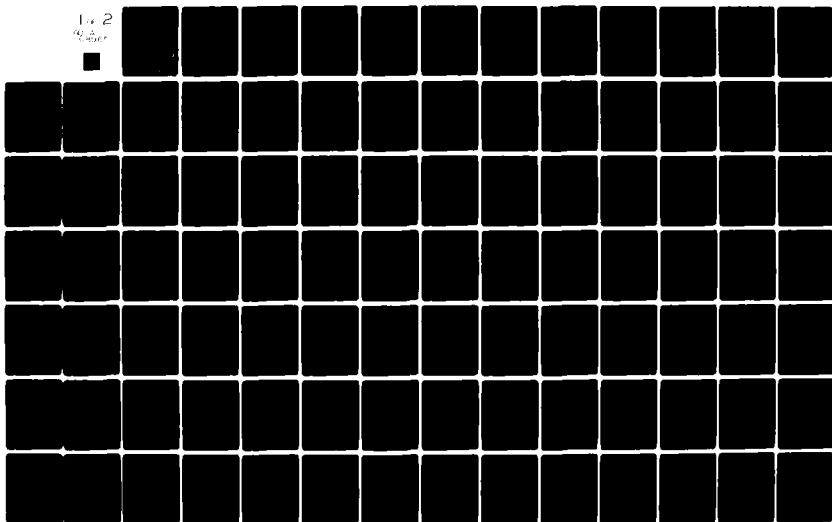
F/G 17/1

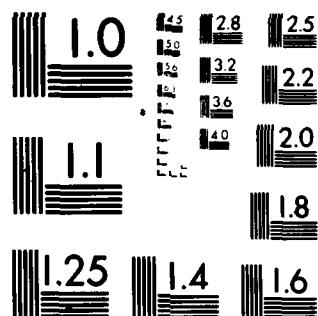
N61331-78-C-0049
NL

UNCLASSIFIED

1 of 2

96 1/2





MICROCOPY RESOLUTION TEST CHART

NATIONAL BUREAU OF STANDARDS-1963-A

AD A089651

LEVEL #

①
B.S.

⑥

TIME-DOMAIN SONAR TARGET RESPONSE MODELING

⑩

H. Mieras and C. L. Bennett

Sperry Research Center, Sudbury, MA 01776 ✓

FINAL REPORT

Contract No. N61331-78-C-0049 ✓

⑪

⑪ 101

⑭

SRC-CR-79-74 ✓

⑪

October 1979

SECRET
SEP 29 1980
A

Prepared for
NAVAL COASTAL SYSTEMS LABORATORY
PANAMA CITY, FLORIDA 32407

DISTRIBUTION STATEMENT A

Approved for public release;
Distribution Unlimited

SPERRY
RESEARCH CENTER

JCB

DDC FILE COPY

4/21/79

80 9 15 002

LIST OF ILLUSTRATIONS

Figure		Page
2-1	Scattering geometry.	4
2-2	Frequency response of sphere: (a) hard, (b) aluminum, and (c) brass.	10
2-3	Frequency response of aluminum sphere with (a) $c_1 = 9300$, (b) $c_1 = 6200$, and (c) $c_1 = 4130$.	11
2-4	Frequency response of aluminum sphere with (a) $c_2 = 4650$, (b) $c_2 = 3100$, and (c) $c_2 = 2065$.	12
2-5	Frequency response of aluminum sphere with (a) $\rho = 2.7$ and (b) $\rho = 1.5$.	13
2-6	Frequency response of aluminum sphere, fluid approximation, with (a) $c_1 = 9300$, (b) $c_1 = 6200$, and (c) $c_1 = 4130$.	14
2-7	Smoothed impulse response of aluminum sphere: (a) hard, (b) aluminum, and (c) brass.	17
2-8	Smoothed impulse response of aluminum sphere with (a) $c_1 = 9300$, (b) $c_1 = 6200$, and (c) $c_1 = 4130$.	18
2-9	Smoothed impulse response of aluminum sphere with (a) $c_2 = 4650$, (b) $c_2 = 3100$, and (c) $c_2 = 2065$.	19
2-10	Smoothed impulse response of aluminum with (a) $\rho = 2.7$ and (b) $\rho = 1.5$.	20
2-11	Smoothed impulse response of aluminum sphere, fluid approximation, for (a) $c_1 = 9300$, (b) $c_1 = 6200$, and (c) $c_1 = 4130$.	21
2-12	Time reference for scattering from unit sphere.	22
2-13	Aluminum variations — responses vs. $c_2 t$ with $c_1 = 6200$.	24
2-14	Aluminum variations — responses vs. $c_2 t$ with $c_1 = 9300$.	25
3-1	Plane wave refraction at plane boundary.	27
3-2	Impulse response of hard sphere (leading edge).	32
3-3	Local influence theory: reflection and refraction.	42
3-4	Glory paths for sphere.	43
3-5	Glory wave model — fluid sphere response.	46
3-6	Glory wave model — aluminum and variations.	47
3-7	Glory wave model — brass and variations.	48
3-8	Principal scattering modes involving shear waves.	49
3-9	Simplified impulse response.	51

Accession For	
NRLS - G-1001	<input checked="" type="checkbox"/>
DDO 128	<input type="checkbox"/>
Unprocessed	<input type="checkbox"/>
Justification	
By	
Date	
Approved by	
Dist	Call and/or special

LIST OF ILLUSTRATIONS (Cont.)

<u>Figure</u>	<u>Page</u>
3-10 Aluminum response model — time domain.	53
3-11 Aluminum response model — frequency domain.	54
3-12 Brass response model — time domain.	55
3-13 Brass response model — frequency domain.	56
4-1 STIE response for fluid aluminum right circular cylinder.	64
4-2 STIE response for fluid brass right circular cylinder.	65
4-3 STIE response — small angle deviation.	66
4-4 Surface pressure for elastic sphere — classical and STIE.	70
4-5 Status of elastic STIE calculation — far field response.	72
4-6 Shell scattering problem.	72
4-7 STIE solution — scattering from spherical membrane.	76
5-1 Shell responses as a function of thickness — frequency domain, thick shell.	83
5-2 Shell responses as a function of thickness — frequency domain, thin shell.	84
5-3 Shell responses as a function of thickness — frequency domain, very thin shell.	85
5-4 Shell responses as a function of thickness — time domain, $a_n = 4$, thick shell.	86
5-5 Shell responses as a function of thickness — time domain, $a_n = 4$, thin shell.	87
5-6 Shell responses as a function of thickness — time domain, $a_n = 4$, very thin shell.	88
5-7 Responses of very thin shell with variations in elastic parameters, $h = 0.001$.	90
5-8 Responses of very thin shell with variations in ρ and h , keeping $\rho_1 h$ constant.	91
5-9 Comparison of responses of soft sphere and soft core (gas-filled) spherical shell — frequency domain.	91
5-10 Comparison of responses of soft sphere and soft core (gas-filled) spherical shell — time domain.	92
5-11 Frequency and time domain responses of heavy core (glycerin-filled) spherical shell.	92

SECTION 1
INTRODUCTION

↙

The acoustic response of simple metallic targets submerged in water is studied under this contract. The aim is to develop an interpretation of the process which would permit its characterization by a simple model. This work is a continuation of a previous contract [1], which should be referred to for the general background of this problem and for greater detail of the space-time integral equation approach.

The classical solution for acoustic scattering from a penetrable homogeneous sphere is studied first in Section 2. It is seen that hard or soft target approximations are not valid for metallic targets (except at very low frequencies), but that resonances are present which are characteristic of the interior composition. Viewed in the time domain, the impulse response of a target consists of a sequence of pulses following the specular impulse. The arrival times of these pulses can be related directly to the elastic constants of the target and medium. Moreover they can be interpreted simply as pulse traversal times at the several speeds along certain paths. The description of this model (the 'glory-wave' model) is the subject of Section 3, along with the first steps toward a complete quantitative theory. A semi-quantitative computer program which generates time and frequency domain responses is given in an appendix.

↘

In Section 4, the space-time integral equation approach is described. Whereas classical solutions can only be found for targets conforming to separable coordinate systems, the integral equation approach is applicable to targets of arbitrary shape. An exact solution is presented for a fluid right circular cylinder. The space-time integral equation formulation is presented for elastic targets (which exhibit interior shear waves as well as compression waves), although numerical difficulties have so far prevented computational results. A procedure is described whereby the scattering

↘
next page

center responses can be computed for use in the simple model of Section 3.

→ In Section 5, the results of previous sections are extended to the hulled target. The classical solution is derived for the thick spherical shell. Results for the shell are given as functions of elastic parameters and shell thickness, including the very-thin shell limit. It is seen that the thick shell response is much more complicated than the already complicated homogeneous sphere, but that in the limit of the thin shell the response becomes a stepped sinusoid with exponential decay. Also given, in subsection 4.3, is the space-time integral equation formulation for the thin hulled target of general geometry.

SECTION 2

ANALYSIS OF HOMOGENEOUS SPHERE RESPONSE

The solution for scattering from a homogeneous penetrable sphere was first given by Anderson in 1950 for the fluid sphere [2] and by Faran in 1951 for the elastic sphere [3]. These were classical solutions; found by expanding interior and exterior fields as sums of eigenfunctions and equating these at the boundary. The applicability of the method is limited to simple shapes which form constant surfaces in separable coordinate systems. However, the advantage is that the solution is straightforward. The only numerical difficulty arises in the evaluation of the spherical Bessel functions at large order and argument. In this section, the classical solution for the sphere, transformed to the time domain, will be used as a starting point for understanding acoustic scattering.

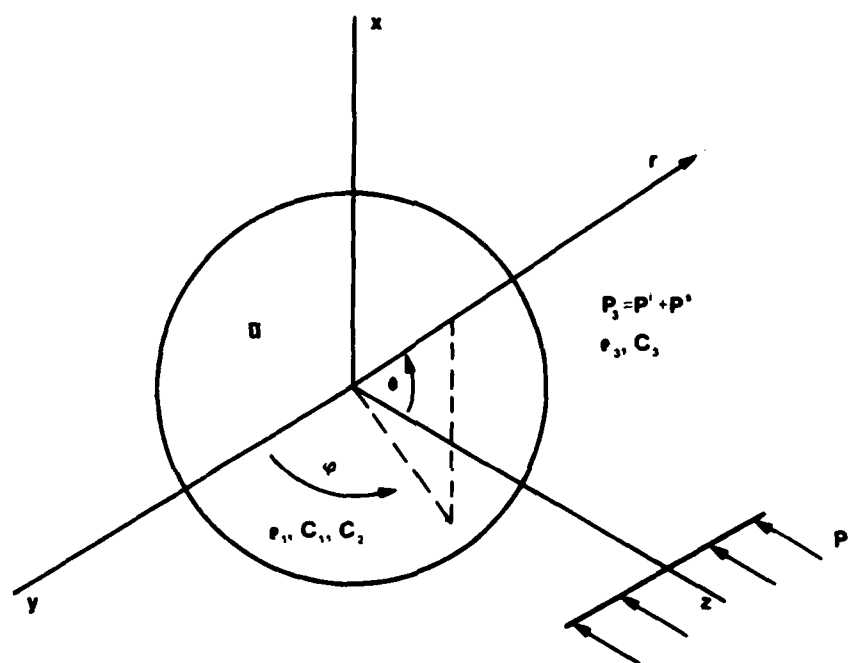
2.1 CLASSICAL SOLUTION FOR HOMOGENEOUS SPHERE

The elastic sphere is completely characterized by its radius, a , and three elastic constants: density ρ_1 , compression speed c_1 , and shear speed c_2 (see Appendix 8.1). It is embedded in a fluid with density ρ_3 and speed of sound c_3 . Let a monochromatic plane wave $p^i(\vec{r}, t)$ be incident upon it from the positive z direction (Fig. 2-1). The incident plane wave can be expanded, for $r \geq a$:

$$p^i(\vec{r}, t) = P_0 \sum_{n=0}^{\infty} (2n+1) (-i)^n P_n(\cos \theta) j_n(kr) e^{-i\omega t} . \quad (2-1)$$

The time dependence $e^{-i\omega t}$ will be suppressed in the equations to follow. The scattered pressure is given by

$$p^s(\vec{r}) = P_0 \sum_{n=0}^{\infty} c_n h_n^{(1)}(kr) P_n(\cos \theta) . \quad (2-2)$$



79-888

FIG. 2-1 Scattering geometry.

Here,

$P_n(\cos \theta)$ are the Legendre polynomials;

$j_n(kr)$, $n_n(kr)$, $h_n^{(1)}(kr)$ are the spherical Bessel functions of the first, second and third kind;

P_0 is an arbitrary constant, or could represent $P_0(\omega)$, the frequency content of the incident pulse;

$k = 2\pi/\lambda = \omega/c_3$, the wave number; and

c_n is the coefficient which is to be found.

Note that p^s satisfies the radiation condition, since asymptotically $h_n^{(1)}(kr) e^{-i\omega t} \rightarrow (-i)^{n+1} (1/kr) e^{i(kr - \omega t)} \rightarrow 0$ as $r \rightarrow \infty$ and is outward traveling.

Following Faran, it can be argued that the displacement \vec{u} inside the target can be written

$$\vec{u} = -\nabla\psi + \nabla \times \vec{A}, \quad (2-3)$$

where ψ , \vec{A} are of the form

$$\psi = \sum_{n=0}^{\infty} a_n j_n(k_1 r) P_n(\cos \theta) \quad (2-4)$$

$$\vec{A} = \hat{\phi} A_{\phi} = \hat{\phi} \sum_{n=0}^{\infty} b_n j_n(k_2 r) \frac{d}{d\theta} P_n(\cos \theta), \quad (2-5)$$

with unknowns a_n and b_n . The latter two equations are the results of symmetry arguments. These expressions are now evaluated at the boundary; $r = a$, and related via the boundary conditions, such as to permit solution for the unknown coefficients a_n , b_n , and c_n .

The boundary conditions are continuity of normal stress, normal

displacement and tangent shear stress. Or, in order, in spherical coordinates at $r = a$:

$$-(p^i + p^s) = \lambda(\nabla \cdot \vec{u}) + 2\mu \frac{\partial u_r}{\partial r} ; \quad (2-6)$$

$$-\frac{1}{\rho_3} \left(\frac{\partial p^i}{\partial r} + \frac{\partial p^s}{\partial r} \right) = \ddot{u}_r ; \quad (2-7)$$

$$\left. \begin{aligned} 0 &= \frac{\partial u_\theta}{\partial r} - \frac{u_\theta}{r} + \frac{1}{r} \frac{\partial u_r}{\partial \theta} , \\ 0 &= \frac{1}{r \sin \theta} \frac{\partial u_r}{\partial \phi} + \frac{\partial u_\phi}{\partial r} - \frac{u_\phi}{r} . \end{aligned} \right\} \quad (2-8)$$

(The last of these is trivially satisfied due to axial symmetry.) See Appendix 8.1 for the relationships between the Lamé coefficients λ , μ and other elastic constants and for the relationships between pressure and displacement. The equation of motion in the solid is (see [1] for discussion)

$$\rho_1 \ddot{\vec{u}} = (\lambda + 2\mu) \nabla(\nabla \cdot \vec{u}) - \mu \nabla \times \nabla \times \vec{u} , \quad (2-9)$$

so that $(\nabla \cdot \vec{u})$ and $(\nabla \times \vec{u})$ inside as well as $p = p^i + p^s$ outside satisfy their respective wave equations with velocities c_1 , c_2 , and c_3 .

The equations (2-6) through (2-8) must be satisfied for each mode n . We thus obtain the following set of three equations (in the same order) for each value of n , by direct substitution of (2-1) through (2-3) in the boundary condition equations:

$$\left. \begin{aligned} M_{11}^n a_n + M_{12}^n b_n + M_{13}^n c_n &= v_1^n \\ M_{21}^n a_n + M_{22}^n b_n + M_{23}^n c_n &= v_2^n \\ M_{31}^n a_n + M_{32}^n b_n &= 0 \end{aligned} \right\} \quad (2-10)$$

where $M_{11}^n = \left(\alpha(n^2 + n) - x_1^2 \right) j_n(x_1) - 2\alpha x_1 j_n'(x_1) \quad (2-11)$

$$M_{12}^n = (n^2 + n) \alpha \left(x_2 j_n'(x_2) - j_n(x_2) \right)$$

$$M_{13}^n = \beta D_0 a^2 h_n^{(1)}(x)$$

$$M_{21}^n = x x_1 j_n'(x_1)$$

$$M_{22}^n = (n^2 + n) x j_n(x_2)$$

$$M_{23}^n = -D_0 a^2 h_n^{(1)'}(x)$$

$$M_{31}^n = x_1 j_n'(x_1) - j_n(x_1)$$

$$M_{32}^n = \left(n^2 + n - 1 - x_2^2/2 \right) j_n(x_2) - x_2 j_n'(x_2)$$

$$M_{33}^n = 0$$

$$V_1^n = -\beta D_0 (2n+1) (-i)^n a^2 j_n(x)$$

$$V_2^n = D_0 (2n+1) (-i)^n a^2 j_n'(x)$$

$$V_3^n = 0$$

and where

$$x = ka = \omega a/c_3,$$

$$x_1 = k_1 a = \omega a/c_1,$$

$$x_2 = k_2 a = \omega a/c_2.$$

It was useful in the above to note that the Bessel functions j_n , n_n , and h_n all satisfy

$$x^2 f_n''(x) = (n^2 + n - x^2) f_n(x) - 2x f_n'(x) \quad (2-12)$$

The following constants were defined in conformance with [1]

$$\beta = \frac{\rho_3 c_3^2}{\rho_1 c_1^2}$$

$$\alpha = \frac{2c_2^2}{c_1^2} \quad (2-13)$$

$$D_o = - \frac{P_o}{\rho_3 c_3^2}$$

We can now solve for the coefficients a_n , b_n , c_n by inverting the matrix M^n . This must be done for all modes n .

By trial and error it is found that the number of modes $n = NMAX$ required to achieve convergence is about $NMAX = 2 + 8\sqrt{ka}$ for low values of ka and about $NMAX = ka + 15$ for ka greater than 5. The applications considered in the following pages required ka up to 40 and $NMAX$ up to 55. The evaluation of Bessel functions for such high order and argument is non-trivial. In these calculations Univac subroutines were used, which were based on the work by Goldstein and Thaler [4]. These utilize forward recurrence for n_n and backward recurrence for j_n . There are still difficulties with these evaluations which occur when n is large but the argument x_1 is small. Overflows in the computation of n_n then limit the calculations to lower values of n and x . This situation arises when c_1/c_3 is very large. For the materials considered here (brass and aluminum), it was found that the calculations could be made for ka up to 60. Since the

effect of parameter changes was also considered, the calculations of frequency responses were generally limited to $ka = 40$. Further, the solution was found at about 200 or 500 equally spaced points on the frequency scale.

The normalized far scattered field can be found from a simplification of (2-2), namely

$$\frac{r_o i^S(\vec{r})}{a} = P_o H(\omega) ,$$

$$H(\omega, \theta) = \sum_{n=0}^{\infty} \frac{c_n (-i)^{n+1}}{k} P_n(\cos \theta) . \quad (2-14)$$

This is obtained from the asymptotic form of $h_n^{(1)}$ which is

$$h_n^{(1)}(kr) \rightarrow \frac{(-i)^{n+1}}{kr} e^{ikr} \quad \text{as} \quad kr \rightarrow \infty$$

(Note that dropping the factor e^{ikr} in (2-14) is equivalent, in the time domain, to referencing the far field time origin to the space origin or sphere center. That is, a pulse scattered from the origin arrives in the far field at time $t = 0$.)

The magnitude of the frequency response, $|H(\omega)|$, in the back-scatter direction ($\theta = 0$) is plotted in Figures 2-2 through 2-6. Some of these results were essentially previously obtained by Hickling [5]. (When making comparisons, see the note on "Scaling" Section 3.8 in [1].) Responses for sound-hard, aluminum, and brass spheres are given in Figure 2.2. In Figures 2-3 through 2-6 the responses of aluminum are given and compared with their modifications due to parameter changes. This will be discussed further in the next section. It is seen that a dominant feature of the elastic responses is the regular occurrence of deep nulls which is absent in the hard target and fluid target approximations. The spacing of the

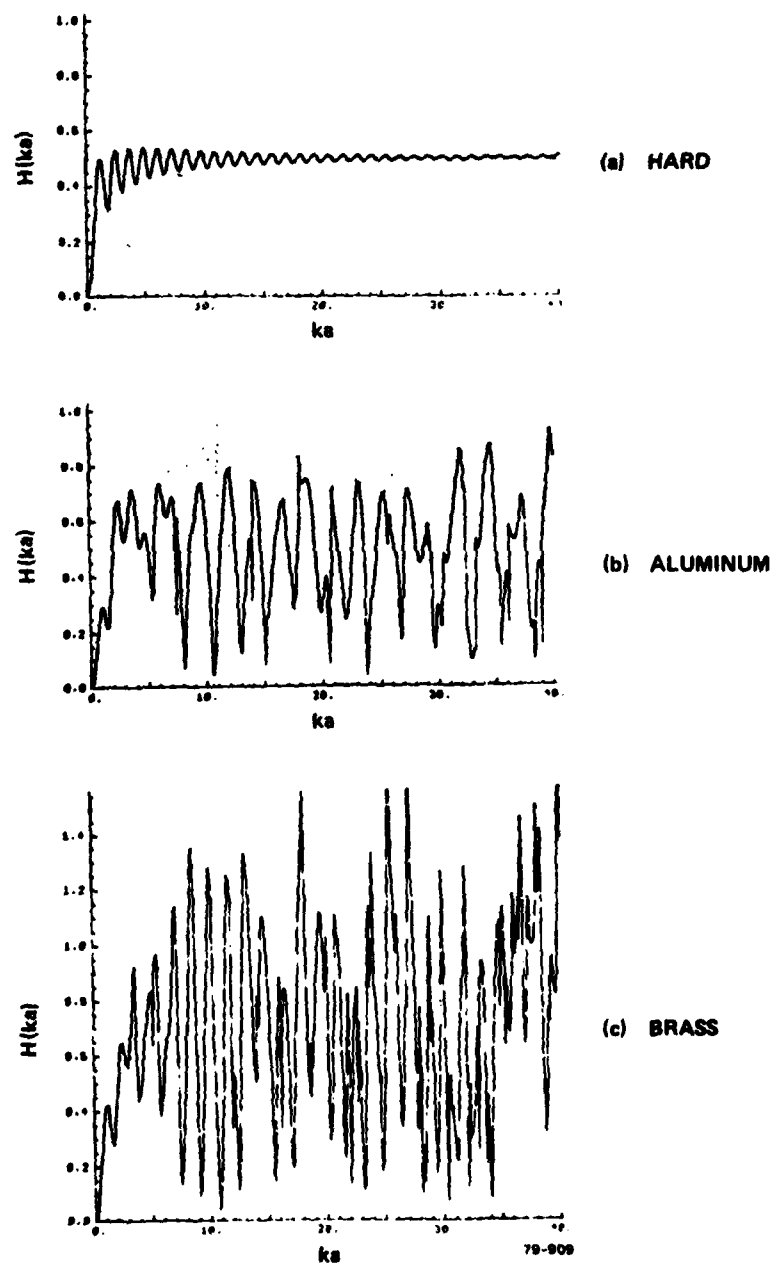


FIG. 2-2 Frequency response of sphere: (a) hard, (b) aluminum, and (c) brass.

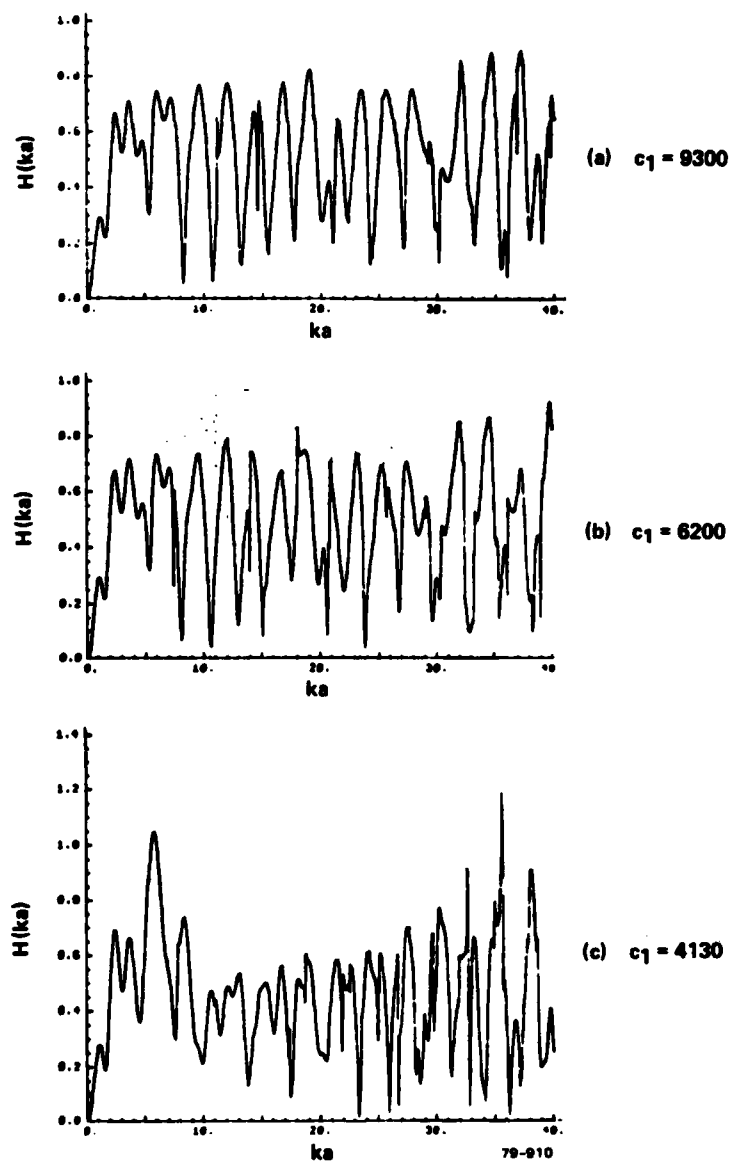


FIG. 2-3 Frequency response of aluminum sphere with (a) $c_1 = 9300$, (b) $c_1 = 6200$, and (c) $c_1 = 4130$.

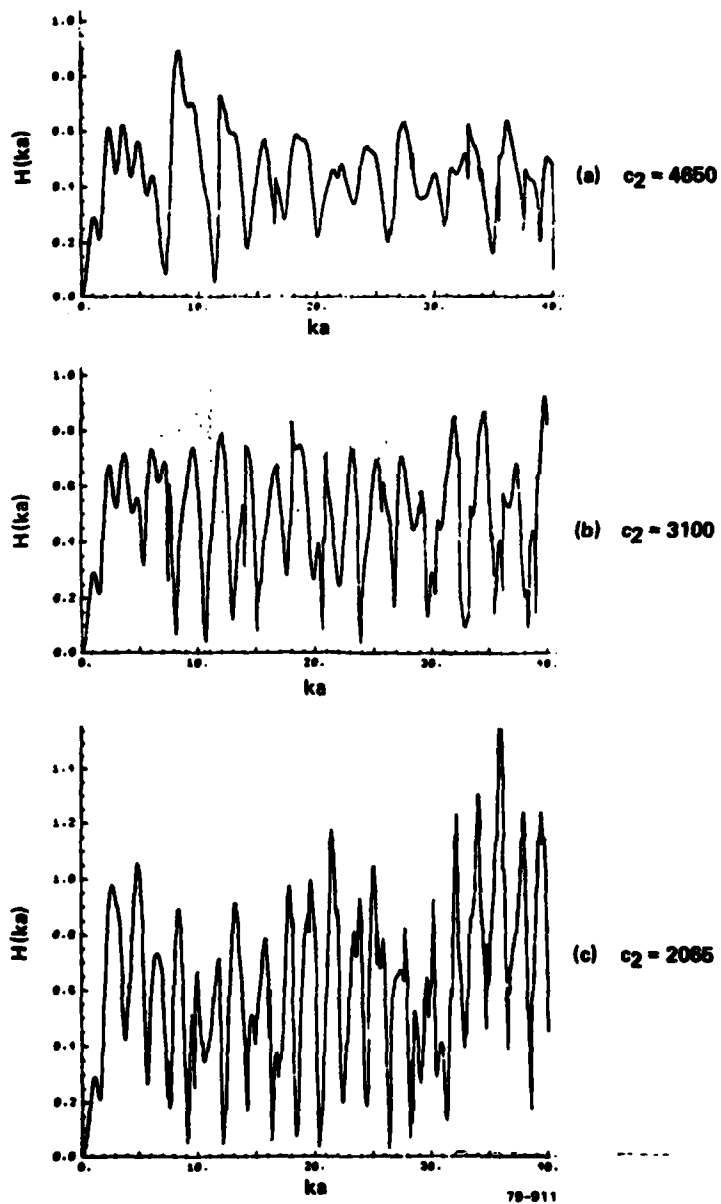


FIG. 2-4 Frequency response of aluminum sphere with (a) $c_2 = 4650$, (b) $c_2 = 3100$, and (c) $c_2 = 2065$.

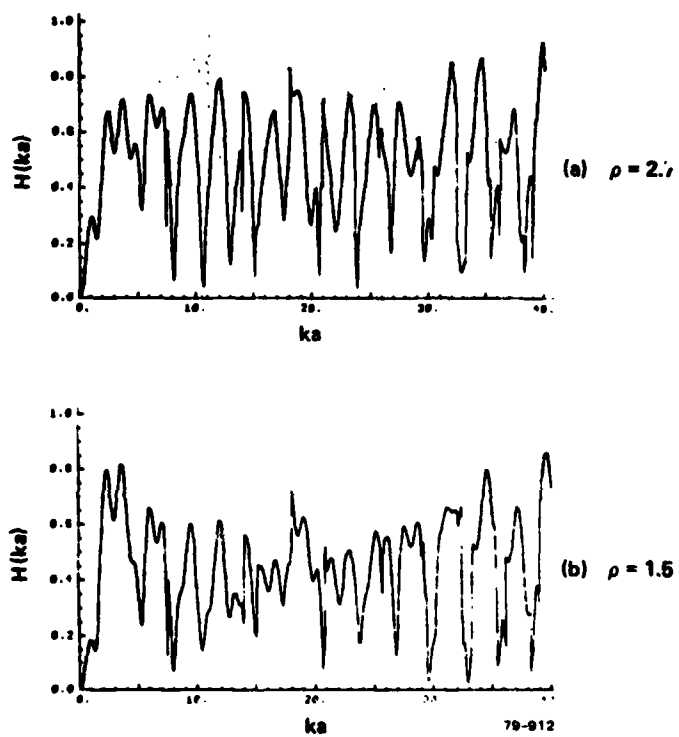


FIG. 2-5 Frequency response of aluminum sphere with (a) $\rho = 2.7$ and (b) $\rho = 1.5$.

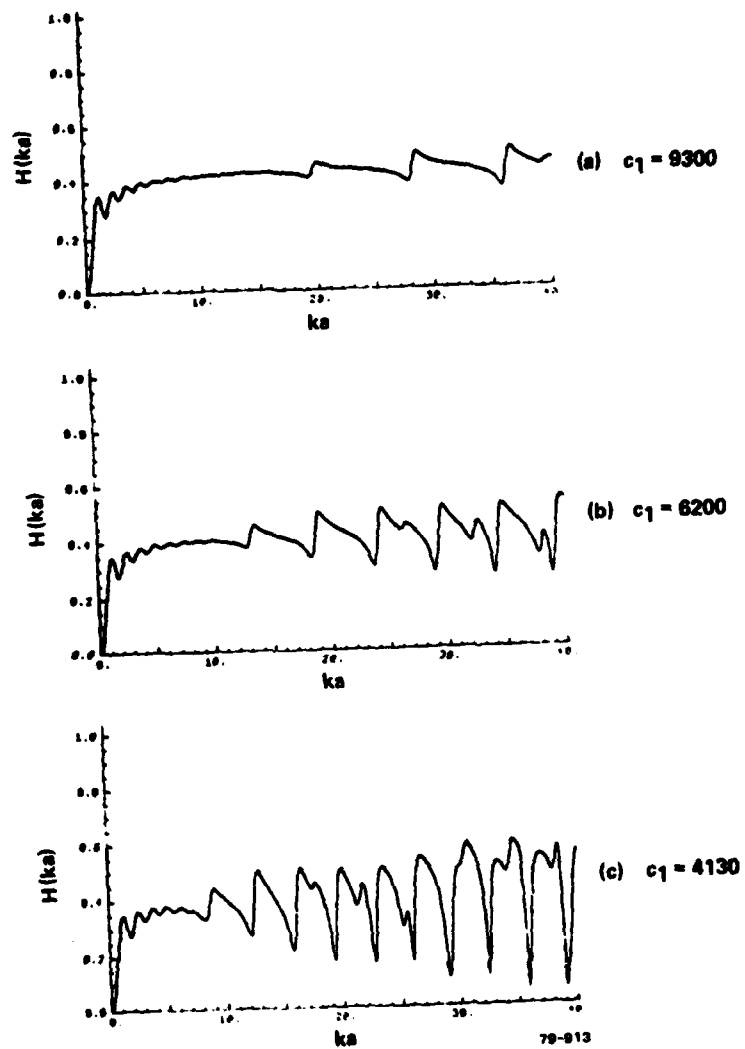


FIG. 2-6 Frequency response of aluminum sphere, fluid approximation, with (a) $c_1 = 9300$, (b) $c_1 = 6200$, and (c) $c_1 = 4130$.

nulls is affected by the velocities c_1 and c_2 , whereas the density affects mainly the amplitude of the response. The fluid response differs from the hard approximation mainly by amplitude at lower frequencies; although at higher frequencies a complex structure develops.

These features are difficult to explain in the frequency domain. After all, these pictures contain only half the available information, the phase of $H(\omega)$ is as important (or more so) as the magnitude.

It is to be noted, that the aluminum and brass sphere responses have been well verified by measurement [1].

2.2 SMOOTHED IMPULSE RESPONSE FOR SPHERE

It is instructive to study the sphere response in the time domain. To do this, a band and time limited pulse is chosen, the "smoothed impulse":

$$e(t') = \frac{a_n}{\sqrt{\pi}} e^{-(a_n t')^2} \quad (2-15)$$

This pulse has been normalized to give unit time integral with the normalized time $t' = c t_3/a$ and has a frequency domain representation

$$E(ka) = e^{-(ka/2a_n)^2} \quad (2-16)$$

(Refer to [6] appendix for a discussion on normalization.) In equation (2-14), P_0 is replaced by $E(ka)$: the product is then transformed to the time domain, resulting in the far field, normalized, "smoothed impulse response", $r_0 p^s(r, \vec{t}')/a$. The larger a_n , the sharper the smoothed impulse, but the higher the range of ω for which the response must be computed. A practical value here (consistent with the considerations of Section 2.1) is $a_n = 8$, which requires the computation of $H(ka)$ up to $ka = 40$.

2.3 EFFECT OF TARGET PARAMETERS ON SPHERE RESPONSE

The time domain responses corresponding to the cases already given in the frequency domain, are plotted in Figures 2-7 through 2-11. The time axes are in units of $c_3 t/a$.

Consider the hard sphere response of Figure 2-7a. The initial part is the specular return, an impulse at time $t = -2$. This is immediately followed by a negative step, a ramp, etc. decaying to zero. This is due to radiation from the region immediately surrounding the specular point (see Section 3.2). Then, centered at a time $t = \pi$, is the creep response. Note that the time of occurrence is just that of a pulse impinging on the target at $z = 0$, traveling at the speed of the medium c_3 around the back-side of the sphere and reradiating tangentially at $z = 0$.

It is seen immediately that the hard target cannot be an adequate model for scattering of wideband radiation from an elastic target: there is a small change in the specular response amplitude and backswing. But mainly, there have appeared large pulses at times 0 through 2. (One can verify readily that interference between these pulses and the specular impulse causes the resonant structure of the frequency response.) Significantly, these pulses are also absent from the fluid model response (Fig. 2-11). The time of occurrence of these pulses is strongly affected by the shear velocity c_2 (Figure 2-9) but only slightly by the compression velocity c_1 (Figure 2-8): we thus identify these features as due mainly to internal propagation of shear waves. Also present, and particularly noticeable in the fluid model are smaller pulses with arrival times proportional to compression velocity. These features can be associated with internal compression waves.

Aiding this discussion, Figure 2-12 illustrates the time references for various reflection paths. Suppose the distances a_1 , a_2 , a_3 are travelled by a plane wave at velocities c_1 , c_2 , c_3 respectively

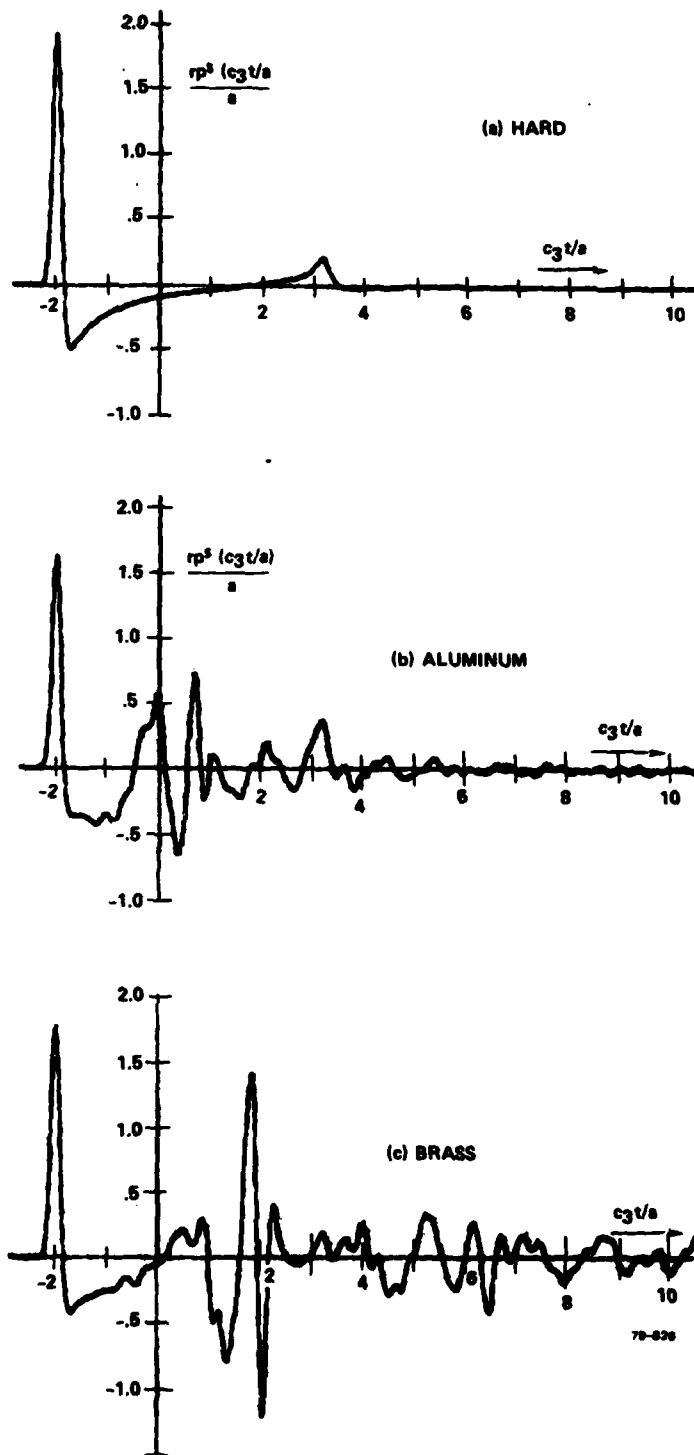


FIG. 2-7 Smoothed impulse response of aluminum sphere: (a) hard, (b) aluminum, and (c) brass.

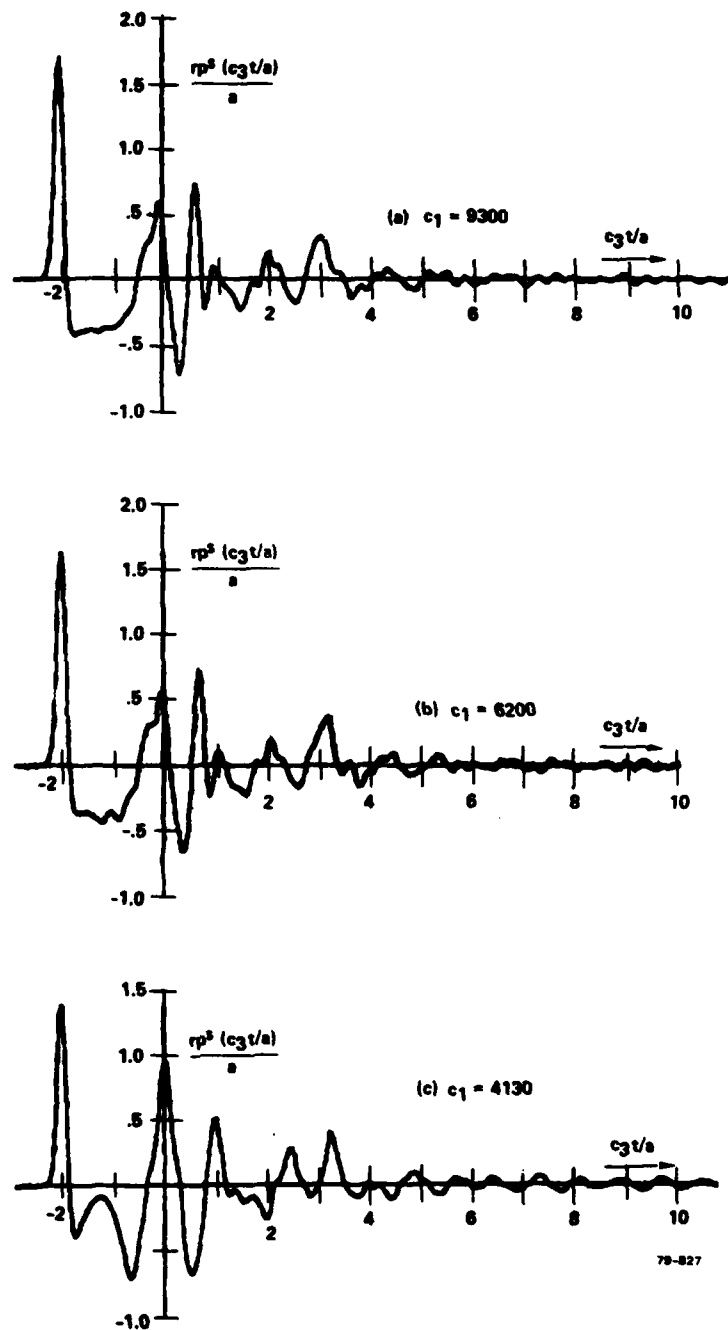


FIG. 2-8 Smoothed impulse response of aluminum sphere with (a) $c_1 = 9300$, (b) $c_1 = 6200$, and (c) $c_1 = 4130$.

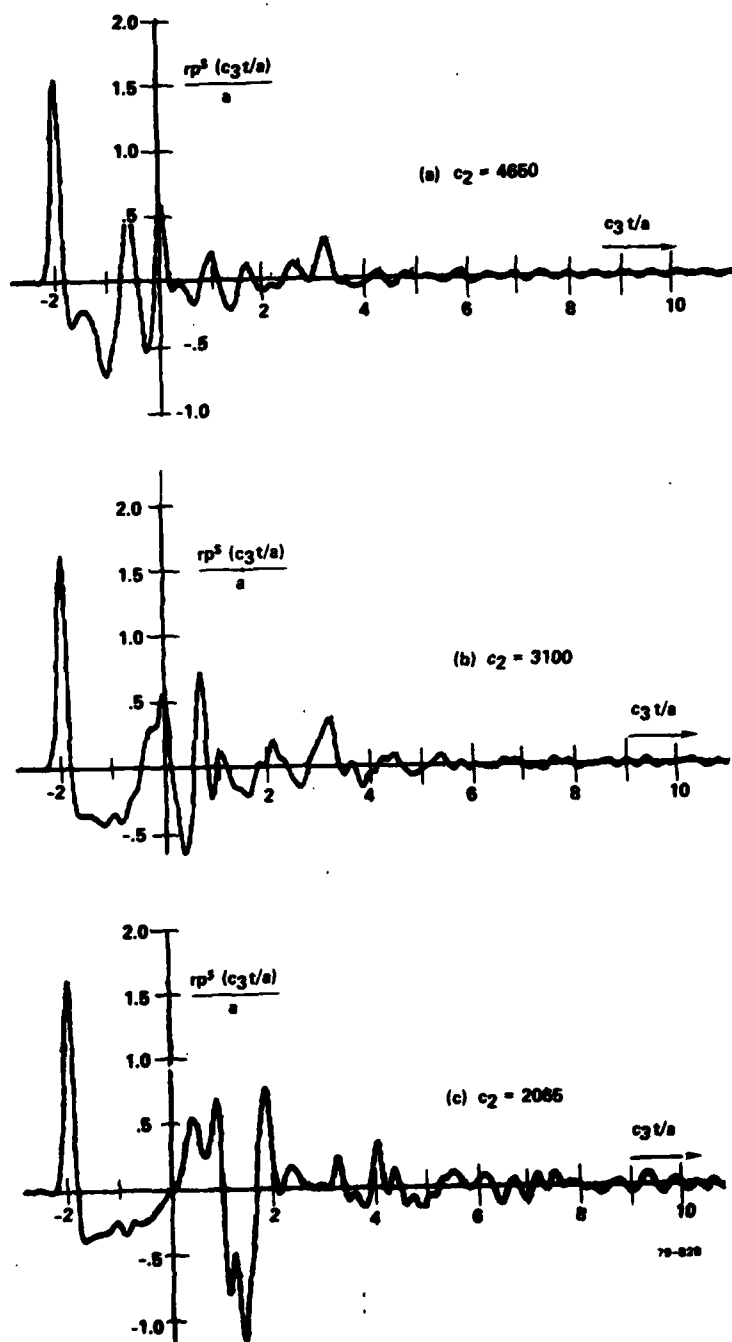


FIG. 2-9 Smoothed impulse response of aluminum sphere with (a) $c_2 = 4650$, (b) $c_2 = 3100$, and (c) $c_2 = 2065$.

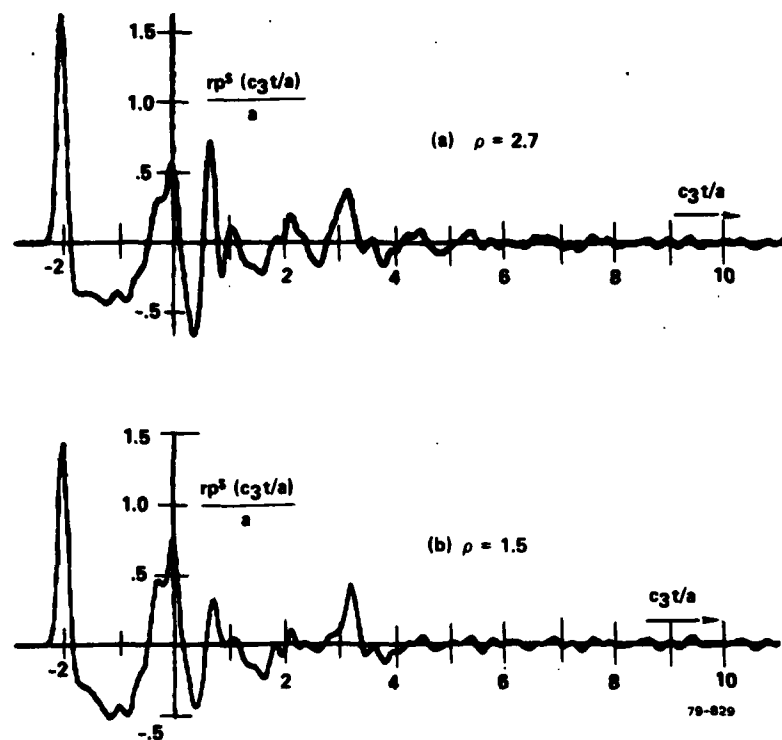


FIG. 2-10 Smoothed impulse response of aluminum with (a) $\rho = 2.7$ and (b) $\rho = 1.5$.

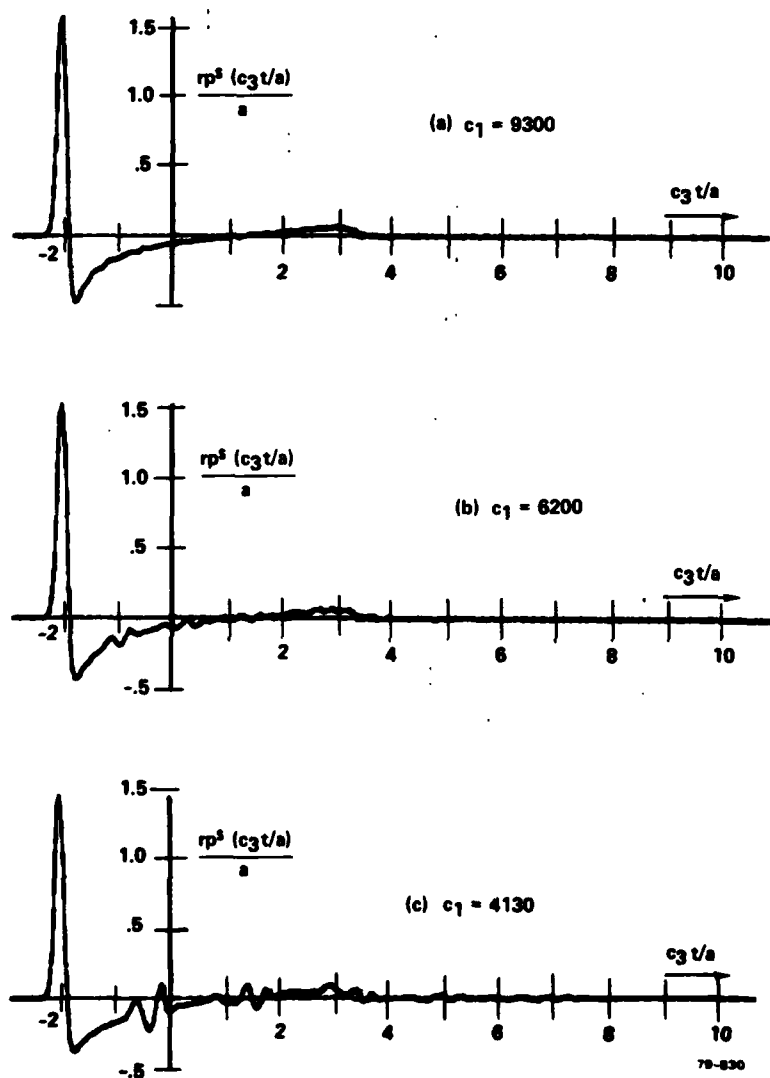
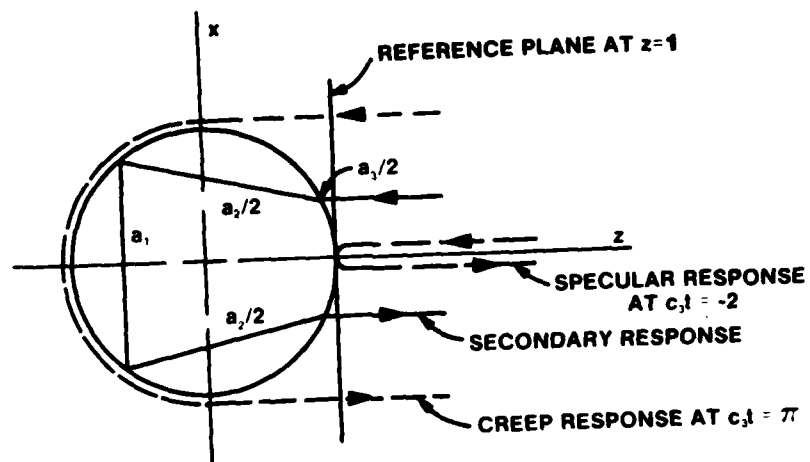


FIG. 2-11 Smoothed impulse response of aluminum sphere, fluid approximation, for (a) $c_1 = 9300$, (b) $c_1 = 6200$, and (c) $c_1 = 4130$.



SECONDARY RESPONSE AT $c_1 t = -2 + \frac{a_1}{c_1} + \frac{a_2}{c_2} + \frac{a_3}{c_3}$

79-869

FIG. 2-12 Time reference for scattering from unit sphere.

(as compared with the specular wave for which the distance is $a_3 = -2$).
Then the time of arrival is

$$t = \frac{a_1}{c_1} + \frac{a_2}{c_2} + \frac{a_3}{c_3} . \quad (2-17)$$

In Figure 2-13 responses are plotted versus time scale $c_2 t = c_2/c_1 a_1 + a_2 + c_2/c_3 a_3$, for several values of c_2 . If the path were entirely at speed c_2 then the features would remain at the same value of $c_2 t$. This is nearly the case: while c_2 is changed by a factor of 4, the time $c_2 t$ at which the "shear wave features" appear is nearly the same. The slight variation of the arrival time in units of $c_2 t$ associated with these features is then due to the fact that the paths of traversal are in small part at c_1 and c_3 . The vertical offset in Figures 2-13 and 2-14 is proportional to c_2 . Figure 2-14 is the same as 2-13 but with a higher value for c_1 . Only for large values of c_2 is there a significant difference between the curves. These results are sufficient to allow estimating path lengths through the target at the various velocities for the principal features of the response. Physical considerations (Snell's law -- Section 3.1) then can give the likely path associated with these features. In Section 3.3 they will be identified as the principal modes of a glory-wave effect.

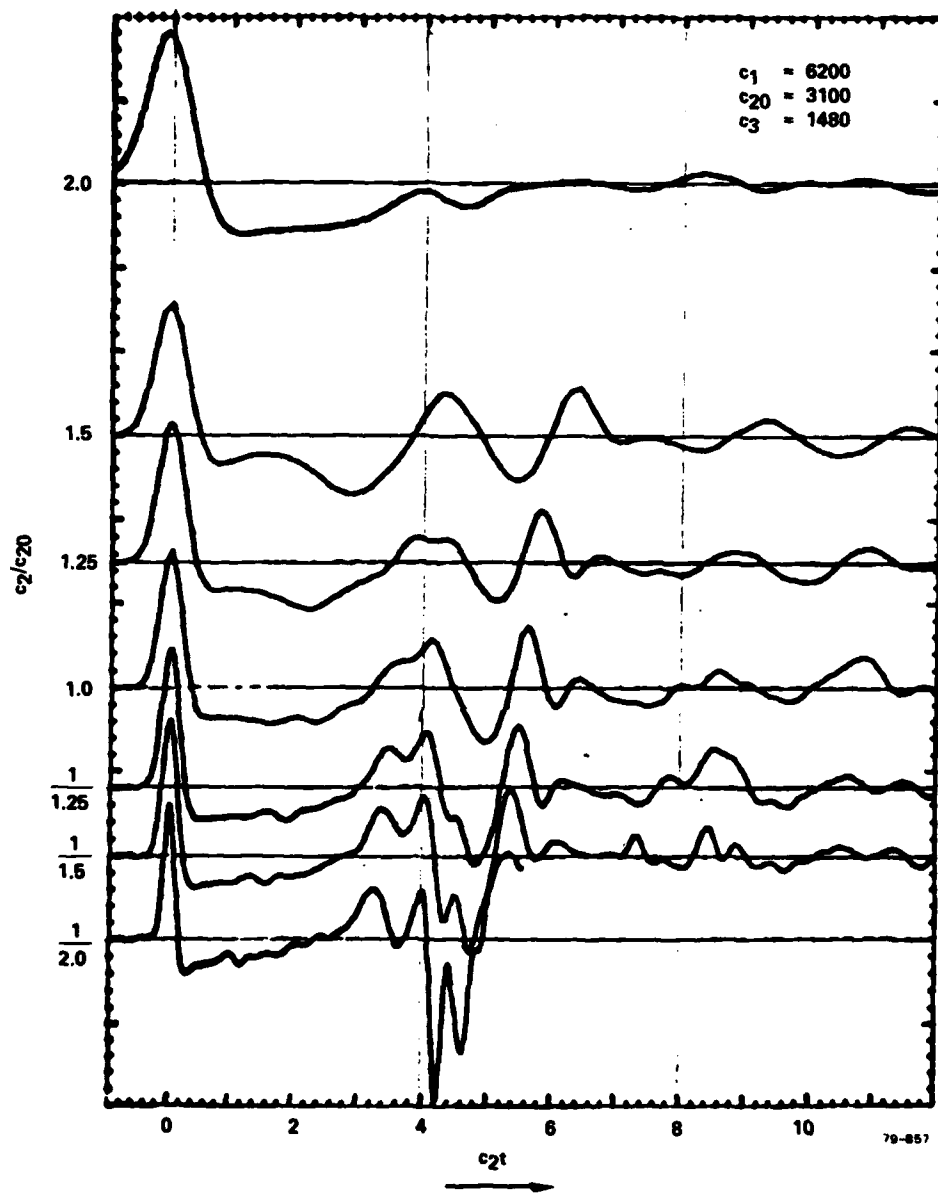


FIG. 2-13 Aluminum variations — response vs. c_2t with $c_1 = 6200$.

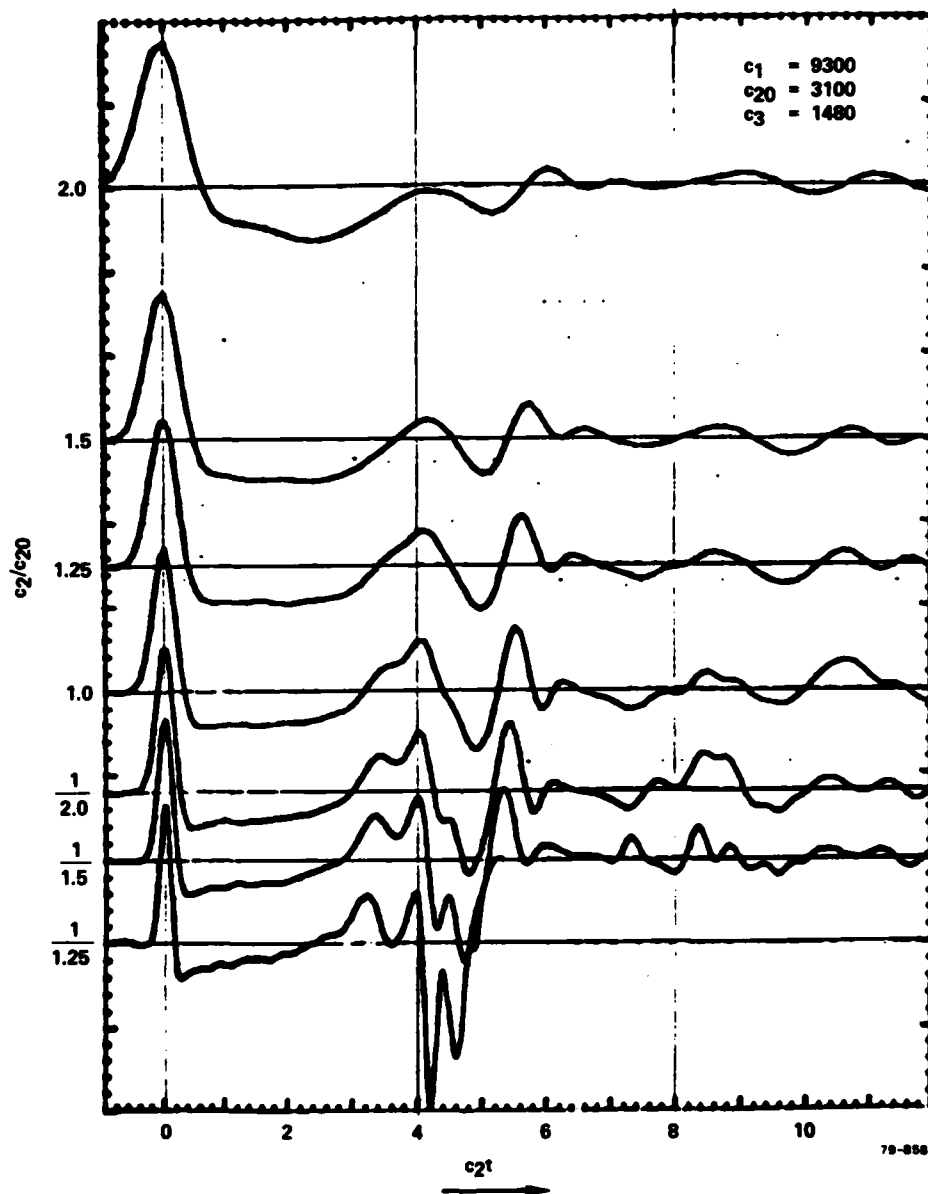


FIG. 2-14 Aluminum variations — response vs. c_2t with $c_1 = 9300$.

SECTION 3

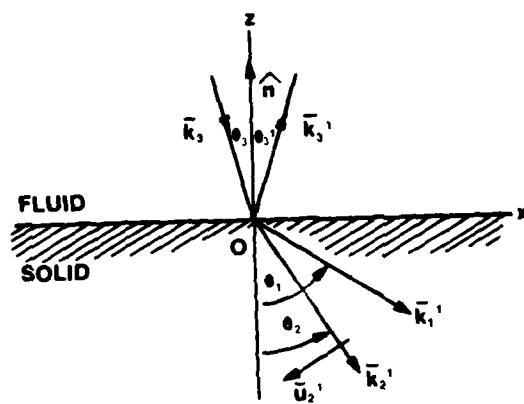
SCATTERING MODEL

It is apparent from both frequency and time domain points of view that the scattering process, for even such a simple target as a sphere, is inherently complicated. The aim of this section is to identify the essential attributes of the responses in order to obtain a reasonable approximation with a relatively simple model. Such a model is possible based on the glory-wave effect. This theory, developed originally for the scattering of light from water droplets, undergoes considerable complication (due to the existence of two sound speeds in the target) when applied to the acoustic case. However, the qualitative aspects of the theory, particularly when viewed in the time domain, are helpful in providing useful insight into the scattering process; it will be seen that the impulse response consists of a string of impulses which arrive after traveling through the target along the readily identifiable glory paths. On the other hand, quantitatively (i.e., for the magnitude of the impulse response) the theory is difficult to apply (see the extensive work of Uberall et al. [7]). It is suggested that a useful approach is a hybrid approximate method, using the quantitative considerations of the next two subsections together with the simple glory-path model.

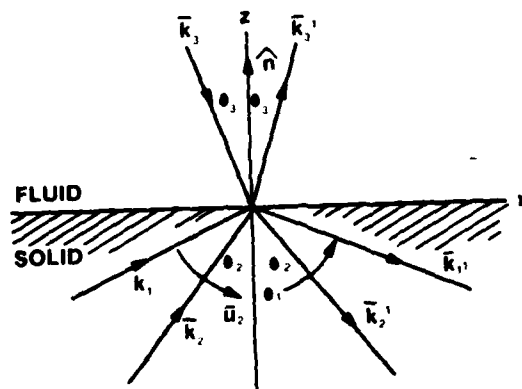
3.1 REFLECTION AND REFRACTION AT A PLANE ELASTIC BOUNDARY

The following is an exact treatment of the interaction of a plane compressional wave with a plane fluid-elastic interface, and of the reverse problem.

Let the displacement in a fluid medium be given by \vec{u}_3 , and in the solid by \vec{u}_1 and \vec{u}_2 corresponding to compressional and shear waves respectively. Primes are used to denote the part of the wave after reflection or refraction. Consider the plane interface of Figure 3-1. Then we



(a) WAVE INCIDENT FROM FLUID



(b) GENERAL CASE

79-870

FIG. 3-1 Plane wave refraction at plane boundary.

have

$$\text{incident wave } \vec{u}_3 = \vec{u}_{30} e^{j\vec{k}_3 \cdot \vec{r} - j\omega t} , \quad (3-1)$$

$$\text{reflected wave } \vec{u}'_3 = \vec{u}'_{30} e^{j\vec{k}'_3 \cdot \vec{r} - j\omega t} , \quad (3-2)$$

$$\text{refracted wave } \vec{u}'_1 = \vec{u}'_{10} e^{j\vec{k}'_1 \cdot \vec{r} - j\omega t} , \quad (3-3)$$

$$\vec{u}'_2 = \vec{u}'_{20} e^{j\vec{k}'_2 \cdot \vec{r} - j\omega t} . \quad (3-4)$$

The zero subscript refers to the value at the origin. Assume that the wave normals are in the x,z plane so that:

$$\begin{aligned} \vec{k}_3 &= (\hat{x} \sin \theta_3 - \hat{z} \cos \theta_3) k_3 , \\ \vec{k}'_3 &= (\hat{x} \sin \theta'_3 + \hat{z} \cos \theta'_3) k'_3 , \\ k'_1 &= (\hat{x} \sin \theta_1 - \hat{z} \cos \theta_1) k'_1 , \\ k'_2 &= (\hat{x} \sin \theta_2 - \hat{z} \cos \theta_2) k'_2 \end{aligned} \quad (3-5)$$

where

$$k_i = \omega/c_i .$$

Snell's laws for reflection and refraction follow directly from these definitions, independent of the nature of the boundary conditions (see Jackson, p. 217 [8]): whatever boundary conditions prevail, the same conditions are satisfied at the point (0,0) as at every other point on the interface. Hence the variation in phase for (3-1) through (3-4) must be

the same for all under translation on the interface. That is:

$$k'_1 \sin \theta_1 = k'_2 \sin \theta_2 = k'_3 \sin \theta'_3 = k_3 \sin \theta_3 \quad (3-6)$$

(The same argument for phase variation with time can be used to establish that the frequencies, ω , are the same for all waves.) Hence Snell's Law:

$$\sin \theta'_3 = \sin \theta_3$$

$$\sin \theta_1 = \frac{c_1}{c_3} \sin \theta_3 \quad (3-7)$$

$$\sin \theta_2 = \frac{c_2}{c_3} \sin \theta_3$$

Note that for solids we generally have $c_1 > c_2 > c_3$, so that rays are refracted away from the normal after entering the solid, as in Figure 3-1. Also note that for some real incident angle, θ_{3c1} (the critical angle), we will have $\sin \theta_{1c} = c_1/c_3 \sin \theta_{3c1} = 1$. There is no transmission at speed c_1 for $\theta_3 \geq \theta_{3c1}$. Similarly, at θ_{3c2} such that $\sin \theta_{2c} = c_2/c_3 \sin \theta_{3c2} = 1$, there is no transmission at c_2 (nor at c_1); so that there is total reflection for $\theta_3 \geq \theta_{3c2}$. At angles between these two critical angles, there is transmission only at c_2 , that is as a shear wave. The boundary conditions can be satisfied through the existence of an evanescent wave which travels along the surface.

We will now derive the relative magnitudes of these waves, for which it is necessary to know the dynamics or boundary conditions. These are

- (1) continuity of normal stress,
- (2) continuity of normal displacement,
- (3) continuity of tangent shear stress.

In Cartesian coordinates these are written [1]:

$$\begin{aligned}\lambda_3 \left[(\nabla \cdot \vec{u}_3) + (\nabla \cdot \vec{u}_3') \right] &= \lambda (\nabla \cdot \vec{u}) + 2\mu \frac{\partial u_n}{\partial n} , \\ \hat{n} \cdot \left[\vec{u}_3 + \vec{u}_3' \right] &= \hat{n} \cdot \vec{u} , \\ \mu \left[\frac{\partial u_n}{\partial x} + \frac{\partial u_x}{\partial n} \right] &= 0\end{aligned}\tag{3-8}$$

where $\vec{u} = \vec{u}_1 + \vec{u}_2$ and the elastic constants are

$$\begin{aligned}\lambda_3 / \rho_3 &= c_3^2 \\ (\lambda + 2\mu) / \rho &= c_1^2 \\ \mu / \rho &= c_2^2 .\end{aligned}\tag{3-9}$$

Substituting equation (3-1) etc. into the boundary conditions, we obtain respectively

$$\lambda_3 k_3 (u_{30} + u_{30}') = \lambda k_1 u_{10}' + 2\mu \left[u_{10}' k_1 \cos^2 \theta_1 + u_{20}' k_2 \cos \theta_2 \sin \theta_2 \right] ,\tag{3-10}$$

$$(u_{30} - u_{30}') \cos \theta_3 = u_{10}' \cos \theta_1 + u_{20}' \sin \theta_2 ,\tag{3-11}$$

$$2 u_{10}' k_1 \sin \theta_1 \cos \theta_1 - u_{20}' k_2 (\cos^2 \theta_2 - \sin^2 \theta_2) = 0 .\tag{3-12}$$

Solving simultaneously we obtain the transmitted amplitude (that is u_{10}' , u_{20}' , and u_{30}') in terms of the incident amplitude u_{30} . It is convenient to define the quantities

$$A = \left(\frac{\rho_1 c_1}{\rho_3 c_3} \right) \left(\left(1 - \alpha \sin^2 \theta_1 \right) + \alpha Q \sin \theta_1 \cos \theta_2 \right), \quad (3-13)$$

$$B = \frac{\cos \theta_1}{\cos \theta_3 \left(\cos^2 \theta_2 - \sin^2 \theta_2 \right)} \quad (3-14)$$

$$Q = \frac{2 c_2 \sin \theta_1 \cos \theta_1}{c_1 \left(\cos^2 \theta_2 - \sin^2 \theta_2 \right)} \quad (3-15)$$

where $\alpha = 2 c_2^2 / c_1^2$. Then the transmission coefficients are found to be

$$R_{33} = \frac{u'_{30}}{u_{30}} = \frac{A - B}{A + B}, \quad (3-16)$$

$$R_{31} = \frac{u'_{10}}{u_{30}} = \frac{2}{A + B}, \quad (3-17)$$

$$R_{32} = \frac{u'_{20}}{u_{30}} = \frac{2Q}{A + B}. \quad (3-18)$$

The first subscript of R refers to the incident wave, the second to the reflected or refracted wave.

The above derivation can be performed more generally, as indicated in Figure 3-2, to also permit waves incident from inside the solid. The results are as follows. For an incident compression wave in the solid, u_{10} , the refractions and reflections are

$$R_{11} = \frac{u'_{10}}{u_{10}} = \frac{B - C + QD}{A + B} \quad (3-19)$$

$$R_{12} = \frac{u'_{20}}{u_{10}} = - \frac{2QC}{A + B} \quad (3-20)$$

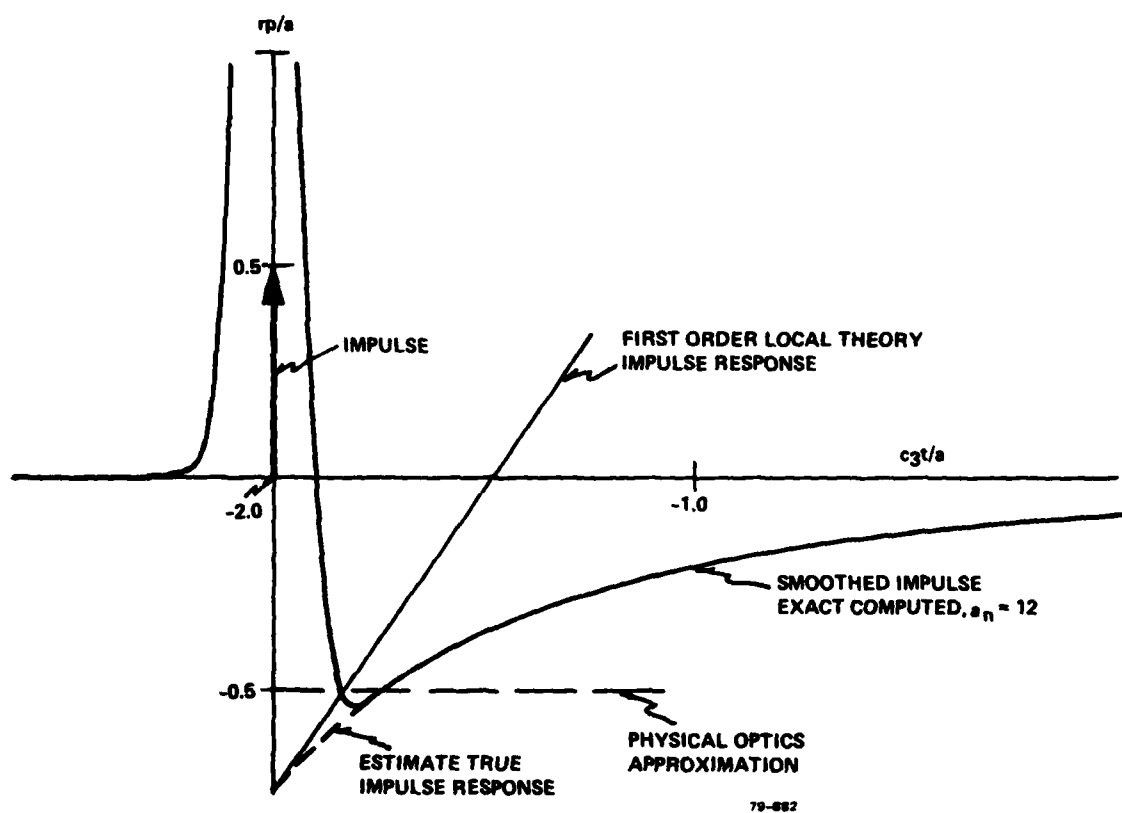


FIG. 3-2 Impulse response of hard sphere (leading edge).

$$R_{13} = \frac{u'_{30}}{u_{10}} = \frac{2BC}{A+B} \quad (3-21)$$

Here we have also used the definitions

$$C = \frac{\rho_1 c_1}{\rho_3 c_3} \left(\cos^2 \theta_2 - \sin^2 \theta_2 \right), \quad (3-22)$$

$$D = \frac{\rho_1 c_2}{\rho_3 c_3} \left(2 \sin \theta_2 \cos \theta_2 \right). \quad (3-23)$$

For an incident shear wave, u_{20} , the refractions and reflections are

$$R_{21} = \frac{u'_{10}}{u_{20}} = \frac{2D}{A+B} \quad (3-24)$$

$$R_{22} = \frac{u'_{20}}{u_{20}} = \frac{2D - B - C}{A+B} \quad (3-25)$$

$$R_{23} = \frac{u'_{30}}{u_{20}} = -\frac{2BD}{A+B} \quad (3-26)$$

Note that R_{13} , R_{23} represent energy transmitted from solid to fluid medium, while R_{12} and R_{21} represent mode conversions.

For normal incidence, $\theta_1 = \theta_2 = \theta_3 = 0$, these expressions simplify to

$$R_{33} = \frac{A-1}{A+1} = \frac{\rho_1 c_1 - \rho_3 c_3}{\rho_1 c_1 + \rho_3 c_3}$$

$$R_{31} = \frac{2}{A+1} = \frac{2\rho_3 c_3}{\rho_1 c_1 + \rho_3 c_3} \quad (3-27)$$

$$R_{32} = 0$$

Also, it is interesting to investigate the case of critical incidence for c_1 , that is $\theta_1 = 90^\circ$. We then have that $R_{33} = 1$, that's total reflection. As the incident angle increases slightly and θ_1 becomes imaginary, there is transmission of energy as a shear wave at c_2 , while on the surface there exists an evanescent compression wave at c_1 .

In closing, it is noted that the fluid, hard, and soft cases are included in the analysis by appropriately letting the densities ρ_1 , ρ_3 go to zero or ∞ .

3.2 TIME DOMAIN SPECULAR RESPONSE - LOCAL STIE

In the physical optics limit, the impulse response of a target is given by $1/2\pi$ times the second derivative of its projected area function. This was given by Kennaugh & Cosgriff in 1958 [9] for the electromagnetic case and is valid, as will be seen, in the limit, for the acoustic case as well. For example, the projected area of a unit sphere with specular point at the origin (Figure 2-1) for an incident plane wave traveling in the z -direction is

$$S_p = \pi \rho^2 = \pi (2az - z^2). \quad (3-28)$$

Taking the speed of sound $c = 1$, we have that $z = t/2$. The area function is then

$$S_p(t) = \pi \left(at - \frac{t^2}{4} \right) u(t), \quad (3-29)$$

and

$$\frac{1}{2\pi} \frac{d^2 S_p}{dt^2} = \frac{1}{2} \delta(t) - \frac{1}{4} u(t) \quad (3-30)$$

is the physical optics impulse response. This can be considered to be the

first two terms of an expansion in singularity functions. An improvement to this approximation can be obtained by including the effect of surface interactions.

3.2.1 Sound Hard Convex Specular Point

For a sound hard target the far backscattered pressure is given by

$$r_o p^s(t) = \frac{1}{4\pi} \int_S (\hat{r}_o \cdot \hat{n}') \frac{\partial p(\vec{r}', t')}{\partial t'} ds' , \quad (3-31)$$

where $t' = t + (\hat{r}_o \cdot \vec{r}')$ and \hat{r}_o is the direction of observation. The pressure on the surface can be shown [1] to be

$$p(\vec{r}', t') = 2 p^i(z', t') + \frac{1}{2\pi} \int_S (\hat{R} \cdot \hat{n}'') \left(\frac{1}{R} + \frac{1}{R} \frac{\partial}{\partial t''} \right) p(\vec{r}'', t'') ds'' , \quad (3-32)$$

where $t'' = t' - R$, $\vec{R} = \vec{r} - \vec{r}'$, and t is in units of sound-meters. It is easier to consider the step response first. Let the incident plane wave be a step traveling in the positive z -direction (i.e., $\hat{r}_o \cdot \vec{r}' = -z'$)

$$p^i(z', t') = u(t' - z') ,$$

or

$$p^i(z', t) = u(t - 2z') . \quad (3-33)$$

As a first approximation we will consider the surface pressure, $p(\vec{r}'', t'')$, constant over the illuminated region (and zero outside). Then $\partial p / \partial t'' = 0$, except at the boundary of the illuminated region where

$$\frac{\partial p}{\partial t''}(\vec{r}'', t'') = p(\vec{r}'', t'') \delta(t'' - z'') ,$$

or

$$\frac{\partial p}{\partial t''}(\vec{r}'', t'') = p(\vec{r}'', t'') \delta(t' - z'' - R) .$$

We want to substitute this in the integral (3-32). To evaluate the integral we use the fact that for a circular patch ΔS of radius γ

$$\epsilon = \frac{1}{2\pi} \int_{\Delta S} dS'' \frac{(\hat{R} \cdot \hat{n}'')}{R^2} = \frac{\bar{\kappa}}{2} \int_0^\gamma dR = \frac{\gamma \bar{\kappa}}{2} , \quad (3-34)$$

where κ is the average curvature. This approximation applies to smooth convex surfaces. This was derived in [1] p. 16, but due to a typographical error, the value of ϵ is given incorrectly in [1]. Here, ΔS is the elliptical patch around \vec{r}' at time t' which is illuminated at the retarded times $t'' = t' - R$. Some reflection reveals that the approximate radius of ΔS is given

$$\gamma = t - 2z' . \quad (3-35)$$

For the second term in (3-32) involving $\partial p / \partial t''$ we need

$$\frac{1}{2\pi} \int_{\Delta S} dS'' \frac{(\hat{R} \cdot \hat{n}'')}{R} \delta(t' - z'' - R) = \frac{\bar{\kappa}}{2} \int_0^\gamma R \delta(t' - z'' - R) dR = \frac{\gamma \bar{\kappa}}{2} \quad (3-36)$$

This follows since $\partial p / \partial t$ is nonzero at the boundary of the patch ΔS . The result of the first order evaluation of (3-32) is thus

$$p(\vec{r}', t') = 2 p^i(z', t') + \gamma \bar{\kappa} p(\vec{r}', t') ,$$

where $\gamma = t - 2z'$. Solving for p and expanding $1/(1 - \gamma \bar{\kappa})$ this can be

written

$$p(\vec{r}', t') = 2 p^i(z', t') \left\{ 1 + \gamma \bar{\kappa} + \gamma^2 \bar{\kappa}^2 + \dots \right\} ,$$

and making the substitution (3-33)

$$\frac{1}{2} p(\vec{r}', t') = u(t - 2z') \left\{ 1 + \bar{\kappa}(t - 2z') + \bar{\kappa}^2(t - 2z')^2 + \dots \right\} ; \quad (3-37)$$

$$\begin{aligned} \frac{1}{2} \frac{\partial p}{\partial t}(\vec{r}', t') &= \delta(t - 2z') \left\{ 1 + \bar{\kappa}(t - 2z') + \dots \right\} \\ &+ u(t - 2z') \bar{\kappa} \left\{ 1 + 2\bar{\kappa}(t - 2z') + \dots \right\} . \end{aligned} \quad (3-38)$$

This expression for the surface pressure can now be used to evaluate the far-scattered step response.

Using $(\hat{r}_o \cdot \hat{n}') dS' = 2\pi \rho a \cos \theta d\theta = 2\pi(a - z') dz'$, the integral (3-31) can be rewritten

$$\begin{aligned} r_o p^S(t) &= \int_0^{t/2} (a - z') \delta(t - 2z') \left\{ 1 + \bar{\kappa}(t - 2z') + \bar{\kappa}^2(t - 2z')^2 + \dots \right\} dz' \\ &+ \int_0^{t/2} (a - z') u(t - 2z') \bar{\kappa} \left\{ 1 + 2\bar{\kappa}(t - 2z') + 3\bar{\kappa}^2(t - 2z')^2 + \dots \right\} dz' \end{aligned} \quad (3-39)$$

Direct evaluation and the substitution $a\bar{\kappa} = -1$, yields for the step response

$$r_o p^S = a \left\{ \frac{1}{2} - \frac{3}{4} (t/a) + \frac{5}{8} (t/a)^2 + \dots \right\} u(t) .$$

Differentiating and normalizing, the impulse response of the hard sphere is then

$$h(t/a) \equiv \frac{r_o p^s(t/a)}{a} = \frac{1}{2} \delta(t/a) - \frac{3}{4} u(t/a) + \frac{5}{4} r_p(t/a) + \dots \quad (3-40)$$

The third term (ramp) of this expansion is inaccurate and could be improved upon by the use of (3-37) and (3-38) in (3-32) as the next approximation; and so on. The main result here is the correction of the step coefficient as given by the simpler physical optics theory in equation (3-30). The result of approximating the impulse response by the methods of Section 2, using $a_n = 12$, is plotted in Figure 3-2, superposed on the present results. The agreement, including the r_p term is seen to be excellent.

3.2.2 Fluid Sphere Convex Specular Point

Consider now the case where energy penetrates the target in the form of compression waves. We then have two integral equations (see Section 4) corresponding to pressure outside, p , and inside, p_1 :

$$\begin{aligned} p(\vec{r}', t') &= 2 p^i(z', t) + \frac{1}{2\pi} \int_{\Delta S} (\hat{R} \cdot \hat{n}'') \left(\frac{1}{R} + \frac{1}{R} \frac{\partial}{\partial t''} \right) p(\vec{r}'', t'') dS'' \\ &\quad - \frac{1}{2\pi} \int_{\Delta S} \frac{1}{R} \frac{\partial}{\partial n''} p(\vec{r}'', t'') dS'' \\ p_1(\vec{r}', t') &= - \frac{1}{2\pi} \int_{\Delta S_1} (\hat{R} \cdot \hat{n}'') \left(\frac{1}{R} + \frac{1}{Rc_1} \frac{\partial}{\partial t''} \right) p_1(\vec{r}'', t_1'') dS'' \\ &\quad + \frac{1}{2\pi} \int_{\Delta S_1} \frac{1}{R} \frac{\partial}{\partial n''} p_1(\vec{r}'', t_1'') dS'' \end{aligned} \quad (3-41)$$

where $t'' = t' - R$, $t_1'' = t' - R/c_1$. The patch ΔS has radius $\gamma = t - 2z'$ as before. The interior integral is over the larger patch ΔS_1 with radius

$\gamma_1 = c_1 t - 2z'_1$. The above equations are related by the boundary conditions

$$p = p_1$$

$$\frac{\partial p}{\partial n} = \frac{\partial p_1}{\rho_1 \partial n} ; \quad (3-42)$$

c_1, p_1 are the sound speed and density inside relative to outside. The integrations over the surface patch are similar to that of the previous section and result in

$$p(\vec{r}', t') = 2p^i + \gamma \bar{\kappa} p - \gamma \frac{\partial p}{\partial n}$$

and

$$p(\vec{r}', t') = -c_1 \gamma \bar{\kappa} p + \gamma \rho_1 c_1 \frac{\partial p}{\partial n} ,$$

where the last equation is obtained from the last of (3-41) and the application of the boundary conditions. Again, we use a step function as the incident field. Solving, we obtain on the surface

$$p(\vec{r}', t') = 2 \left(\frac{\rho_1 c_1}{1 + \rho_1 c_1} \right) (1 + \epsilon + \epsilon^2 + \dots) u(t - 2z') ,$$

$$\frac{\partial p}{\partial n}(\vec{r}', t') = 2 \left(\frac{1}{1 + \rho_1 c_1} \right) (1 + \epsilon + \epsilon^2 + \dots) \left(\frac{1 + c_1 \bar{\kappa} \gamma}{\gamma} \right) u(t - 2z') , \quad (3-43)$$

where we have defined

$$\epsilon = \left(\frac{\rho_1 - 1}{1 + \rho_1 c_1} \right) \bar{\kappa} c_1 \gamma .$$

The integral equation for far field scattering from an elastic or fluid

target is

$$r_o p^s(t) = \frac{1}{4\pi} \int_s (\hat{r}_o \cdot \hat{n}') \frac{\partial p(\vec{r}', t')}{\partial t'} dS' - \frac{1}{4\pi} \int_s \frac{\partial p(\vec{r}', t')}{\partial n'} dS' \quad (3-44)$$

Substituting (3-43) into this, results in terms similar to that for the hard target step response except for constants. The result is that the impulse response of a smooth curved specular point for a fluid target is given by

$$h(t/a) = \left(\frac{\rho_1 c_1}{1 + \rho_1 c_1} \right) \left\{ \frac{1}{2} \delta(t/a) - \left[\frac{1}{4} + \frac{\beta}{2} \right] u(t/a) + \dots \right\} \\ - \left(\frac{1}{1 + \rho_1 c_1} \right) \left\{ \frac{1}{2} \delta(t/a) - \left[\frac{\beta + c}{2} \right] u(t/a) + \dots \right\}, \quad (3-45)$$

where

$$\beta = \frac{\rho_1 c_1 - c_1}{\rho_1 c_1 + 1}.$$

Note that as $\rho_1 \rightarrow \infty$ (3-45) reduces to the sound-hard case. Also, the factor $(\rho_1 c_1 - 1)/(\rho_1 c_1 + 1)$, by which the impulse term differs from the sound-hard (perfectly reflecting) case, is the same as the reflection coefficient found in (3-27) for normal reflection from an elastic plane surface.

3.2.3 Extensions of These Techniques

At the next level of complexity it is possible to determine by these analytic methods the response of an elastic specular point. The expressions become very complicated however when shear wave effects are included; hence this approach was not pursued here. A direct approach is

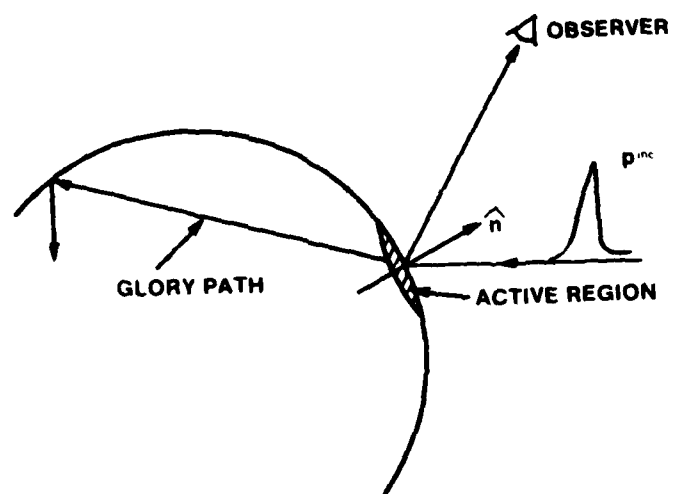
the numerical evaluation of the integrals of the preceding section using a very short smoothed impulse incident pressure. The result is the leading edge of the impulse response and requires the numerical integration over only a small part of the target surrounding the specular point. Furthermore, the technique may be applied to a bistatic configuration and also to refraction. This approach, known as the local influence theory, is based on the observation that at a given time only a few identifiable points are active as scatterers; see Figure 3-3. (The approach has been used successfully for the electromagnetic case [10].) Attempts to implement this technique for elastic targets have been, to date, thwarted by the numerical difficulties further described in Section 4. It is felt that, once these difficulties are removed, these calculations of scattering center responses, combined with the glory-wave model to be described, will yield a fully quantitative but greatly simplified scattering model.

3.3 GLORY-WAVE EFFECTS

The glory phenomenon is the halo surrounding the viewer's own shadow cast by the sun upon a mist (or a cloud, when observed by airplane). It is caused by light entering water droplets and, after multiple internal reflections, being returned to the observer [11][12]. It is a monostatic effect as distinguished from the rainbow effect which, although also involving internal reflections, is bistatic, resulting from local maxima in scattering intensity at certain bistatic angles. The phenomena involve surface (creep) waves as well as Snell's law reflection and refraction.

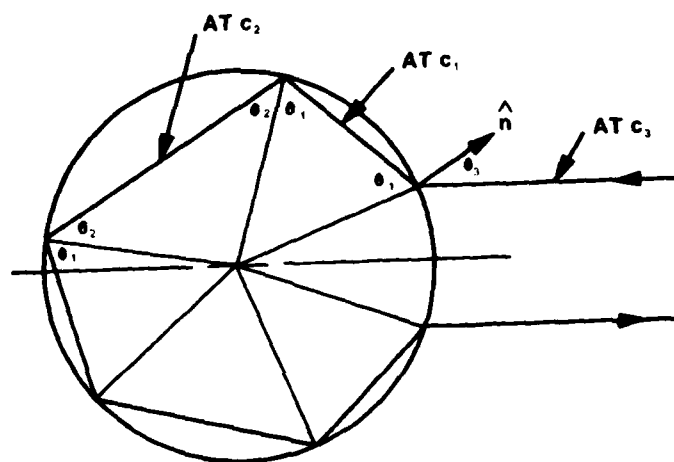
The nomenclature is here applied to the acoustic case. (Since the refractive index for most acoustical situations will be greater than 1 while for the optical case it is generally less than 1, there are some qualitative differences between the two cases.) A semiquantitative understanding of the phenomenon can be obtained using ray-optics theory.

Consider the glory path as illustrated in Figure 3-4 for a



79-871

FIG. 3-3 Local influence theory: reflection and refraction.



ILLUSTRATED FOR $c_1 > c_2 > c_3$; $m_1 = 4, m_2 = 1$

79-872

FIG. 3-4 Glory paths for sphere.

sphere. At each change in direction Snell's law is obeyed

$$\frac{\sin \theta_1}{c_1} = \frac{\sin \theta_2}{c_2} = \frac{\sin \theta_3}{c_3} \quad (3-46)$$

where c_1 , c_2 , c_3 are the compression, shear, and external velocities respectively. Each chord of the path is thus the base of an isosceles triangle. The requirement is that after k traverses around the sphere the rays return to the source. Let m_1 and m_2 be the number of chords at c_1 and c_2 respectively. Then

$$2\theta_3 + m_1(\pi - 2\theta_1) + m_2(\pi - 2\theta_2) = 2\pi k \quad (3-47)$$

With the constraints (3-46), this equation has at most one solution θ_3 for each set (m_1, m_2, k) .

The extra time required to traverse this path compared to direct reflection from the center of the sphere is

$$t_{m_1 m_2 k} = 2a \left(\frac{m_1}{c_1} \cos \theta_1 + \frac{m_2}{c_2} \cos \theta_2 - \cos \theta_3 \right), \quad (3-48)$$

where a is the sphere radius.

The cases m_1 or $m_2 \rightarrow \infty$ are identified as creep waves along the (inner) surface of the sphere, which are launched when θ_3 is at one of the critical angles. By this model, then, the impulse response of an elastic sphere is a sequence of pulses occurring at the times $t_{m_1, m_2, k}$. The magnitudes and shapes of these pulses depend upon the detailed interaction of the local wavefront with the boundary at each of the reflection points.

3.4 GLORY MODEL EVALUATION

Consider first the fluid sphere response (that is, considering only compression waves). Figure 3.5 illustrates two cases, comparing the smoothed impulse response with the impulses predicted by the glory wave model. It is seen that the agreement is virtually perfect. All possible glory paths are observed with decreasing amplitude in proportion to the number of reflections.

In Figures 3.6 and 3.7 the model is compared with the elastic target response. First, note that the pure compression modes as observed for the fluid target are still observed (for the sake of clarity not all of them are indicated), though these effects are overwhelmed by the shear effects. The agreement between the glory modes and the main features of the response is only approximate. It is significant that the change in times of occurrence with changing c_2 and c_1 agree.

It is seen from the figures that the dominant modes are those with $m_2 = 1$, $m_2 = 2$, or $m_2 = \infty$ (creep). There is little time difference between $(m_1, m_2) = (2, 1)$ and $(\infty, 1)$ or between $(1, 2)$ and $(\infty, 2)$, where $m_1 = \infty$ means that the path at speed c_1 is an internal creep path. A more quantitative theory is required to determine the relative contributions from those modes. These principal modes are illustrated in Figure 3-8.

3.5 SIMPLE MODEL

It is apparent that pure compressional modes can be neglected in a simple scattering model for elastic solids. We will base our model on the paths a, b, c, d of Figure 3-8. For path (a), the specular response, the return occurs at time

$$t_a = - \frac{2a}{c_3} \quad (3-49)$$

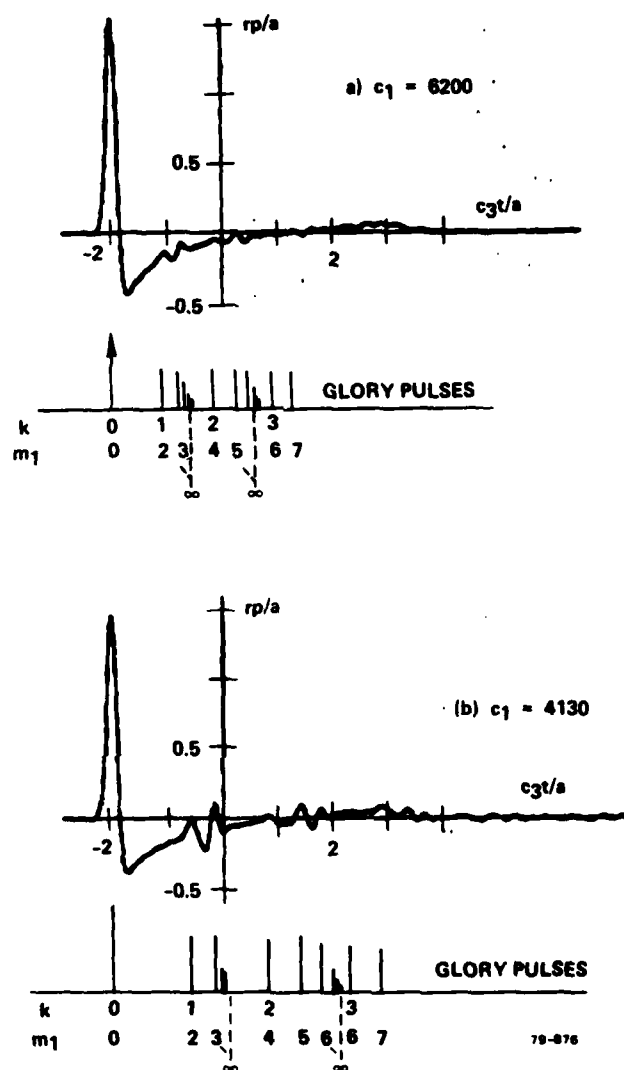


FIG. 3-5 Glory wave model — fluid sphere response.

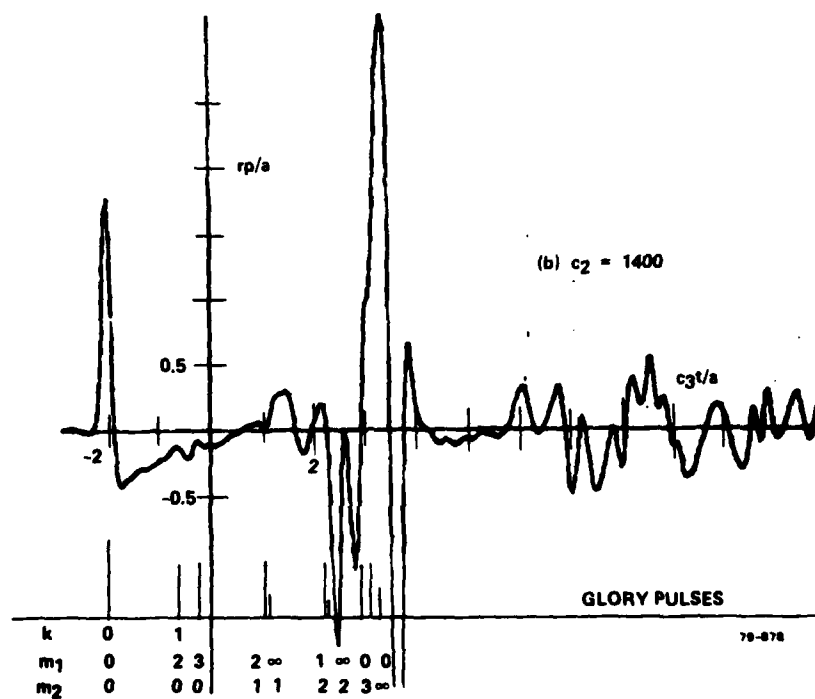
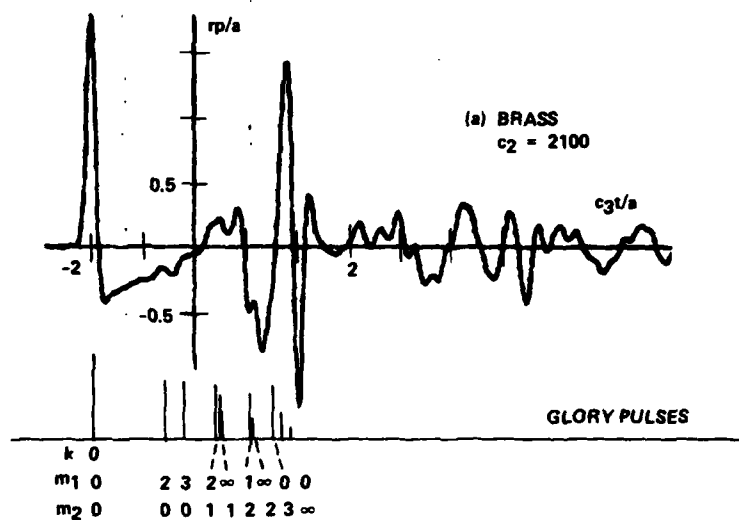
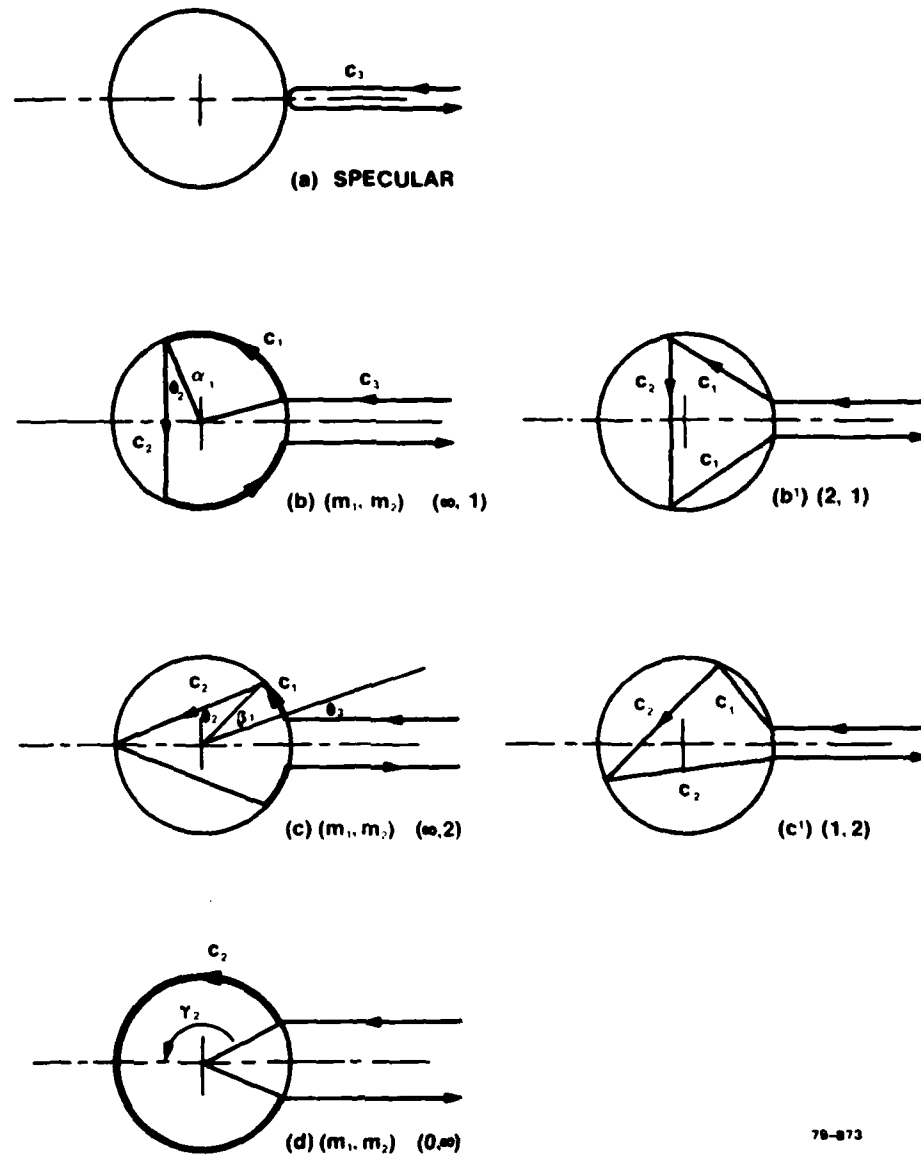


FIG. 3-7 Glory wave model – brass and variations.



79-873

FIG. 3-8 Principal scattering modes involving shear waves.

For paths (b) and (c) we are at the critical angle for c_1 . That is $\theta_1 = 90^\circ$ and $\theta_{3c1} = \sin^{-1}(c_3/c_1)$ and $\theta_2 = \sin^{-1}(c_2/c_1)$. The creep path length travelled at c_1 is just sufficient to satisfy the requirement that the ray return to the source. (Actually, the creep wave at c_1 is continually radiating so that all orientations of the path at c_2 occur. Also, at other observation angles, the same model can be expected to apply with a different arc length at c_1 .) The arc at c_1 spans in case (b): $\alpha_1 = \theta_2 + (\pi/2 - \theta_{3c1})$ and in case (c): $\beta_1 = 2\theta_2 - \theta_{3c1}$.

The return times are thus

$$t_b = 2a \left[\frac{\alpha_1}{c_1} + \frac{\cos \theta_2}{c_2} - \frac{\cos \theta_{3c1}}{c_3} \right], \quad (3-50)$$

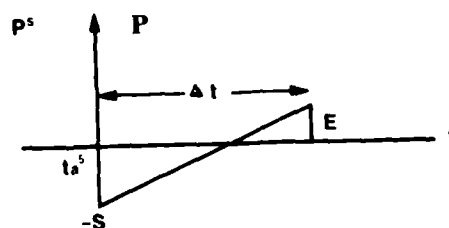
$$t_c = 2a \left[\frac{\beta_1}{c_1} + \frac{2 \cos \theta_2}{c_2} - \frac{\cos \theta_{3c1}}{c_3} \right]. \quad (3-51)$$

Path (d) has the critical angle associated with c_2 , $\theta_{3c2} = \sin^{-1}(c_3/c_2)$, and half arc length $\gamma_2 = (\pi - \theta_{3c2})$. Hence the return time is

$$t_d = 2a \left[\frac{\gamma_2}{c_2} - \frac{\cos \theta_{3c2}}{c_3} \right]. \quad (3-52)$$

A computer program was written to implement this model. The response for each mode is assumed to be of the form illustrated in Figure 3-9, namely impulse, step, ramp, and backswing (P, S, R, and E) such that the total area (DC response) is zero.

$$r(t) = \sum_k p_k \delta(t - t_k) + S_k u(t - t_k) + R_k(t - t_k) [u(t - t_k) - u(t - t_k + \Delta t)] + E_k u(t - t_k + \Delta t) \quad (3-53)$$



79-874

FIG. 3-9 Simplified impulse response.

At this stage P , S , and E are inputs to the program; with $\Delta t = -2P/(E + S)$, $R = (E - S)/\Delta t$. It is expected that development of the methods in Sections 3-1 and 3-2 will yield theoretical values. The times of occurrence of these pulses are computed from the relations (3-49) to (3-52). It is seen in Figure 3-10 for aluminum that a simple representation for the impulse response can be found in this way. In the frequency domain (Figure 3-11), the model and actual response (as computed by Section 2 methods) agree in the main features. Brass is illustrated in Figures 3-12 and 3-13.

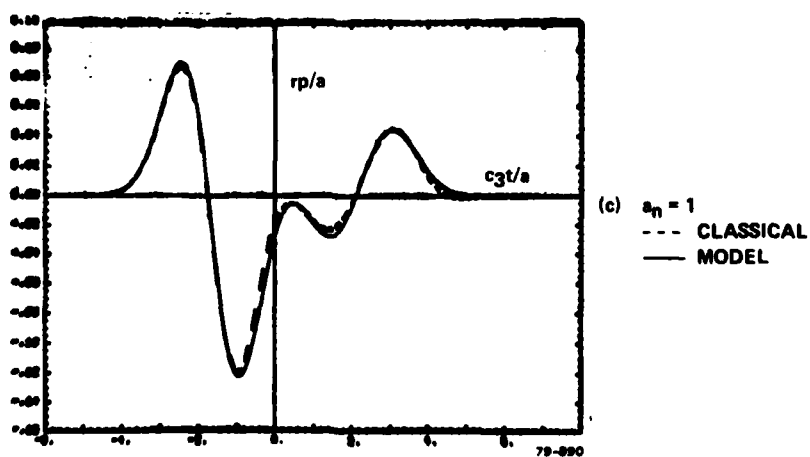
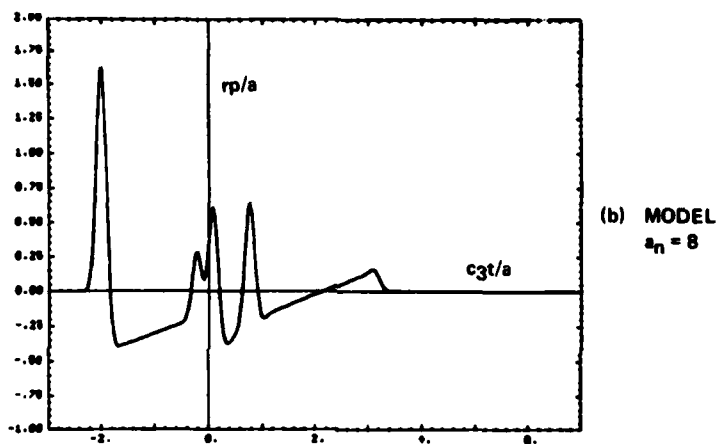
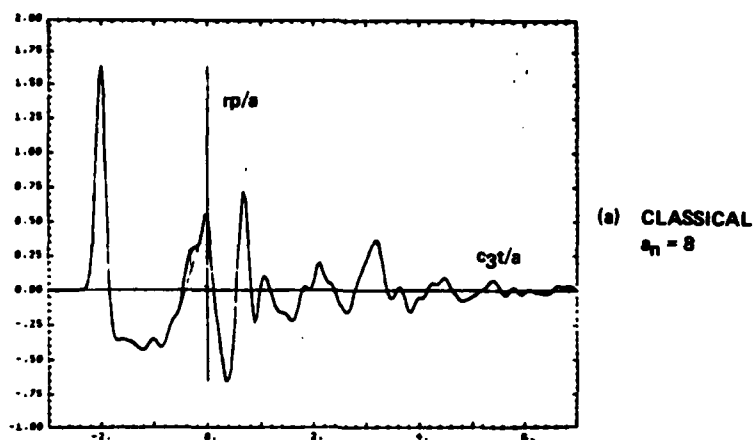


FIG. 3-10 Aluminum response model – time domain.

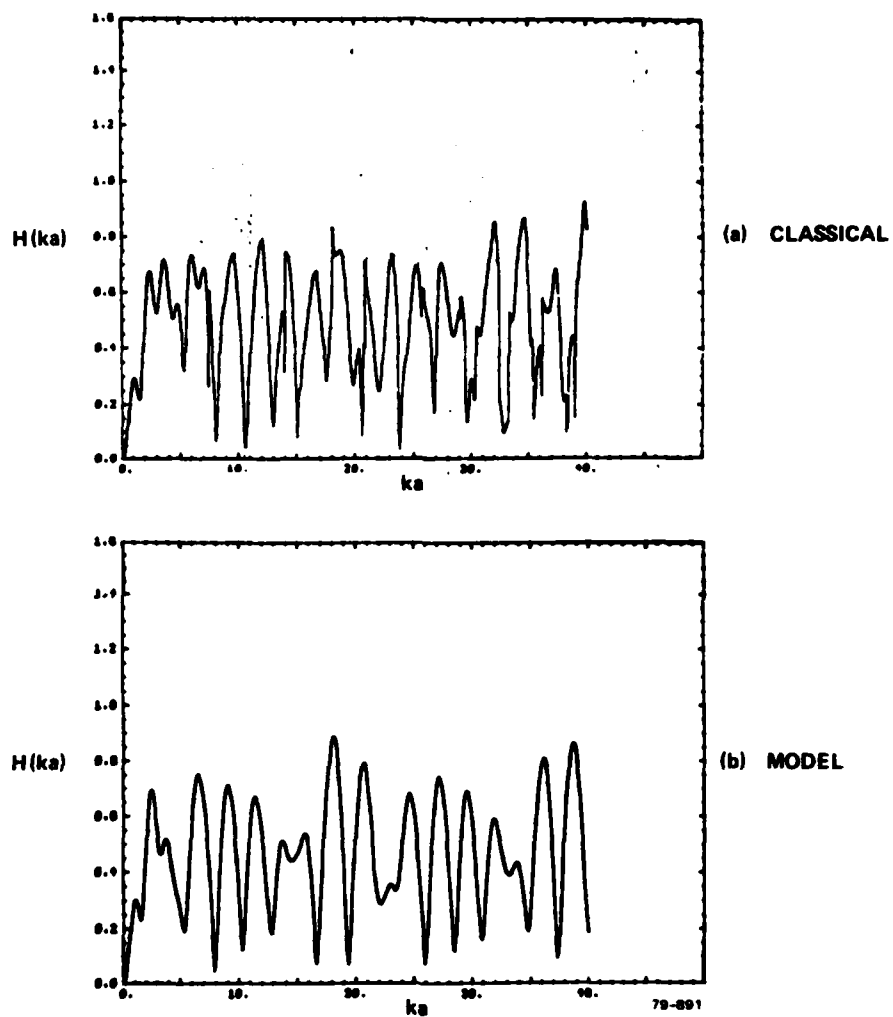


FIG. 3-11 Aluminum response model – frequency domain.

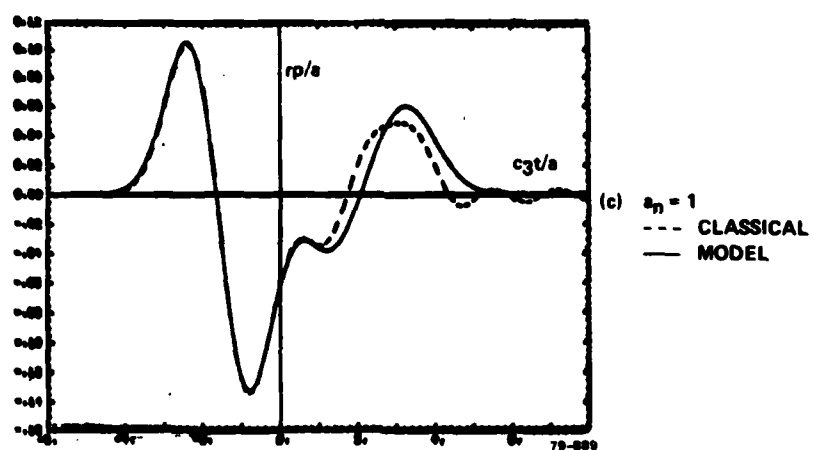
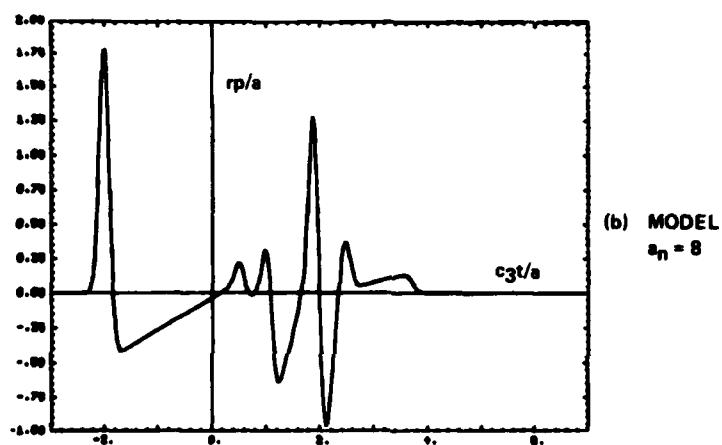
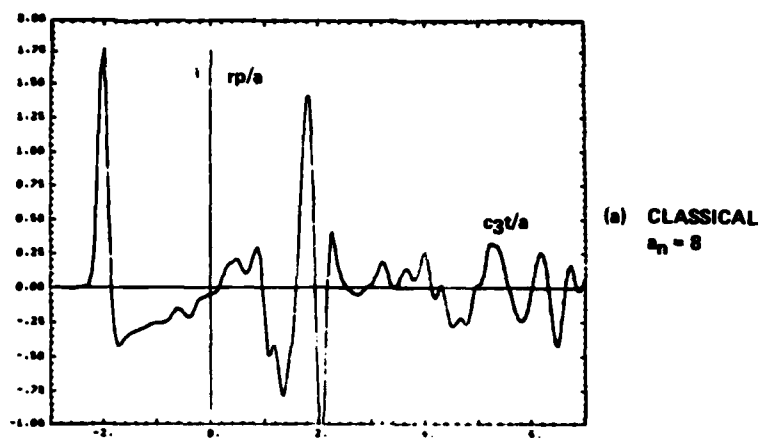


FIG. 3-12 Brass response model – time domain.

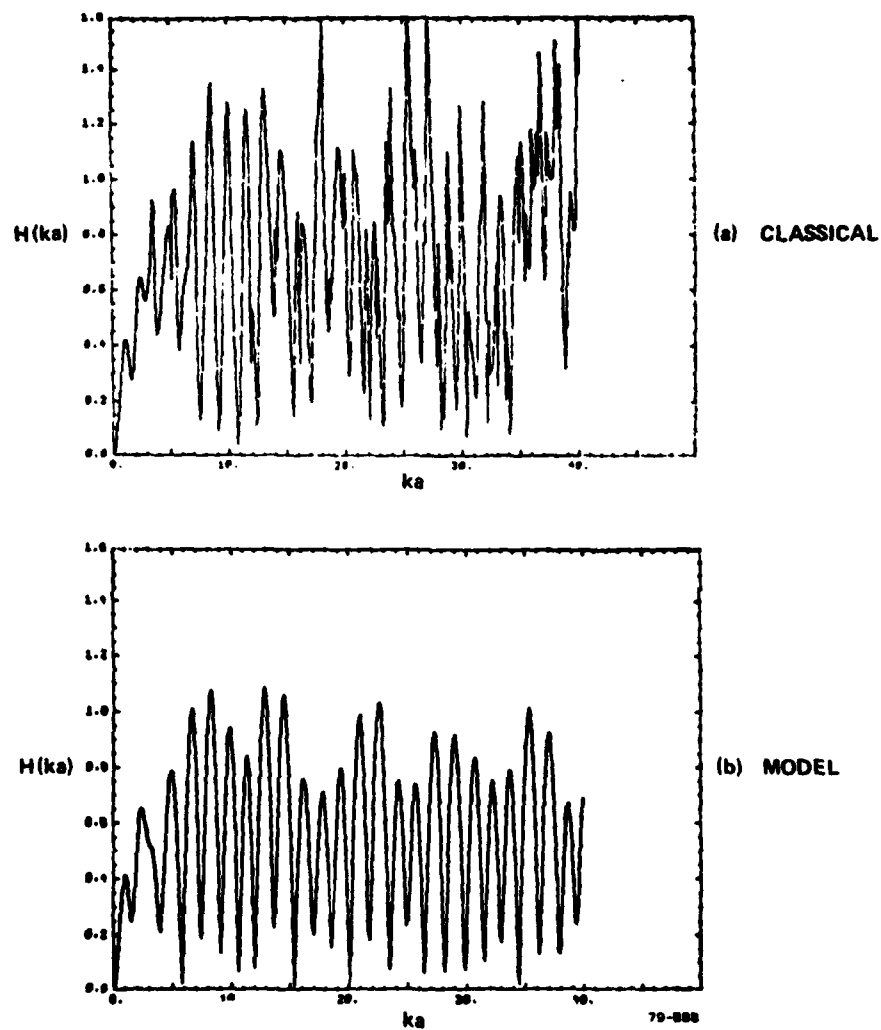


FIG. 3-13 Brass response model — frequency domain.

SECTION 4

SPACE-TIME INTEGRAL EQUATION APPROACH (SOLID TARGETS)

A major advantage of an integral equation formulation of the scattering problem is that it yields exact responses for targets of arbitrary three dimensional shape. The integral equation technique (STIE) used at the Sperry Research Center operates in the time domain, solving the problem by stepping in time rather than by matrix inversion. Using the excitation described in Section 2.2, the result is a smoothed impulse response. Such a time domain response is highly suggestive of target shape. If desired, the response can be deconvolved with the incident pulse and transformed to the frequency domain to obtain a frequency response. The latter is valid for values of ka from zero to an upper limit determined by the frequency content of the excitation pulse. The latter is limited primarily by computation time. To date most experience with this type of solution has been with electromagnetic scattering and with acoustic scattering from sound hard and sound soft targets [6, 13, 14]. It has been found that practical values on the upper frequency limit are $ka = 6$ to 12.

To date the STIE approach has been applied with complete success to impenetrable targets such as conducting solids and thin surfaces in the electromagnetic case and to sound hard and sound soft targets in the acoustic case. Results have been published [6, 13, 14] for three dimensional targets of varying complexity.

In the present effort, this technique is extended to penetrable targets. The approach is reported in detail in reference 1, and will here be outlined in a somewhat more convenient form. At time of writing, targets penetrated only by compression waves are treated successfully, whereas numerical difficulties plague the solution when shear waves are added. We will first concentrate on the fluid target solution and present

computational results.

4.1 FLUID TARGET FORMULATION

In an ideal fluid the excess pressure satisfies the wave equation

$$\ddot{p} = c_3^2 \nabla^2 p, \quad (4-1)$$

where c_3 is the speed of sound. The pressure is related to particle displacement \vec{u} by

$$\nabla p = -\rho_3 \ddot{\vec{u}} \quad (4-2)$$

where ρ_3 is the density (see [1], Section 2.1).

4.1.1 Derivation of Integral Equation

Consider a closed surface S in the medium with pressure sources, p^i , originating outside of S . Using the Green's function

$$G(\vec{r}|\vec{r}', t|\tau) = \frac{1}{R} \delta\left(\tau - R/c_3 - t\right)$$

where $\vec{R} = \vec{r} - \vec{r}'$, a solution to the wave equation can be developed, known as the Kirchhoff integral representation:

$$p(\vec{r}, t) = p^i(\vec{r}, t) - \frac{1}{4\pi} \int_S \left\{ \frac{1}{R} \frac{\partial p(\vec{r}', \tau)}{\partial n'} - (\hat{n}' \cdot \hat{R}) \nabla p(\vec{r}', \tau) \right\} dS' \quad (4-3)$$

where the integral is over the surface

\hat{n}' is the unit normal out of the surface

R is the magnitude of $\vec{R} = \vec{r} - \vec{r}'$

\hat{R} is the unit direction of \vec{R}

$$L = \frac{1}{R^2} + \frac{1}{Rc_3} \frac{\partial}{\partial \tau}$$

$$\tau = t - R/c_3$$

The above is valid for \vec{r} outside of S.

Let the inside of S be source-free and filled with a fluid with properties c_1, ρ_1 ; then (maintaining the same direction for \hat{n})

$$p_1(\vec{r}, t) = \frac{1}{4\pi} \oint_S \left\{ \frac{1}{R} \frac{\partial p_1}{\partial n'}(\vec{r}', \tau_1) - (\hat{n}' \cdot \hat{R}) L_1 p_1(\vec{r}', \tau_1) \right\} ds' \quad (4-4)$$

for \vec{r} inside S, where

$$L_1 = \frac{1}{R^2} + \frac{1}{Rc_1} \frac{\partial}{\partial \tau_1}$$

$$\tau_1 = t - R/c_1$$

and $p_1, \partial p_1 / \partial n$ are the values just on the inside of the surface.

That is, the pressure can be calculated everywhere if the values of p and $\partial p / \partial n$ are known on S. In particular, in the far field as $R \rightarrow r \rightarrow \infty$, the scattered part of the field is given by

$$r p^s(\vec{r}, t) = \frac{1}{4\pi} \oint \left\{ - \frac{\partial p}{\partial n}(\vec{r}', \tau) + (\hat{n}' \cdot \hat{r}) \frac{\partial p}{c_3 \partial \tau}(\vec{r}', \tau) \right\} ds' \quad (4-5)$$

To evaluate this expression, it is first required to solve (4-3) and (4-4) on S. A limiting procedure must be applied to make these valid on the surface since the term $(\hat{n} \cdot \hat{R}) L p$ in the integral becomes singular as $r' \rightarrow r$. This singularity is removed in the following way: consider the singular term separately and define the integral written as $\oint ds'$ to have its

singular term removed. (Usually this is written as $\oint dS'$.) Now require that (4-3), the "outside equation" results in $p(\vec{r}) \equiv 0$ for \vec{r} inside S . This requirement remains to be justified. Comparing the results of evaluating (4-3) for \vec{r} just inside and just outside of S , we see that the non-singular parts of the equation I_{NS} give the same value at these two points, but that the singular portion changes sign (due to $\hat{r} \cdot \hat{n}$). That is, we have

$$\begin{aligned} \vec{r} \text{ outside: } p &= p^i + I_{NS} - I_S \\ \vec{r} \text{ inside: } 0 &= p = p^i + I_{NS} + I_S \end{aligned} \quad (4-6)$$

Combining these, we obtain $p = 2p^i + 2I_{NS}$. The singular point has been removed and we have introduced a factor of 2. We thus obtain for \vec{r} on the (outside layer of the) surface S :

$$p(\vec{r}, t) = 2p^i(\vec{r}, t) - \frac{1}{2\pi} \int_S \left\{ \frac{1}{R} \frac{\partial p}{\partial n'}(\vec{r}', \tau) - (\hat{n}' \cdot \hat{R}) L p(\vec{r}', \tau) \right\} dS' \quad (4-7)$$

This equation contains two unknowns p and $\partial p / \partial n$ so that another relation is needed to solve. In the case of an impenetrable target the requirement $p = 0$ inside is exactly physically true so that p and $\partial p / \partial n$ in (4-7) represent actual physical quantities. The additional boundary condition $\partial p / \partial n = 0$ for sound-hard or $p = 0$ for sound-soft then permits solution of (4-7).

In the case of the fluid target we apply an analogous argument, requiring inside equation (4-5) to yield $p(\vec{r}) = 0$ for \vec{r} outside, resulting in

$$p_1(\vec{r}, t) = \frac{1}{2\pi} \int_S \left\{ \frac{1}{R} \frac{\partial p_1}{\partial n'}(\vec{r}', \tau_1) - (\hat{n}' \cdot \hat{R}) L_1 p_1(\vec{r}', \tau_1) \right\} dS' \quad (4-8)$$

We now have two integral equations in 4 unknowns. S is a surface of discontinuity with two sides. The two sides of S are related by the boundary conditions. Imposition of the boundary conditions justifies the above $p = 0$ requirement and also permits the system (4-7), (4-8) to be solved. These conditions are

$$\left. \begin{aligned} p_1(\vec{r}, t) &= p(\vec{r}, t) \\ \frac{\partial p_1}{\rho_1 \partial n}(\vec{r}, t) &= \frac{\partial p}{\rho_3 \partial n}(\vec{r}, t) \end{aligned} \right\} \vec{r} \text{ on } S \quad (4-9)$$

corresponding to continuity of pressure and normal displacement.

4.1.2 Numerical Implementation

To solve these equations numerically, the surface is divided into patches ΔS_k and p , $\partial p / \partial t$, $\partial p / \partial n$ are assumed to be constant in value over a patch. Time is also quantized. That is, for (4-7) at \vec{r}_i :

$$\begin{aligned} p(\vec{r}_i, t_j) &= 2p^i(\vec{r}_i, t_j) - \frac{1}{2\pi} \sum_{k \neq i} \left\{ \frac{1}{R_{ik}} \frac{\partial p}{\partial n}(\vec{r}_k, \tau_{ijk}) - (\hat{n}_k \cdot \hat{R}_{ik}) L_{ik} p(\vec{r}_k, \tau_{ijk}) \right\} \Delta S_k \\ &\quad - \gamma_i \frac{\partial p}{\partial n}(\vec{r}_i, t_j) + \epsilon_i p(\vec{r}_i, t_j) \end{aligned} \quad (4-10)$$

where $\tau_{ijk} = t_j - R_{ik}/c_3$. In the above, the integral over the "self-patch" which contains \vec{r}_i (i.e., for $k = i$), has been performed analytically.

$$\frac{1}{2\pi} \int_{\Delta S_i} \frac{dS'}{R} = \sqrt{\frac{\Delta S_i}{\pi}} \equiv \gamma_i \quad (4-11)$$

$$\frac{1}{2\pi} \int_{\Delta S_i} (\hat{n}' \cdot \hat{R}) \left(\frac{1}{R^2} + \frac{1}{Rc} \frac{\partial}{\partial \tau} \right) p(\vec{r}', \tau) dS' = \frac{\gamma_i}{2} K_i p \equiv \epsilon_i p \quad (4-12)$$

where K_i is the average curvature of the patch at \vec{r}_i . The derivation of (4-11) is straightforward, by approximating the patch by a circle with radius γ_i . For (4-12) it is necessary to expand \vec{R} and \hat{n} in curvilinear coordinates (see Appendix in reference 13). A similar numerical expression is written for (4-8). Writing I and I_1 for these sums (the "non-self integrals") and applying the boundary conditions, we obtain the system

$$\begin{aligned} (1 - \epsilon_i) p(\vec{r}_i, t_j) + \gamma_i \frac{\partial p}{\partial n}(\vec{r}_i, t_j) &= 2p^i(\vec{r}_i, t_j) - I(\vec{r}_i, t_j) \\ (1 + \epsilon_i) p(\vec{r}_i, t_j) - \gamma_i \frac{\rho_1}{\rho_3} \frac{\partial p}{\partial n}(\vec{r}_i, t_j) &= I_1(\vec{r}_i, t_j) \end{aligned} \quad (4-13)$$

This can be solved simultaneously for p , $\partial p / \partial n$ for time t_j at each \vec{r}_i on S . Note that the non-self integrals can be evaluated at time t_j since the arguments τ are earlier than t_j . Hence (4-13) can be solved for all time by stepping in time.

The stepping in time procedure is valid so long as the distance ΔR to the nearest patch is greater than $c_1 \Delta t$ (or $c_3 \Delta t$, whichever is greater) for Δt = time step. It may be desirable to use smaller patches in regions of rapid change, for which ΔR is smaller than the above limit. For these cases a local iterative procedure is used involving only these nearby patches: first the contributions from all the non-near (properly retarded) patches are calculated to each patch. These values are then used to determine the near-patch contributions by simple linear interpolation between the new values and those at the previous time point. Then, one more iteration of this process is sufficient to assure convergence. This procedure, involving only the nearby patches is quick and does not add much time to the overall solution.

Typical values for a target dimension is $a = 1$ (representing, for instance, cylinder radius) and for the pulse length parameter $a_n = 1$ (see equation 2-15). Then, for time expressed in sound-meters ($c_3 = 1$),

a time step of $\Delta t = .2$ (or even $.3$) is adequate to obtain good results in the case of sound-hard or soft targets. Since the pulsewidth measured between 2% points is about $W = 4/a_n = 4$, this represents about 20 time steps per pulsewidth. The typical patch separation then is somewhat larger than 0.2 . For the fluid case, the time step must be reduced by about the ratio c_3/c_1 . It was found that $\Delta t = .075$ was sufficiently fine.

In the integral (4-10) it is necessary to interpolate in the table of previously computed values of p to obtain p and $\partial p/\partial t$ at time τ . One way to do this is by fitting a fourth-order polynomial to the five values surrounding τ . This worked very successfully and accurately for the sound-hard case. However, numerical inaccuracies tend to develop toward the end of the response in time which may be amplified by high order polynomial fitting, resulting in a rapidly growing instability. This effect was particularly noticeable for the sound-soft case. This problem can be eliminated by linearly smoothing the five points and then fitting a simple quadratic to the inner three points. This method causes a small loss in accuracy and hence requires the use of a somewhat smaller Δt (say $.1$ for sound soft, or $.05$ for fluid with $c_1/c_3 = 4$).

4.1.3 Responses of Right Circular Cylinders

Responses were computed by these methods for a fluid right circular cylinder with the properties of aluminum and brass but neglecting the shear velocity:

	ρ_1	c_1
"Fluid Al"	2.70 g/cm^3	6200 m/s
"Fluid Brass"	8.39	4400
Medium (Water)	1.00	1480

the incident pulse was $a_n = 1$. Results are plotted in Figures 4-1 through 4-3. The cylinder has length/radius ratio $L/a = 6/1$. Time is in units of

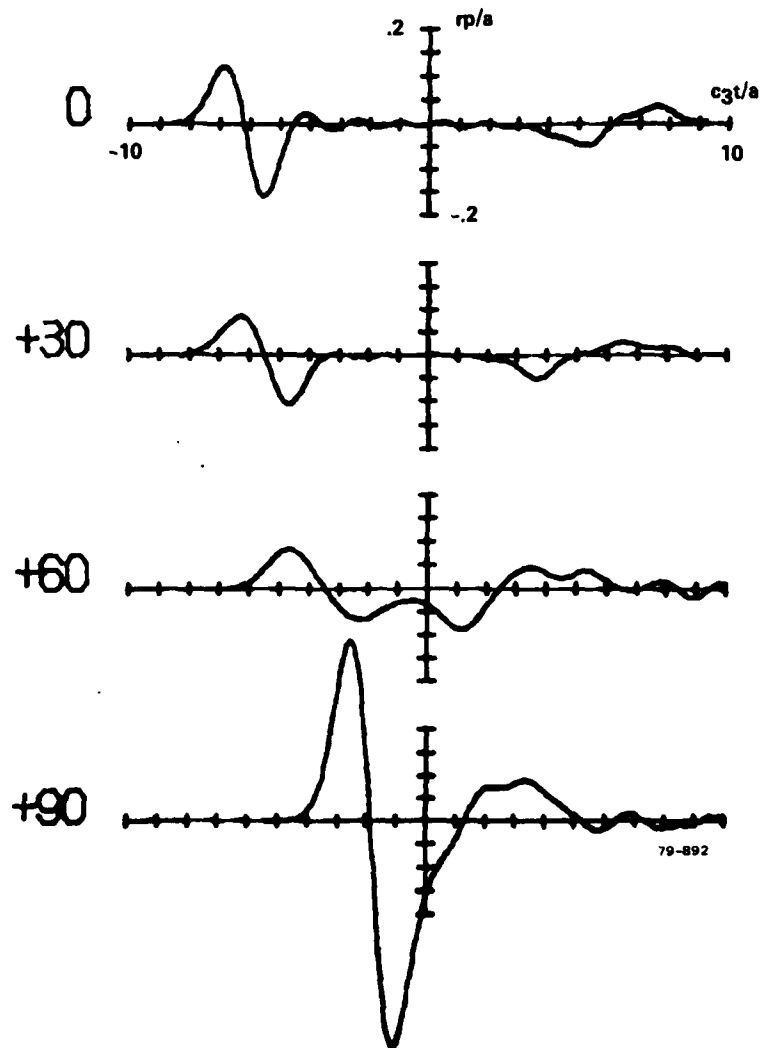


FIG. 4-1 STIE response for fluid aluminum right circular cylinder.

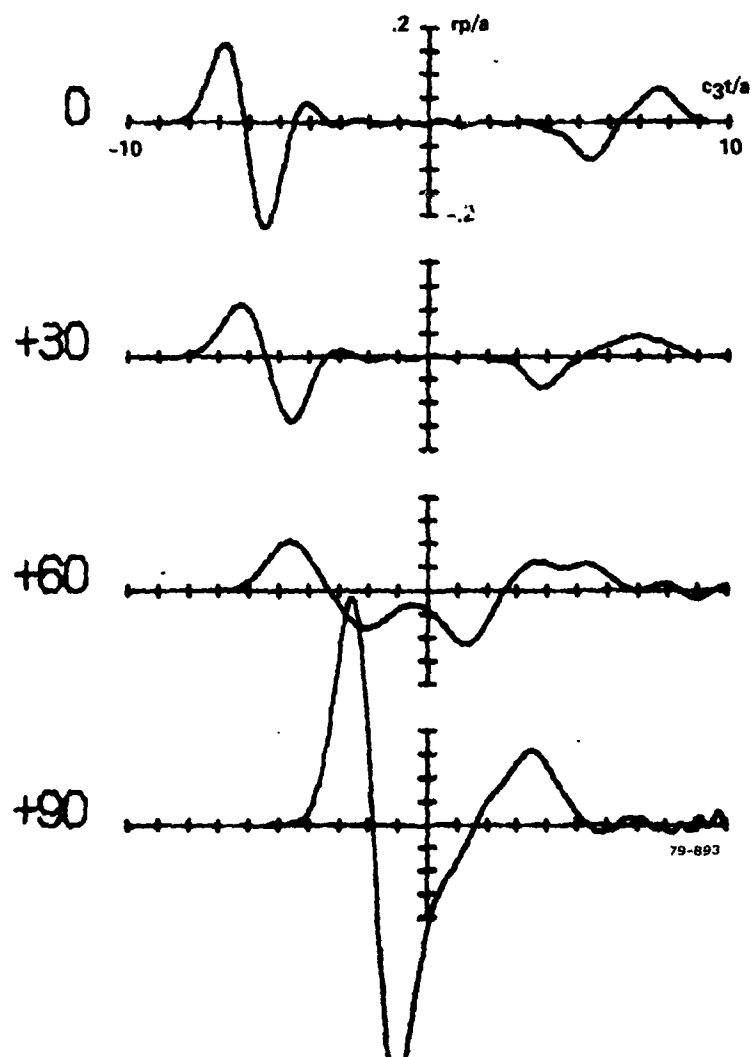


FIG. 4-2 STIE response for fluid brass right circular cylinder.

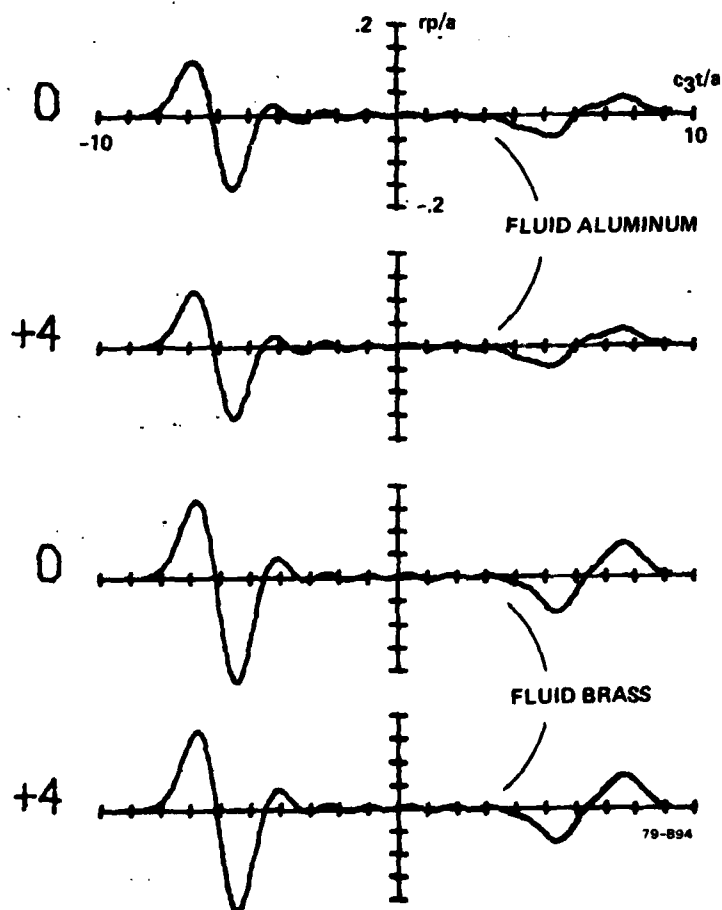


FIG. 4-3 STIE response — small angle deviation.

$c_3 t/a$. Consider the 0° aspect; the initial part of the response is from the flat end of the cylinder and looks somewhat like the derivative of the incident pulse, centered on $t = -6$. The small peak at about $t = -4$ can be interpreted as interaction with the edge. This part of the response is similar in shape to the response of a hard cylinder (see [13] or [1]) except for a reduction in amplitude. The small peak at $t = -4$ is also somewhat earlier, indicating that edge effects occur at both c_1 and c_3 . The next major part of the return is the creep return at $t = 6$ to 8 . This has been changed in shape and moved slightly earlier in comparison with the hard cylinder response. In between these two extreme times, the hard cylinder has a near-zero response, whereas the fluid target exhibits ringing. The latter must be interpreted as the result of internal reflections (end to end) of compression waves at c_1 . As the aspect angle changes the two parts of the response move closer together.

A similar set of responses is given for brass in Figure 4-2. Also given, in Figure 4-3, is a comparison for each of these targets at the 0° and 4° aspects. The difference is extremely small.

4.2 ELASTIC TARGET FORMULATION

A complete elastic target formulation must also include the effect of internal shear waves. As seen in Section 2, these can be the dominant effects. This formulation is treated in detail in [1] and will only be cursorily treated here. Instead of pressure it is easier to deal with the divergence of displacement. The two quantities are proportional:

$$p_1 = -c_1^2 \rho_1 (\nabla \cdot \vec{u}) \quad (4-14)$$

The equation of motion inside the solid is

$$\ddot{\vec{u}} = c_1^2 \nabla (\nabla \cdot \vec{u}) - c_2^2 \nabla \times \nabla \times \vec{u}, \quad (4-15)$$

from which it may be found (by taking the $\nabla \times$ and $\nabla \cdot$ of the above) that both $(\nabla \cdot \vec{u})$ and $(\nabla \times \vec{u})$ separately satisfy wave equations:

$$(\nabla \times \ddot{\vec{u}}) = c_2^2 \nabla^2 (\nabla \times \vec{u}) \quad (4-16)$$

In addition to equations (4-7) and (4-8), with p_1 replaced by $(\nabla \cdot \vec{u})$, we have a vector Kirchhoff integral:

$$\nabla \times \vec{u}(\vec{r}, t) = \frac{1}{2\pi} \int_S \left\{ \frac{1}{R} \frac{\partial}{\partial n'} (\nabla \times \vec{u}') - (\hat{n}' \cdot \hat{R}) L_2 (\nabla \times \vec{u}') \right\} dS' \quad (4-17)$$

for \vec{r} on S . Here, the equation has already been specialized to the boundary S .

$$\nabla \times \vec{u}' \text{ means } \nabla \times \vec{u}(\vec{r}', \tau_2)$$

$$\tau_2 = t - R/c_2.$$

Another form for this equation, which may be useful in practice is

$$\nabla \times \vec{u} = - \frac{1}{2\pi} \int_S \left\{ \frac{1}{R} (\hat{n}' \times \nabla \times \nabla \times \vec{u}') + L_2 \left((\hat{n}' \cdot \nabla \times \vec{u}') \hat{R} + (\hat{n}' \times \nabla \times \vec{u}') \times \hat{R} \right) \right\} dS' \quad (4-18)$$

This form is obtained from (4-17) by vector manipulations and the use of the divergence theorem. (See Jackson [8], pp. 283.) It may be useful to observe that another equation can be written, namely for the $(\nabla \times \nabla \times \vec{u})$. The quantities $(\nabla \times \vec{u})$, and $(\nabla \times \nabla \times \vec{u})$ now play somewhat similar roles to \vec{E} and \vec{H} of electromagnetics, so that techniques found useful there are possibly applicable here.

The boundary conditions are the two stated in Section 4.1, continuity of normal stress and normal displacement, although the first looks

somewhat more complicated for elastic solids (see [1]). An additional boundary condition on the shear states that the tangential shear stress is continuous across S. Since this quantity is zero in the fluid, it is zero at the solid side of S. The boundary conditions may be written (see [1] for derivation; here the form in which these relations are written is more precise):

$$-p = \rho_1 \left(c_1^2 - 2c_2^2 \right) (\nabla \cdot \vec{u}) + 2 \rho_1 c_2^2 \frac{\partial u_n}{\partial n} \quad (4-19)$$

$$-\frac{\partial p}{\rho_3 \partial n} = c_1^2 \frac{\partial}{\partial n} (\nabla \cdot \vec{u}) - c_2^2 (\nabla \times \nabla \times \vec{u})_n = \ddot{u}_n \quad (4-20)$$

$$0 = (\nabla \times \vec{u})_{\text{tan}} - 2 \frac{\partial}{\partial n} (\hat{n} \times \vec{u}) \quad (4-21)$$

where \hat{n} is the outward normal direction. The set of 2 scalar and one vector STIE's plus the two scalar and one vector boundary equations can be solved for the unknowns p , $\nabla \cdot \vec{u}$, $\nabla \times \vec{u}$ and their normal derivatives. However it requires the formation, numerically, of certain space-derivatives on the surface of S, and the numerical solution of the equation of motion (4-15) [1]. The need for differentiation on a curved surface results in numerical instabilities in the solution, which have to date not been solved. Only the initial portion of the response from the region around the specular point can be computed successfully.

Figure 4-4 illustrates the status of the space-time integral equation calculation. Plotted is the surface pressure as a function of time $p(c_3 t/a)$ for the smooth impulse incidence at several points on the surface. The pressure as predicted by the classical solution of Section 2 is plotted in part (a); the current status of the integral equation solution in part (b). The shape of p more or less follows that of the incident pulse with significant deviations. In particular, at the backside ($\theta = 180^\circ$) there is a bump a little before $t = 0$ which represents

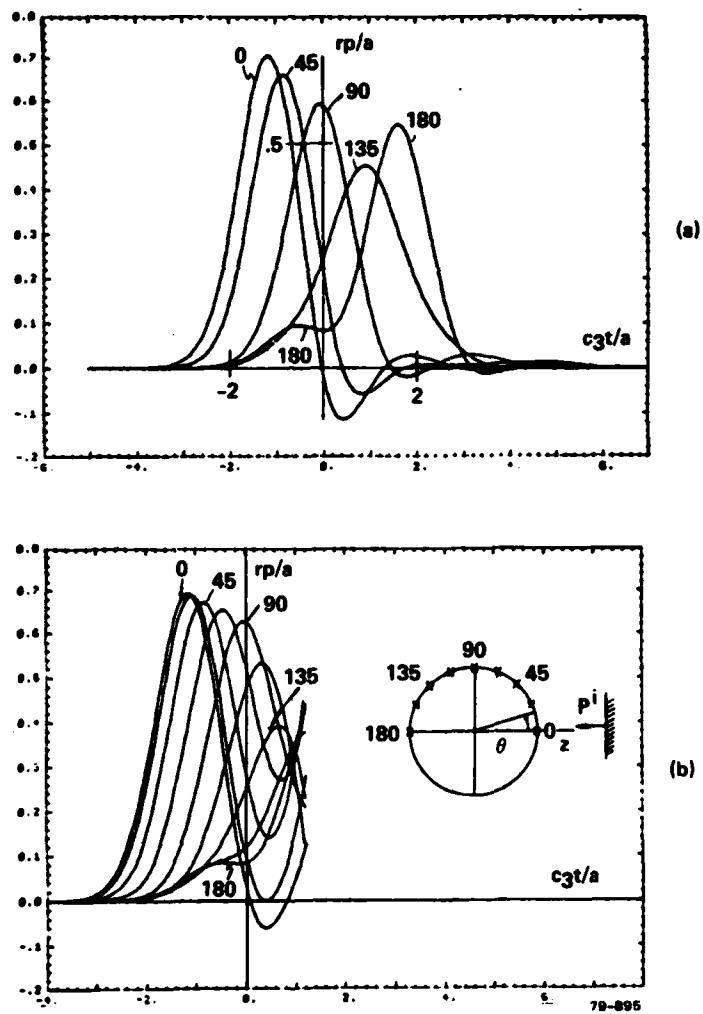


FIG. 4-4 Surface pressure for elastic sphere — classical and STIE.

transmission through the target at the shear velocity, c_2 . It is seen that the initial part of the STIE calculation is correct; in particular the bump at $\theta = 180^\circ$ is computed correctly. The latter is the respect in which elastic targets are distinguished from hard or fluid targets. Unfortunately, inaccuracies which rapidly develop into an instability start near $\theta = 45^\circ$. These inaccuracies have been identified as numerical differentiation problems; particularly since the quantity differentiated, \vec{u} , becomes large as time goes on, although the derivatives to be found remain relatively small. This problem has not yet been circumvented. The solution must lie in a formulation which avoids space-differentiation of the displacement \vec{u} . The far field computed from these surface values is shown in Figure 4-5, with the classical result shown dashed.

4.3 THIN SHELL SPACE-TIME INTEGRAL EQUATION FORMULATION

A direct approach to solving the problem of scattering from an elastic shell with fluid interior and exterior is to formulate integral equations over both boundaries and applying boundary conditions on each. This two-boundary approach is taken in the classical solution of the next section. A computationally simpler approach is to attempt to find the limiting boundary condition between inside and outside media, and avoiding the need for solving any equations in the shell itself.

Consider the sphere of Figure 4-6 with outer and inner radii a and b . The boundary conditions can be written as

$$\begin{aligned} -p &= \rho_1 \left(c_1^2 - 2c_2^2 \right) (\nabla \cdot \vec{u})^a + 2 \rho_1 c_2^2 \left(\frac{\partial u_r}{\partial r} \right)^a \\ -p_4 &= \rho_1 \left(c_1^2 - 2c_2^2 \right) (\nabla \cdot \vec{u})^b + 2 \rho_1 c_2^2 \left(\frac{\partial u_r}{\partial r} \right)^b \end{aligned} \quad (4-22)$$

and

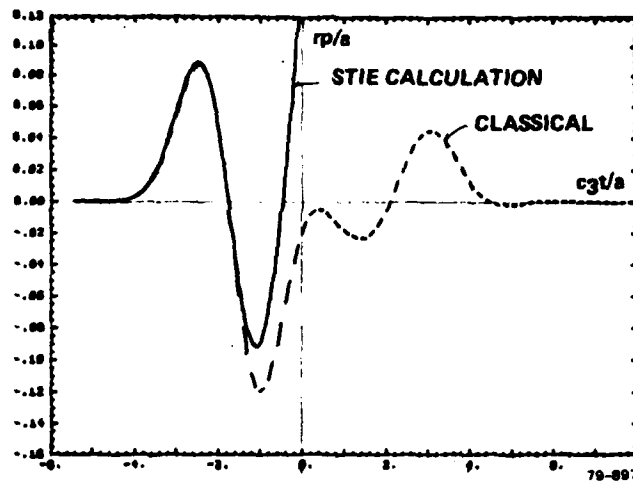


FIG. 4-5 Status of elastic STIE calculation – far field response.

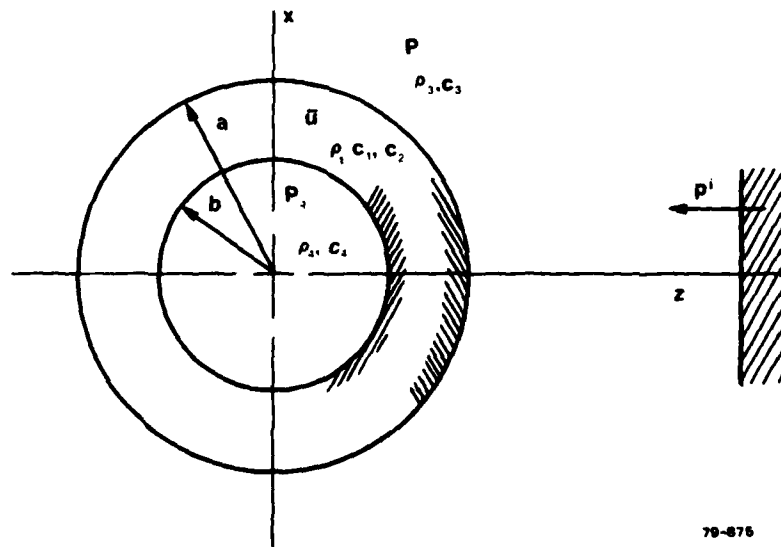


FIG. 4-6 Shell scattering problem.

$$\ddot{u}_r^a = -\frac{\partial p}{\rho_3 \partial r} = c_1^2 \frac{\partial}{\partial r} (\nabla \cdot \vec{u})^a - c_2^2 (\nabla \times \nabla \times \vec{u})_r^a, \quad (4-23)$$

$$\ddot{u}_r^b = -\frac{\partial p_4}{\rho_4 \partial r} = c_1^2 \frac{\partial}{\partial r} (\nabla \cdot \vec{u})^b - c_2^2 (\nabla \times \nabla \times \vec{u})_r^b;$$

where the superscripts a and b refer to the outer and inner surfaces. If we write $(\nabla \times \nabla \times \vec{u})_r$ and the boundary condition (4-21) in spherical coordinates, we obtain

$$(\nabla \times \nabla \times \vec{u})_r^a = 2 \frac{\partial}{\partial r} (\nabla \cdot \vec{u})^a - 2 \frac{\partial}{\partial r} \left[\frac{1}{r^2} \frac{\partial}{\partial r} (r^2 u_r) \right]^a \quad (4-24)$$

We use this to rewrite (4-23):

$$\ddot{u}_r^a = -\frac{\partial p}{\rho_3 \partial r} = \left(c_1^2 - 2c_2^2 \right) \frac{\partial}{\partial r} (\nabla \cdot \vec{u})^a + 2 c_2^2 \frac{\partial}{\partial r} \left[\frac{1}{r^2} \frac{\partial}{\partial r} (r^2 u_r) \right]^a$$

$$\ddot{u}_r^b = -\frac{\partial p_4}{\rho_4 \partial r} = \left(c_1^2 - 2c_2^2 \right) \frac{\partial}{\partial r} (\nabla \cdot \vec{u})^b + 2 c_2^2 \frac{\partial}{\partial r} \left[\frac{1}{r^2} \frac{\partial}{\partial r} (r^2 u_r) \right]^b. \quad (4-25)$$

The aim is to find relations between p , $\frac{\partial p}{\partial r}$, p_4 , $\frac{\partial p_4}{\partial r}$ by applying a limiting process so that the problem reduces to essentially the fluid-in-fluid problem of Section 4.1, but with different boundary conditions.

First, suppose the shell thickness, h , sufficiently thin so that we can use a first order Taylor expansion; for example

$$(\nabla \cdot \vec{u})^a = (\nabla \cdot \vec{u})^b + h \frac{\partial}{\partial r} (\nabla \cdot \vec{u})^b. \quad (4-26)$$

We will then rewrite the boundary conditions

$$p_4 - p = \rho_1 h (c_1^2 - 2c_2^2) \frac{\partial}{\partial r} (\nabla \cdot \vec{u}) + 2 \rho_1 h c_2^2 \frac{\partial^2 u_r}{\partial r^2} \quad (4-27)$$

$$\frac{\partial p_4}{\rho_4 \partial r} - \frac{\partial p}{\rho_3 \partial r} = h (c_1^2 - 2c_2^2) \frac{\partial^2}{\partial r^2} (\nabla \cdot \vec{u}) + 2 h c_2^2 \frac{\partial^2}{\partial r^2} \left[\frac{1}{r^2} \frac{\partial}{\partial r} (r^2 u_r) \right]. \quad (4-28)$$

If both h and ρ are reduced to zero the problem reduces to the fluid-in-fluid problem with no shell. As a next level of approximation, let $h \rightarrow 0$ and let $u_r^b = u_r^a$. Then

$$p_4 - p = \rho_1 h (c_1^2 - 2c_2^2) \frac{\partial}{\partial r} (\nabla \cdot \vec{u}) \quad (4-29)$$

$$\ddot{u}_r = - \frac{\partial p_4}{\rho_4 \partial r} = - \frac{\partial p}{\rho_3 \partial r} = (c_1^2 - 2c_2^2) \frac{\partial}{\partial r} (\nabla \cdot \vec{u}). \quad (4-30)$$

or

$$p_4 - p = \rho_1 h \ddot{u}_r. \quad (4-29')$$

This represents the equation of motion of a membrane with no internal restoring forces. We can add restoring forces due to an ambient pressure difference, $\tilde{\Delta p}$, between inside and outside which results in a tension $T = \tilde{\Delta p} (a/2)$. Then we have

$$p_4 - p = \rho_1 h \ddot{u}_r - T \nabla_s^2 u_r. \quad (4-29'')$$

This is the equation of motion of a membrane under tension and can be solved in conjunction with the fluid-in-fluid integral equations.

We have simplified more than desired, however, since we wish the elastic properties of the shell to be included. Returning to equations (4-23), we note that we can also write by virtue of the boundary conditions [1]

$$(\nabla \times \nabla \times \vec{u})_r = -2 \nabla_s^2 u_r, \quad (4-31)$$

but it must be realized that the meaning of ∇_s^2 is dependent on the coordinate system. In spherical coordinates (with axial symmetry):

$$\nabla_s^2 u_r \equiv \frac{\partial^2 u_r}{r^2 \partial \theta^2} - \frac{\partial u_\theta}{r^2 \partial \theta} + \frac{\cos \theta}{r^2 \sin \theta} \left(\frac{\partial u_r}{\partial \theta} - u_\theta \right) \quad (4-32)$$

the above is actually a definition of ∇_s^2 , obtained from writing out $(\nabla \times \nabla \times \vec{u})$ and applying the boundary condition in spherical coordinates.

We then write (4-23) as

$$\ddot{u}_r = c_1^2 \frac{\partial}{\partial r} (\nabla \cdot \vec{u}) + 2 c_2^2 \nabla_s^2 u_r \quad (4-33)$$

and use this to eliminate $\partial/\partial r (\nabla \cdot \vec{u})$ in equation (4-29). The result is

$$p_4 - p = (\rho_1 h) \left(1 - 2 \frac{c_2^2}{c_1^2} \right) \left\{ \ddot{u}_r - 2 \frac{c_2^2}{c_1^2} \nabla_s^2 u_r \right\} \quad (4-34)$$

$$\ddot{u}_r = - \frac{\partial p}{\rho_3 \partial r} = - \frac{\partial p_4}{\rho_4 \partial r} \quad (4-25')$$

These equations can be used as the boundary conditions with the system of two space-time integral equations as written for the fluid case of Section 4.1. It requires the time-integration of \ddot{u}_r (which is no problem) and the numerical differentiation in the surface of u_r . Unfortunately, as was the case for the elastic target, the numerical differentiation causes instabilities.

In Figure 4.7 is plotted the result of the numerical implementation of the space-time integral equation solution using the membrane

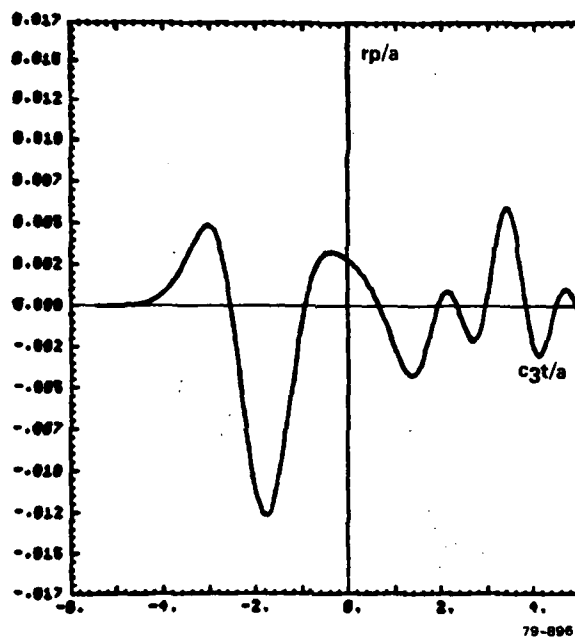


FIG. 4-7 STIE solution — scattering from spherical membrane.

boundary condition between similar fluids. As will be seen in the next section, this result is not a good model for a thin shell. While the general nature of the response is similar, its dominant frequency differs by a factor of 2. It is therefore necessary to solve the problem remaining with implementing boundary condition (4-34).

SECTION 5
SPHERICAL HULLED TARGETS

5.1 CLASSICAL SOLUTION FOR THICK SHELL

The fluid-filled spherical thick shell problem can be solved by expansion in terms of eigenfunctions in a way completely analogous to the elastic solid of Section 2.1 [15]. Let the outer and inner radii be a, b ; and let the core have constants c_4, ρ_4 . In addition to the incident and scattered pressure expansions, we have a compressional wave in the sphere core (ρ_4, c_4). The eigenfunctions must be bounded at the origin and are therefore $j_n(kr) P_n(\cos \theta)$. In the shell, on the other hand, there no longer is the requirement that the eigenfunction be bounded at the origin. Or, alternatively we can say that the shell exhibits both inward and outward traveling waves. The shell solution thus contains both j_n and n_n (or, both $h_n^{(1)}$ and $h_n^{(2)}$, whichever is more convenient).

Suppressing the time dependence $e^{-i\omega t}$, we thus have

$$p^i(\vec{r}) = p_o \sum_{n=0}^{\infty} (2n+1) (-i)^n j_n(kr) P_n(\cos \theta) \quad (5-1)$$

$r \geq a$

$$p^s(\vec{r}) = p_o \sum_{n=0}^{\infty} c_n h_n^{(1)}(kr) P_n(\cos \theta) \quad (5-2)$$

$r \geq a$

$$p^4(\vec{r}) = p_o \sum_{n=0}^{\infty} f_n j_n(k_4 r) P_n(\cos \theta) \quad (5-3)$$

$r \leq b$

$$\psi(\vec{r}) = \sum_{n=0}^{\infty} \left(a_n j_n(k_1 r) + d_n n_n(k_1 r) \right) P_n(\cos \theta) \quad (5-4)$$

$b \leq r \leq a$

$$A_{\phi}(\vec{r}) = \sum_{n=0}^{\infty} \left(b_n j_n(k_2 r) + e_n n_n(k_2 r) \right) \frac{dP_n}{d\theta} \quad (5-5)$$

$b \leq r \leq a$

Again we have that in the elastic shell

$$\vec{u}(\vec{r}) = -\nabla\psi + \nabla \times \vec{A} \quad b \leq r \leq a \quad (5-6)$$

$$\rho_1 \ddot{\vec{u}}(\vec{r}) = (\lambda + 2\mu) \nabla(\nabla \cdot \vec{u}) - \mu \nabla \times \nabla \times \vec{u} \quad b \leq r \leq a \quad (5-7)$$

and that the total pressure in the external medium is

$$p = p^i + p^s \quad r \geq a \quad (5-8)$$

The unknowns are $a_n, b_n, c_n, d_n, e_n, f_n$ for each mode n . The boundary conditions (2-6), (2-7) and (2-8) are applied both at $r = a$ and at $r = b$. The result is a system of 6 equations in 6 unknowns analogous to the system (2-10):

$$M^n Z^n = V^n, \quad (5-9)$$

where Z^n is written for the vector of unknowns (a_n, b_n, \dots, f_n) . The matrix entries M_{ij}^n and the entries V_i^n for $i, j \leq 3$ are exactly those of (2-11). To obtain the other M_{ij}^n , we can avoid a lot of writing by observing the following: each row is augmented by the coefficients of d_n and e_n , which are the same as the corresponding coefficients of a_n and b_n except for the use of n_n instead of j_n . That is:

replace j_n by n_n in M_{i1}^n to obtain $M_{i4}^n \quad (i = 1, \dots, 6);$

replace j_n by n_n in M_{i2}^n to obtain $M_{i5}^n \quad (i = 1, \dots, 6).$

Also, equations 4, 5, and 6 are the same as 1, 2, 3, except that they are

evaluated at $r = b$ instead of $r = a$; and also all occurrences of ρ_3, c_3 are replaced by ρ_4, c_4 . That is: replace Bessel function arguments x, x_1, x_2 by y, y_1, y_2 , where

$$\begin{aligned} y &= k_4 b = \omega b / c_4 \\ y_1 &= k_1 b = \omega b / c_1 \\ y_2 &= k_2 b = \omega b / c_2 \end{aligned} \quad (5-10)$$

in

M_{1j}^n to obtain M_{4j}^n ,

M_{2j}^n to obtain M_{5j}^n ,

M_{3j}^n to obtain M_{6j}^n (all for $j = 1, 2, 4, 5$).

Further, $M_{i6}^n = 0$ for $i = 1, 2, 3$; $M_{i3}^n = 0$ for $i = 4, 5, 6$;

$$M_{46}^n = \beta_4 D_0 b^2 j_n(y),$$

$$M_{56}^n = -D_0 b^2 j_n'(y),$$

$$M_{66}^n = 0,$$

$$v_i^n = 0, \quad i = 4, 5, 6, \quad (5-11)$$

where

$$\beta_4 = \frac{\rho_4 c_4^2}{\rho_1 c_1^2}.$$

For example,

$$M_{45}^n = (n^2 + n) \alpha \left(y_2 n'_n (y_2) - n_n (y_2) \right) .$$

A number of degenerate cases can be obtained from these equations by letting the appropriate ρ or c go to ∞ or 0, and thereby eliminating one or more unknowns and equations.

Degenerate Condition	Shell	Core	Equations (i)	Unknowns (j)
-	Elastic	Fluid	1,2,3,4,5,6	1,2,3,4,5,6
$\rho_4 \rightarrow \infty$	Elastic	Hard	1,2,3,5,6	1,2,3,4,5
$\rho_4 = 0$	Elastic	Soft	1,2,3,4,6	1,2,3,4,5
$b = 0$	Elastic	No	1,2,3	1,2,3
$c_2 = 0$	Fluid	Fluid	1,2,4,5	1,3,4,6
$c_2=0, \rho_4 \rightarrow \infty$	Fluid	Hard	1,2,5	1,3,4
$c_2=0, \rho_4=0$	Fluid	Soft	1,2,4	1,3,4
$c_2=0, b=0$	Fluid	No	1,2	1,3
$\rho_1 \rightarrow \infty$	Hard	No	2	3
$\rho_1 \rightarrow 0$	Soft	No	1	3

It is simplest to solve this set of equations by Gauss elimination and back substitution. Care must be taken, however, since the (complex) entries in M^n vary in magnitude from 10^{20} to 10^{-20} . Successful solution is achieved by normalizing M both by rows and by columns before applying the elimination procedure. The same considerations hold here as discussed in Section 2.1 with regard to the order of the Bessel functions.

Here the problem is somewhat more severe because of the larger range of Bessel function arguments. In the examples to follow, responses will be computed to $ka = 20$ and smoothed impulse responses will be computed for pulsewidth parameter $a_n = 4$.

5.2 THIN SHELL LIMIT

The solution for the thin shell can be obtained nicely from the above without further modification. As the thickness $h = a - b$ becomes small, greater accuracy can be obtained by noting that

$$M_{1j}^n = M_{4j}^n + h \frac{\partial}{\partial r} M_{4j}^n \quad (j = 1, 2, 4, 5) .$$

Row 4 can then be subtracted from row 1. The same can be done with rows 2 and 3. As $h \rightarrow 0$, some elements of M^n can be replaced by zero. However, this is not a great simplification since no unknowns are eliminated. In the calculations that follow, the unmodified thick shell computer program was used for the thin shell as well.

5.3 SHELL RESPONSES AS FUNCTIONS OF ELASTIC PARAMETERS

The sequence of plots in Figure 5-1 through 5-3 gives the magnitude of the frequency response of the spherical aluminum shell with parameter thickness. The thickness, h/a decreases from 1 to .001 through the sequence. The sequence 5-4 through 5-6 gives the same results in the time domain for smoothed impulse incidence with $a_n = 4$. It is seen that the thick shell has a more complex response than the solid. However, as the shell becomes thin, the response becomes simpler again, reducing in the limit to a sequence of spikes in the frequency domain. The magnitude of the response is proportional to h in the thin shell limit.

Whereas the response of a solid is perhaps best understood in the time domain as a sequence of pulses corresponding to various paths,

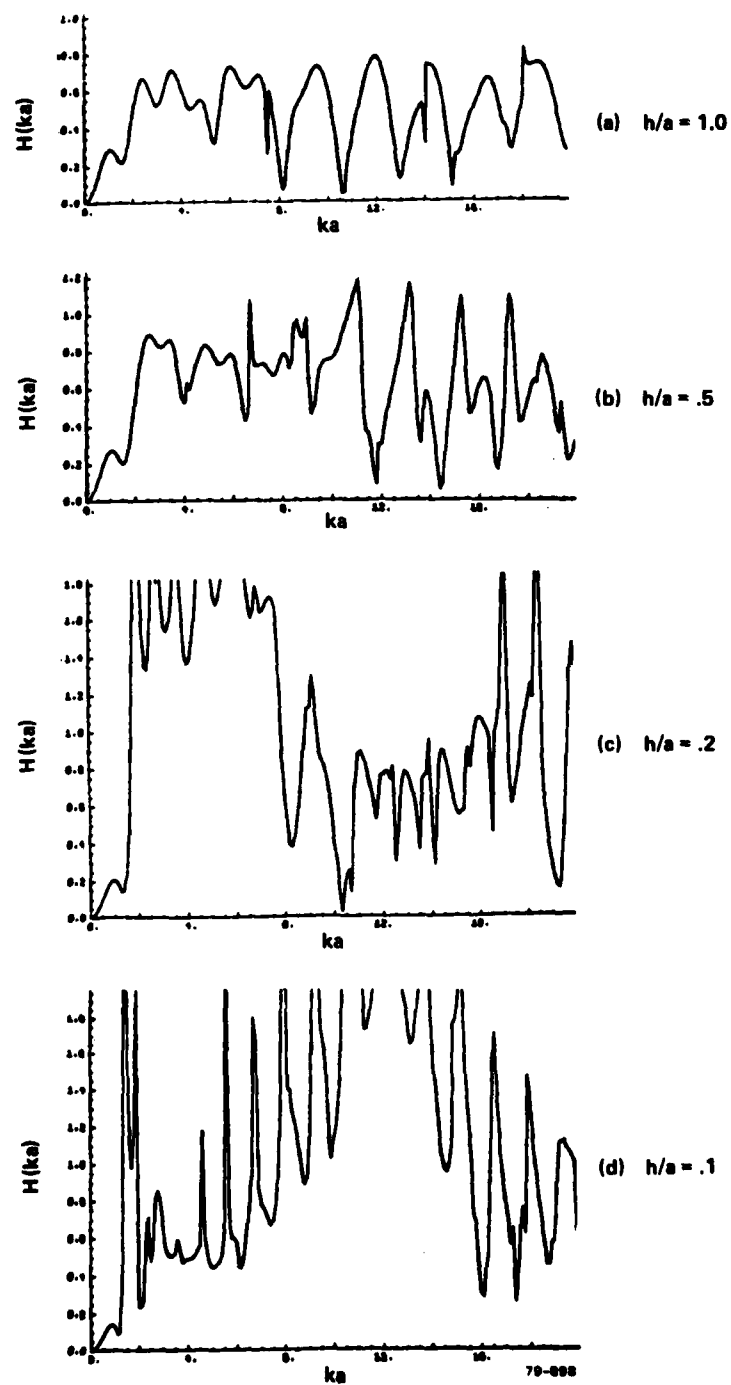


FIG. 5-1 Shell responses as a function of thickness — frequency domain, thick shell.

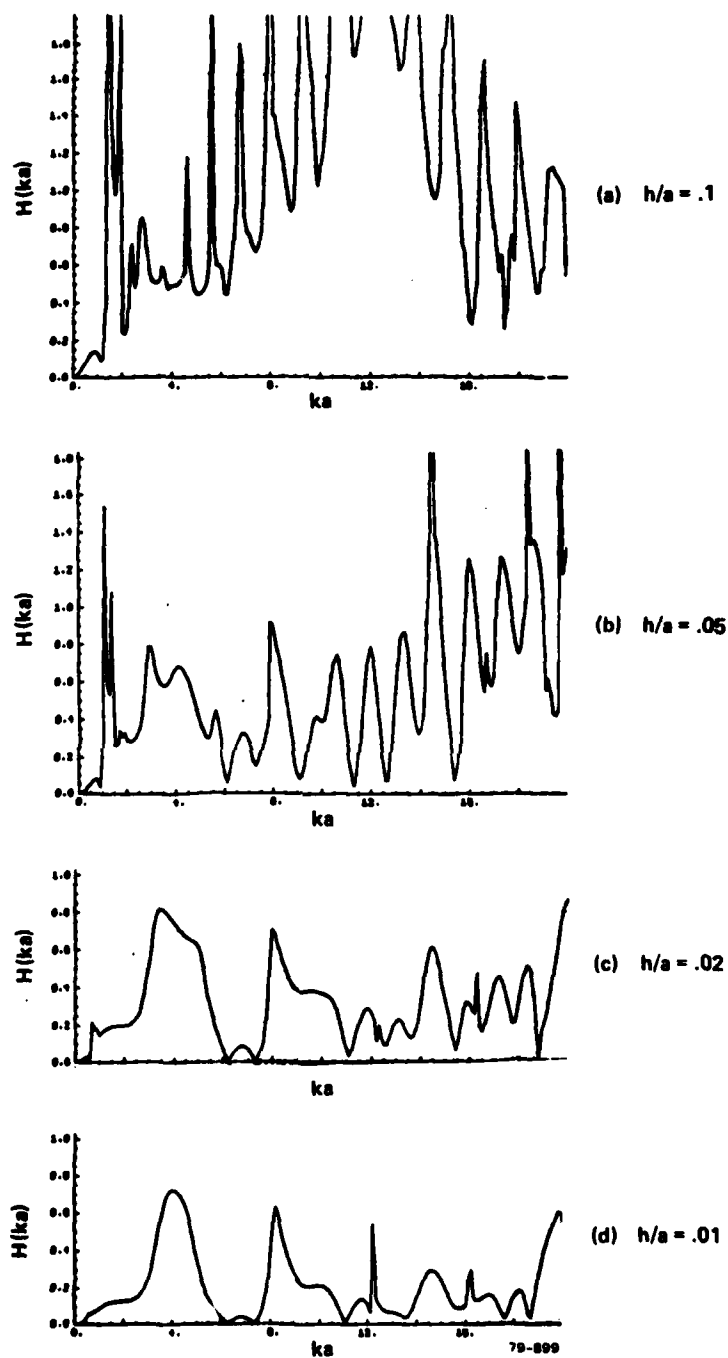


FIG. 5-2 Shell responses as a function of thickness — frequency domain, thin shell.

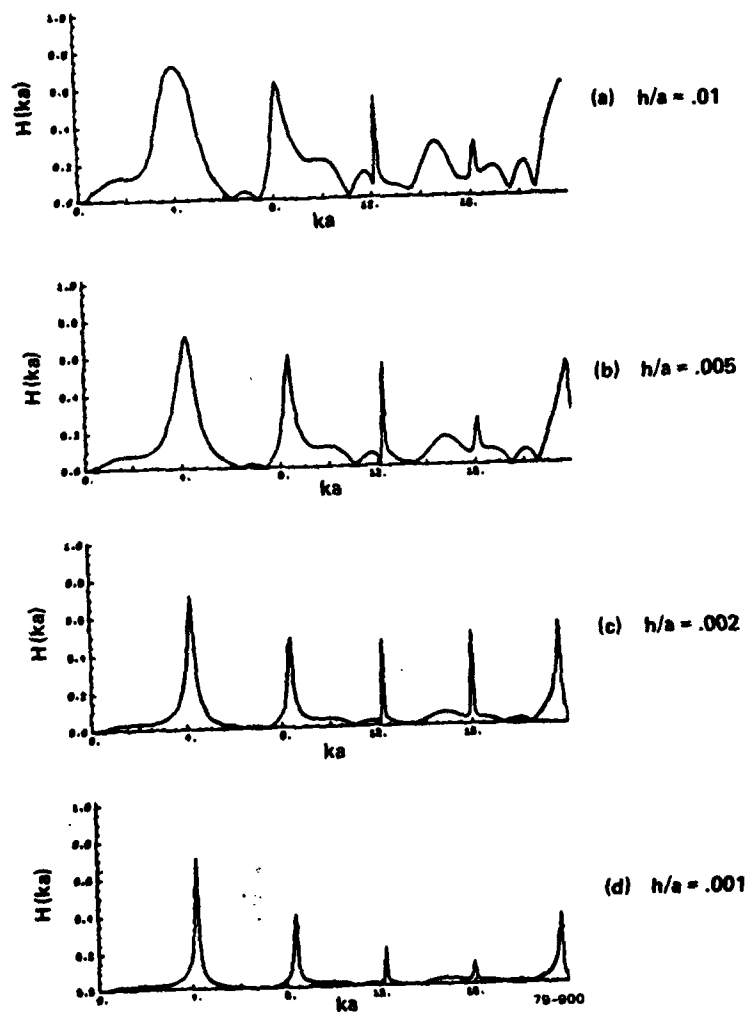


FIG. 5-3 Shell responses as a function of thickness – frequency domain, very thin shell.

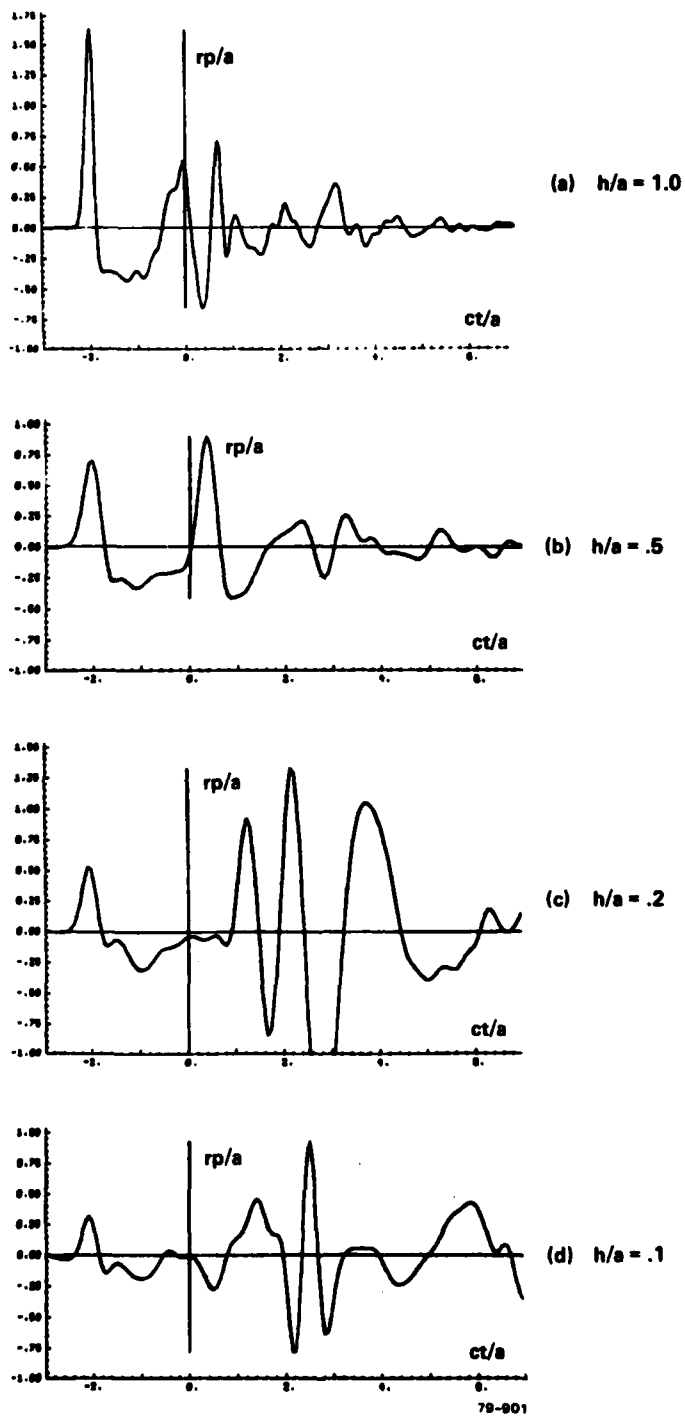


FIG. 5-4 Shell responses as a function of thickness — time domain, $a_n = 4$, thick shell.

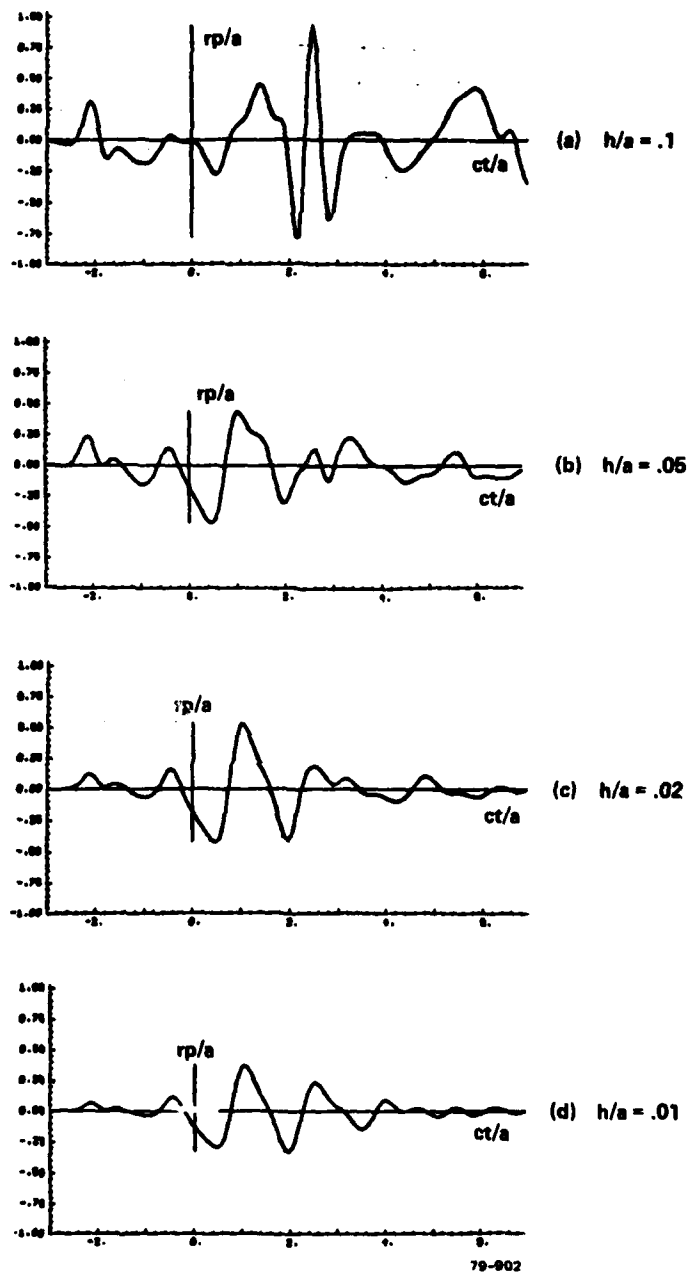


FIG. 5-5 Shell responses as a function of thickness — time domain, $a_n = 4$, thin shell.

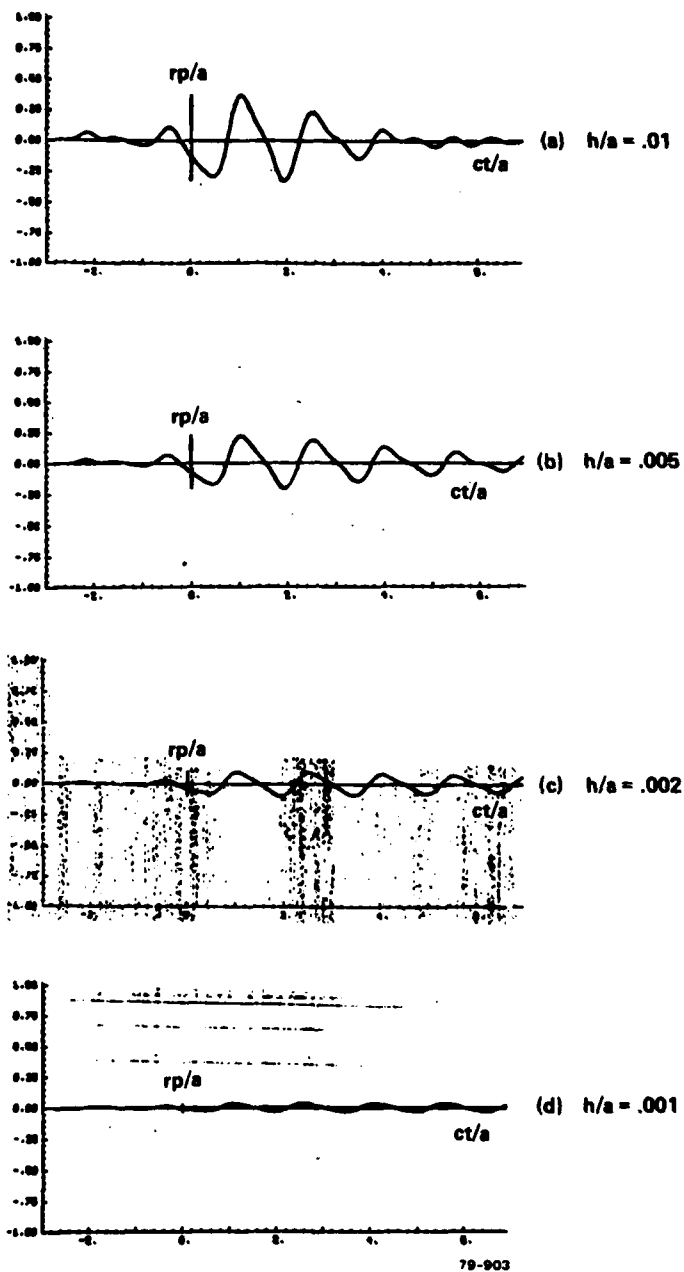


FIG. 5-6 Shell responses as a function of thickness — time domain, $a_n = 4$, very thin shell.

the very thin shell response is best understood in the frequency domain as a resonance with its overtones. The resonant frequency is dependent on both c_1 and c_2 as illustrated in Figure 5-7, where one of the elastic parameters of an aluminum shell with $h = .001$ is changed at a time. If both ρ_1 and h are changed in such a way that the surface density ($\rho_1 h$) remains constant, then the response remains about constant (for the very thin shell). This is illustrated in Figure 5-8.

In all of the above examples, the core was water filled. It is interesting to see the effect of a different core. In Figure 5-9 the response of a soft sphere is compared to that of a soft core (that is, a gas-filled) spherical shell. The difference between the two responses is the same sequence of resonances already found for the water filled shell. In addition, a large very low frequency resonance is observed. The time domain response is given in Figure 5-10. A similar result is found if the core is a heavier fluid. Figure 5-11 illustrates the response of a glycerin core, which has a density about 1.25 times water. This resembles closely the response of a fluid sphere, but with the spikes characteristic of the shell superposed. The very low frequency spike is absent.

It is significant that a thin shell, surrounding a sound-soft or fluid target has a large effect on the response in the form of sharp resonances.

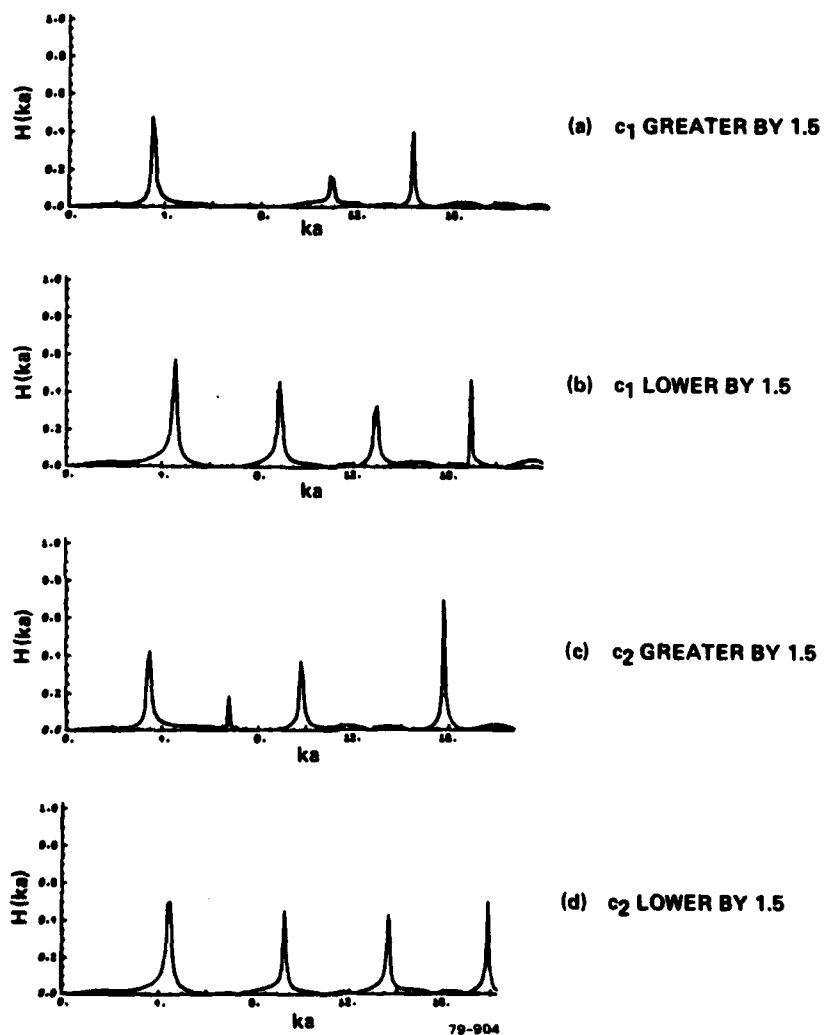


FIG. 5-7 Responses of very thin shell with variations in elastic parameters, $h = 0.001$.

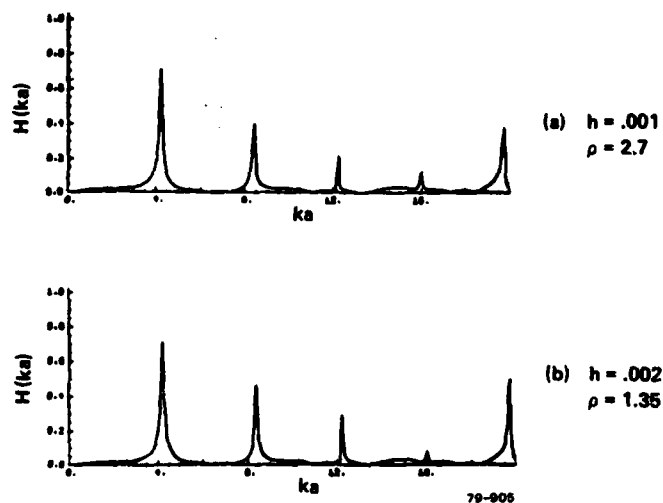


FIG. 5-8 Responses of very thin shell with variations in ρ and h , keeping $\rho_1 h$ constant.

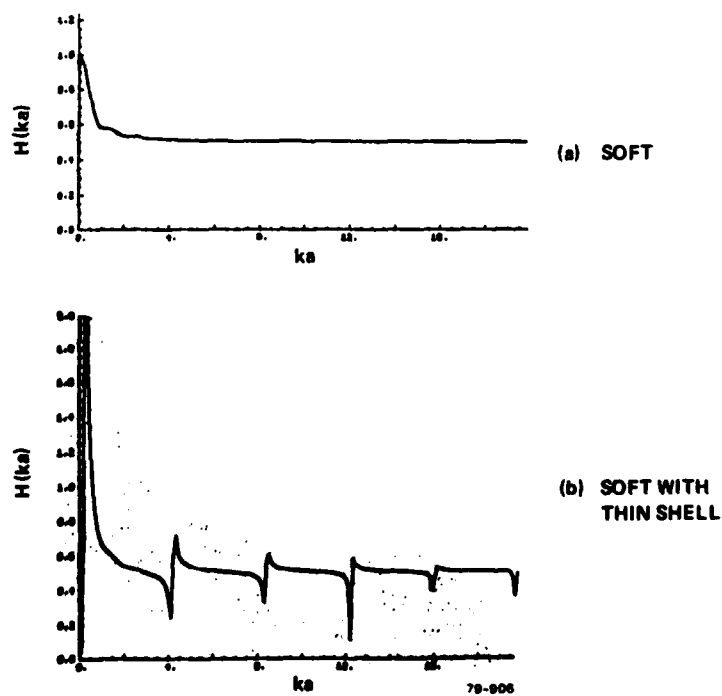


FIG. 5-9 Comparison of responses of soft sphere and soft core (gas-filled) spherical shell — frequency domain.

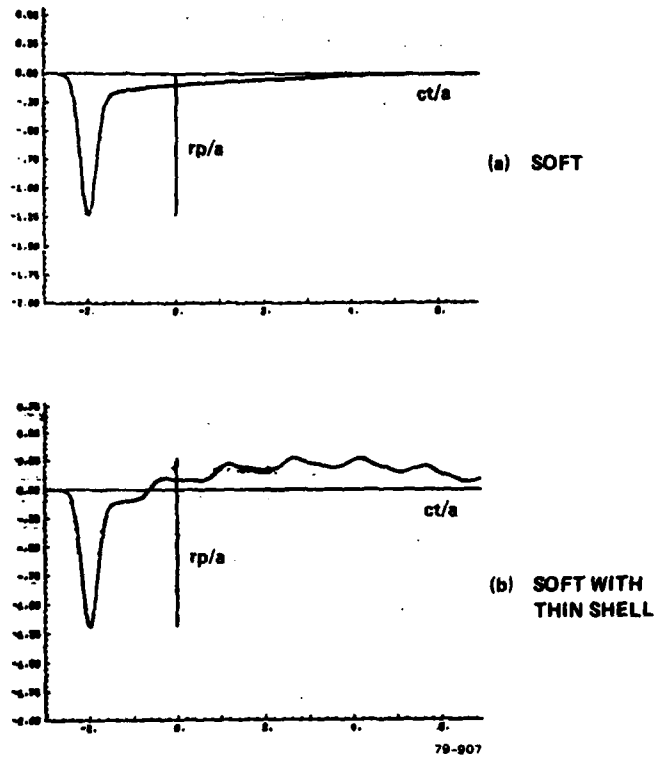


FIG. 5-10 Comparison of responses of soft sphere and soft core (gas-filled) spherical shell — time domain.

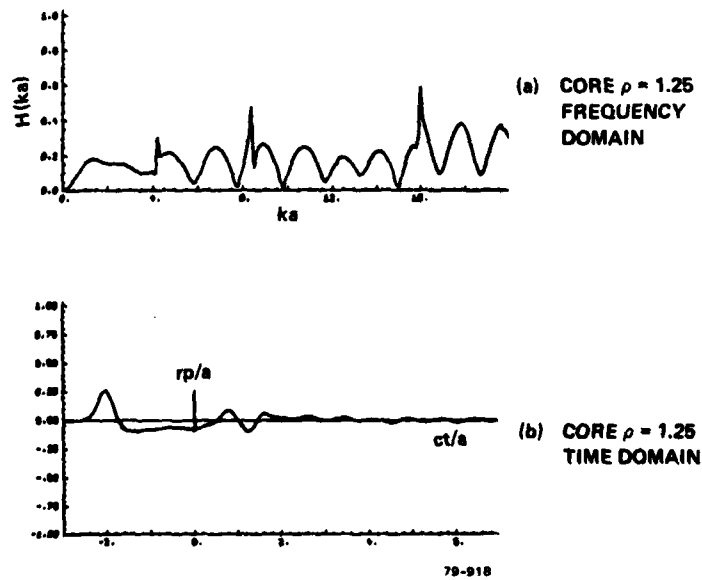


FIG. 5-11 Frequency and time domain responses of heavy core (glycerin-filled) spherical shell.

SECTION 6

REFERENCES

1. H. Mieras and C.L. Bennett, "Active Sonar Modeling," Sperry Research Center, Final Report Contract No. N61339-77-C-0105, August 1978.
2. V.C. Anderson, "Sound Scattering from a Fluid Sphere," JASA 22-4, July 1950.
3. J.J. Faran, "Sound Scattering by Solid Cylinders and Spheres," JASA 23-4, July 1951.
4. M. Goldstein and R.M. Thaler, "Recurrence Techniques for the Calculation of Bessel Functions," MTAC, 1959.
5. R. Hickling, "Analysis of Echoes from a Solid Elastic Sphere in Water," JASA 34-10, October 1962.
6. C.L. Bennett, A.M. Auckenthaler, R.S. Smith and J.D. DeLorenzo, "Space Time Integral Equation Approach to the Large Body Scattering Problem," Final Report, F30602-71-C-0162, RADCR-73-70, AD 763794, May 1973.
7. D. Brill and H. Uberall, "Acoustic Waves Transmitted through Solid Elastic Cylinders," JASA 50-3 (Part 2), p. 921, 1971.
8. J.D. Jackson, Classical Electromagnetics, Wiley, N.Y., 1962.
9. E.M. Kennaugh and R.L. Cosgriff, "The Use of Impulse Response in Electromagnetic Scattering Problems," 1958 IRE National Convention Record, Part 1, pp. 72-77.
10. C.L. Bennett, H. Mieras, S.L. Teeter, and J.P. Toomey, "Low EM Signature Response Techniques," Final Report Contract No. F30602-77-C-0166, October 1978.
11. H.C. Van de Hulst, Light Scattering by Small Particles, Wiley, N.Y., 1957.
12. H.C. Bryant and N. Jarmie, "The Glory," Scientific American, July 1974.
13. C.L. Bennett and R.M. Hieronymus, "Solution of Acoustic Space-Time Integral Equations for Soft and Hard Boundary Conditions," SCRC-RR-74-29, November 1974.

AD-A089 651

SPERRY RESEARCH CENTER SUDBURY MA
TIME-DOMAIN SONAR TARGET RESPONSE MODELING.(U)
OCT 79 H MIERAS, C L BENNETT
SRC-CR-79-74

F/G 17/1

UNCLASSIFIED

N61331-78-C-0049

NL

2 x 2

2 x 2



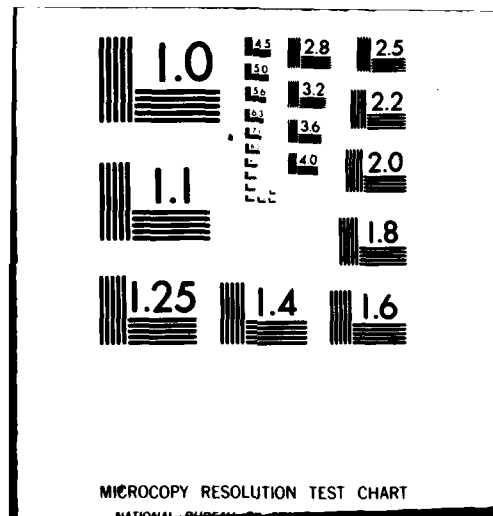
END

DATE

FILED

10-80

DTIC



14. H. Mieras and C.L. Bennett, "Solution of Acoustic Space-Time Integral Equations for Hard or Soft Targets in the Presence of Hard or Soft Planes," SCRC-RR-76-4, February 1976.
15. R.R. Goodman and R. Stern, "Reflection and Transmission of Sound by Elastic Spherical Shells," JASA 34-3, March 1962.

SECTION 7
APPENDICES

7.1 ELASTIC CONSTANTS

Collected here are some useful relationships and equations to do with elastic properties.

λ, μ Lamé Coefficients
 Y, B, μ Young's, Bulk, Shear Moduli
 σ Poisson Ratio
 c_1, c_2 Longitudinal, Transverse Speeds
 ρ Density

$$Y = 3B(1 - \sigma) = 2\mu(1 + \sigma)$$

$$\lambda = B - 2\mu/3$$

$$c_1^2 = \frac{\lambda + 2\mu}{\rho}$$

$$c_2^2 = \frac{\mu}{\rho}$$

$$c_1^2/c_2^2 = 2(1 - \sigma)/(1 - 2\sigma)$$

$$\sigma = (c_1^2 - 2c_2^2)/2(c_1^2 - c_2^2)$$

In a fluid: $\mu = 0$, $\sigma = 1/2$, $c_2 = 0$

\vec{u} displacement

Equation of motion:

$$\ddot{\vec{u}} = c_1^2 \nabla(\nabla \cdot \vec{u}) - c_2^2 \nabla \times \nabla \times \vec{u}.$$

In fluid: p excess pressure,

$$p = -c_1^2 \rho(\nabla \cdot \vec{u}), \quad \nabla p = -\rho \ddot{\vec{u}}.$$

7.2 SCATTERING MODEL - COMPUTER PROGRAM

```

PBTM05  ASYMOD-ASYMOD-TPFS.
L14 081 07217779-16:00(U.)
1000-  PARAMETER 1PM=4
1100-  DIMENSION P2(IPM),TPATH(3,IPM),PATH(3,IPM),IN3D(IPM)
1200-  DIMENSION P2(IPM),P2(IPM),P2(IPM),P2(IPM),DELTA2(IPM)
1300-  PARAMETER MFORT=11, MFORT=2011, NUMM=MFORT/2
1400-  COMPLEX RNFORT), W(NUMM)
1500-  DIMENSION VNFORT), AN(NUMM), AN(NUMM), E(NUMM), AT(MFORT), TINFOR
1600-  ST), SFORT(NUMM)
1700-  DIMENSION XXX(2), VVV(2)
1800-  CHARACTER80 TITLE, LABEL
1900-  CHARACTER=48 VLABEL
2000-  CHARACTER=8 CDATE,CTIME
2100-  C-----
2200-  C----- CONSTANTS & PARAMETERS
2300-  C-----
2400-  C-----
2500-  C-----
2600-  C-----
2700-  C-----
2800-  C-----
2900-  C-----
3000-  C-----
3100-  C-----
3200-  C-----
3300-  C-----
3400-  C-----
3500-  C-----
3600-  C-----
3700-  C-----
3800-  C-----
3900-  C-----
4000-  C-----
4100-  C-----
4200-  C-----
4300-  C-----
4400-  C-----
4500-  C-----
4600-  C-----
4700-  C-----
4800-  C-----
4900-  C-----
5000-  C-----
5100-  C-----
5200-  C-----
5300-  C-----
5400-  C-----
5500-  C-----
5600-  C-----
5700-  C-----
5800-  C-----
5900-  C-----
6000-  C-----
6100-  C-----
6200-  C-----
6300-  C-----
6400-  C-----
6500-  C-----
6600-  C-----
6700-  C-----
6800-  C-----
6900-  C-----
7000-  C-----
7100-  C-----
7200-  C-----
7300-  C-----
7400-  C-----
7500-  C-----
7600-  C-----
7700-  C-----
7800-  C-----
7900-  C-----
8000-  C-----
8100-  C-----
8200-  C-----
8300-  C-----
8400-  C-----
8500-  C-----
8600-  C-----
8700-  C-----
8800-  C-----
8900-  C-----
9000-  C-----
9100-  C-----
9200-  C-----
9300-  C-----
9400-  C-----
9500-  C-----
9600-  C-----
9700-  C-----
9800-  C-----
9900-  C-----

```

```

670. CTM3C1=SQRT(1.-STM3C1**2)  & COSINES
671. CTM2C1=SQRT(1.-STM2C1**2)
672. TM3C1=ASIN(STM3C1)
673. TM2C1=ASIN(STM2C1)

```

```

270. C CRITICAL ANGLE CORRESPONDING TO C2

```

```

770. STM3C2=1./C2
771. CTM3C2=SQRT(1.-STM3C2**2)
772. TM3C2=ASIN(STM3C2)

```

```

270. C PATH 1 IS SPHERICAL REGION

```

```

770. PATH(1,1)=0.  & PATH LENGTH AT SPEED C1
771. PATH(2,1)=0.  & PATH LENGTH AT SPEED C2
772. PATH(5,1)=0.  & PATH LENGTH AT SPEED C3
773. TM30C1)=0.  & INCIDENCE ANGLE

```

```

870. C PATH 2 IS CRITICAL C1 (CREEP) WITH ONE CHORD AT C2

```

```

871. ALPH=PI-5-TM3C1+TM2C1  & ARC LENGTH OF PATH AT C1 (CREEP)
872. PATH(1,2)=2.*ALPH
873. PATH(2,2)=2.*CTM2C1
874. PATH(3,2)=2.*(1.-CTM3C1)
875. TM30C2)=TM3C1+DEG

```

```

970. C PATH 3 IS CRITICAL C1, WITH TWO CHORDS AT C2

```

```

971. ALPH=2.-TM2C1-TM3C1
972. PATH(1,3)=2.*ALPH
973. PATH(2,3)=4.-CTM2C1
974. PATH(3,3)=PATH(3,2)
975. TM30C3)=TM30C2

```

```

970. C PATH 4 IS CRITICAL C2

```

```

971. ALPH=2.-PI-TM3C2)
972. PATH(1,4)=0.
973. PATH(2,4)=ALPH
974. PATH(3,4)=2.*CTM3C2)
975. TM30C4)=TM3C2+DEG

```

```

1070. C TRAVERSAL TIMES

```

```

1071. DO 14 IP=1,IPN
1072. TPATH(1,IP)=PATH(1,IP)/C1
1073. TPATH(2,IP)=PATH(2,IP)/C2

```

```

1074. TPATH(3,IP)=PATH(3,IP)
1075. T2CIP)=2.-TPATH(1,IP)+TPATH(2,IP)+TPATH(3,IP)
1076. CONTINUE

```

```

1170. C -----END GLORY PATH CALCULATION-----

```

```

1171. C PARTS OF IMPULSE RESPONSE CORRESPONDING TO EACH PATH

```

```

1172. C -----INPUT-----

```

```

1173. IPP=IPN

```

```

1174. WRITE(6,230)IPP

```

```

1175. FORMAT(' ENTER IMPULSE RESP. PARAMS P,S,E FOR ',12,' PATHS')

```

```

1176. READ(5,*)P2(1P),S2(1P),E2(1P),IP=1,IPN)

```

```

1177. DO 24 IP=1,IPN

```

```

1178. DELT2(1P)=2.-P2(1P)+S2(1P)+E2(1P)  & DERIVED PULSE PARAMETERS

```

```

1179. R2(1P)=(E2(1P)-S2(1P))/DELT2(1P)  & SUCH THAT DC RESPONSE IS ZERO

```

```

1180. CONTINUE

```

```

1270. C

```

```

1271. WRITE(6,240)

```

```

1700. WRITE(6,250)IP,P2(IP),S2(IP),E2(IP),R2(IP),DELTA2(IP),
1710. A 121P2,TH2P(IP),LTPATH1C,IP,LC=1,3,IP=1,IPM)
1720. 240 FORMAT(' IMPULSE RESPONSE PARAMETERS // IP P2 S2
1730. A'E2 R2 DELTA2 T2 TH2P PL1/C1',
1740. C'PL2/22 PL3/23')
1750. 250 FORMAT(1X,11,10F7.3)
1760. C
1770. WRITE(6,270)
1780. 270 FORMAT(' ENTER FREQUENCY STEP DM, MAX WM, SM,IMPULSE AN")
1790. READ(5,*)DM,WM,AN
1800. NUM=DM/AN*1.5
1810. NUM=MIN(NUM,NUMM)
1820. WM=NUM*DM
1830. WRITE(6,280)DM,WM,AN,NUM,MFORT
1840. 280 FORMAT(1X,F8.3,2F8.3,16," VALUES. FFT ON,"15," POINTS")
1850. CALL FORT(M,MFORT,SFORT,0,LFORT) B SET UP FFT SINETABLES
1860. C
1870. C-----END INPUT-----AND CALC SET-UP-----
1880. C
1890. C COMPUTE FREQUENCY RESPONSE FOR EACH PAIR AND ADD TOGETHER IN M(M)
1900. C
1910. C CALL RESPNS(IPM,T2,P2,S2,E2,R2,DELTA2,DM,NUM,M)
1920. C
1930. C MAGNITUDE OF M
1940. DO 32 I=1,NUM
1950. 32 AM(I)=CABS(M(I))
1960. 32 TIME=I
1970. C-----
1980. 33 CONTINUE A DO IT AGAIN FROM THIS POINT FOR ANOTHER AN
1990. C-----
2000. C
2010. PLB=2.921/DM
2020. DT=PER/MFORT
2030. V1=-INT((3./AN+2.5)/DT+.5)+DT B APPROX START TIME OF PULSE
2040. DO 33 I=1,NUM
2050. 33 V(I)=(I-1)*DT+T1
2060. 33 CONTINUE
2070. C MULTIPLY BY SMOOTHED IMPULSE IN FREQUENCY DOMAIN
2080. C
2090. DO 33 I=1,NUM
2100. 33 WM(I)=V(I)*M(I)
2110. 33 R(I)=E(I)*M(I)
2120. 33 AM(I)=CABS(R(I))
2130. 33 CONTINUE
2140. C
2150. C FILL IN INPUT ARRAY TO FFT
2160. M1=NUM+1
2170. M2=MFORT-NUM+1
2180. DO 342 I=M1,M2
2190. 342 R(I)=0.00)
2200. DO 343 I=2,NUM
2210. 343 M(I)=CONJG(R(I))
2220. C
2230. C
2240. C
2250. C
2260. C
2270. C
2280. C
2290. C
2300. C
2310. C
2320. C
2330. C
2340. C
2350. C
2360. C
2370. C
2380. C
2390. C
2400. C
2410. C
2420. C
2430. C
2440. C
2450. C
2460. C
2470. C
2480. C
2490. C
2500. C
2510. C
2520. C
2530. C
2540. C
2550. C
2560. C
2570. C
2580. C
2590. C
2600. C
2610. C
2620. C
2630. C
2640. C
2650. C
2660. C
2670. C
2680. C
2690. C
2700. C
2710. C
2720. C
2730. C
2740. C
2750. C
2760. C
2770. C
2780. C
2790. C
2800. C
2810. C
2820. C
2830. C
2840. C
2850. C
2860. C
2870. C
2880. C
2890. C
2900. C
2910. C
2920. C
2930. C
2940. C
2950. C
2960. C
2970. C
2980. C
2990. C
3000. C

```

```

C ARRAY N NOW CONTAINS TIME DOMAIN RESPONSE
C TIME SHIFT AND SCALE. PUT INTO RT(7)
RT(7)=T/TOT+.5
MT2=MT1+1
NIN=NBRT
DO 534 I=1,NT1
II=INFORT-MT1+1
RT(I)=R(I)/PER
CONTINUE
534 DO 535 I=MT2,NT3
I(1)=MI
RT(I)=R(I)/PER
CONTINUE
535 -----END TIME DOMAIN RESPONSE CALCULATION-----
C -----PLOT RESULTS-----
IF(LTIME-1).LTED TO AAS
      B SCALES FOR FREQ DOMAIN PLOTS
      HX(1)=0.
      HX(2)=50.
      VV(1)=0.
      VV(2)=1.0
      ENCODE(100,410,TITLE,MCT,NM,CY,CZ
      FORMAT('SCATTERING MODEL = BM,EL,C2M',3BA,3,3AN)
      ENCODE(100,420,XLABEL,MCH)(P2(IP),S2(IP),E2(IP),IP=1,4)
      FORMAT('P,S,E',4F5.2,F5.2,3H),2H)
      CALL ABATECDATE,CTIME) B GET DATE,TIME FOR IDENTIFICATION
      ENCODE(48,434,YLABEL,MCT)(DATE,CTIME
      FORMAT(10H,2A8,22H)
      436 FORMATION,2AB,AH,'AM',SA,1,4A1
      WRITE(6,435)YLABEL
      435 FORMAT(/' RUN IDENTIFICATION ',A48)
C PLOT SCALE
CALL PLOTIC(-1,HXX,VVV,2,0,0,TITLE,MCT,XLABEL,MCH,YLABEL,MCT,1)
C PLAT RESULTS
CALL PLOTIC(6,AM,MUM,0,0, 0,0, 0,0, 0,0, 2)
CALL PLOTIC(6,E, MUM,0,0, 0,0, 0,0, 0,0, 3)
CALL PLOTIC(6,M,AB,MUM,0,0, 0,0, 0,0, 0,0, 4)
HXC(1)=-3. B TIME DOMAIN SCALES
HX(2)=7.
HXC(1)=1.
VV(2)=2.
CONTINUE
441 IS=542,ITYPE
ENCODE(48,430,YLABEL,MCT)(DATE,CTIME,AN
CALL PLOTIC(-1,HXX,VVV,2,0,0,TITLE,MCT,XLABEL,MCH,YLABEL,MCT,10)
IS=10A1
CALL PLOTIC(6,T,MY,MUM,0,0, 0,0, 0,0, 0,0, 10)
C -----END PLOTS-----
C DO CASE AN=1 AS AFTERTHOUGHT
ITIME=TIME+1
HXC(1)=-C. B TIME SCALES FOR AN=1
HXC(2)=0.
VV(1)=-.1
VV(2)=.12
AN=1.
IF(LTIME-10).LTED TO J11

```

2440. C
2450. 9J CONTINUE
2460. STOP
2470. END

END 014 111 10ANK 17115 00ANK

1014.5 ASCRDB-RESPAS-TPFS.

110. C 02/17/79-16:01(0.2)

110. SUMOUTLINE RESPNS(N,TZ,PZ,SZ,EZ,RZ,DELTAZ,DM,MU,M)

110. DIMENSION T2(N),P2(N),S2(N),EZ(N),R2(N),DELTAZ(N)

110. COMPLEX MU(N), DM, CEAZ, CR, JAV

110. C

110. C ADD M RESPONSES IN FREQ DOMAIN

110. C RESPONSE OCCURS AT TIME T2, AND IS COMPOSED OF IMPULSE P2.

110. C STEP SZ, RAMP R2, BACKSLING EZ AT TIME DELTAZ

110. C ASSUME RZ, DELTAZ SET SUCH THAT DC RESPONSE M(0) IS ZERO

110. C CALLED BY MODELING PROGRAM ASCRDB

110. C

110. JAV=(0.,1.)

110. DO 12 I=1,M

110. M(I)=(0.,0.)

110. DO 8 K=1,N 3 FOR M PULSES

110. 2=0.

110. DO 7 I=2,MW 9 AT ALL FREQ. EXCEPT M=0.

110. 2=0.

110. 2=0.

110. 2=0.

110. 2=0.

110. 2=0.

110. 2=0.

110. 2=0.

110. 2=0.

110. 2=0.

110. 2=0.

110. 2=0.

110. 2=0.

110. 2=0.

110. 2=0.

110. 2=0.

110. 2=0.

110. 2=0.

110. 2=0.

110. 2=0.

110. 2=0.

110. 2=0.

110. 2=0.

110. 2=0.

-101-

END 014 750 10ANK 85 00ANK

[illegible]

```

40  N=2000
41  IF (A(1,1)) - 1 ) 20,200,10
42  WE ARE DOING TRANSFORM ONLY. SEE IF PRE-COMPUTED
43  S TABLE IS SUFFICIENTLY LARGE
44  1L 100 N=NP 20,20,12
45  1L 10000
46  GO TO 2,0
47  SCRAMBLE A, BY SANDE'S METHOD
48  DO 22 L=2,M
49  DO 24 L=M,12
50  DO 26 L=2,M
51  DO 28 L=M,12
52  DO 30 L=2,M
53  DO 32 L=M,12
54  DO 34 L=2,M
55  DO 36 L=M,12
56  DO 38 L=2,M
57  DO 40 L=M,12
58  DO 42 L=2,M
59  DO 44 L=M,12
60  DO 46 L=2,M
61  DO 48 L=M,12
62  DO 50 L=2,M
63  DO 52 L=M,12
64  DO 54 L=2,M
65  DO 56 L=M,12
66  DO 58 L=2,M
67  DO 60 L=M,12
68  DO 62 L=2,M
69  DO 64 L=M,12
70  DO 66 L=2,M
71  DO 68 L=M,12
72  DO 70 L=2,M
73  DO 72 L=M,12
74  DO 74 L=2,M
75  DO 76 L=M,12
76  DO 78 L=2,M
77  DO 80 L=M,12
78  DO 82 L=2,M
79  DO 84 L=M,12
80  DO 86 L=2,M
81  DO 88 L=M,12
82  DO 90 L=2,M
83  DO 92 L=M,12
84  DO 94 L=2,M
85  DO 96 L=M,12
86  DO 98 L=2,M
87  DO 100 L=M,12
88  DO 102 L=2,M
89  DO 104 L=M,12
90  DO 106 L=2,M
91  DO 108 L=M,12
92  DO 110 L=2,M
93  DO 112 L=M,12
94  DO 114 L=2,M
95  DO 116 L=M,12
96  DO 118 L=2,M
97  DO 120 L=M,12
98  DO 122 L=2,M
99  DO 124 L=M,12
100  DO 126 L=2,M
101  DO 128 L=M,12
102  DO 130 L=2,M
103  DO 132 L=M,12
104  DO 134 L=2,M
105  DO 136 L=M,12
106  DO 138 L=2,M
107  DO 140 L=M,12
108  DO 142 L=2,M
109  DO 144 L=M,12
110  DO 146 L=2,M
111  DO 148 L=M,12
112  DO 150 L=2,M
113  DO 152 L=M,12
114  DO 154 L=2,M
115  DO 156 L=M,12
116  DO 158 L=2,M
117  DO 160 L=M,12
118  DO 162 L=2,M
119  DO 164 L=M,12
120  DO 166 L=2,M
121  DO 168 L=M,12
122  DO 170 L=2,M
123  DO 172 L=M,12
124  DO 174 L=2,M
125  DO 176 L=M,12
126  DO 178 L=2,M
127  DO 180 L=M,12
128  DO 182 L=2,M
129  DO 184 L=M,12
130  DO 186 L=2,M
131  DO 188 L=M,12
132  DO 190 L=2,M
133  DO 192 L=M,12
134  DO 194 L=2,M
135  DO 196 L=M,12
136  DO 198 L=2,M
137  DO 200 L=M,12
138  DO 202 L=2,M
139  DO 204 L=M,12
140  DO 206 L=2,M
141  DO 208 L=M,12
142  DO 210 L=2,M
143  DO 212 L=M,12
144  DO 214 L=2,M
145  DO 216 L=M,12
146  DO 218 L=2,M
147  DO 220 L=M,12
148  DO 222 L=2,M
149  DO 224 L=M,12
150  DO 226 L=2,M
151  DO 228 L=M,12
152  DO 230 L=2,M
153  DO 232 L=M,12
154  DO 234 L=2,M
155  DO 236 L=M,12
156  DO 238 L=2,M
157  DO 240 L=M,12
158  DO 242 L=2,M
159  DO 244 L=M,12
160  DO 246 L=2,M
161  DO 248 L=M,12
162  DO 250 L=2,M
163  DO 252 L=M,12
164  DO 254 L=2,M
165  DO 256 L=M,12
166  DO 258 L=2,M
167  DO 260 L=M,12
168  DO 262 L=2,M
169  DO 264 L=M,12
170  DO 266 L=2,M
171  DO 268 L=M,12
172  DO 270 L=2,M
173  DO 272 L=M,12
174  DO 274 L=2,M
175  DO 276 L=M,12
176  DO 278 L=2,M
177  DO 280 L=M,12
178  DO 282 L=2,M
179  DO 284 L=M,12
180  DO 286 L=2,M
181  DO 288 L=M,12
182  DO 290 L=2,M
183  DO 292 L=M,12
184  DO 294 L=2,M
185  DO 296 L=M,12
186  DO 298 L=2,M
187  DO 300 L=M,12
188  DO 302 L=2,M
189  DO 304 L=M,12
190  DO 306 L=2,M
191  DO 308 L=M,12
192  DO 310 L=2,M
193  DO 312 L=M,12
194  DO 314 L=2,M
195  DO 316 L=M,12
196  DO 318 L=2,M
197  DO 320 L=M,12
198  DO 322 L=2,M
199  DO 324 L=M,12
200  DO 326 L=2,M
201  DO 328 L=M,12
202  DO 330 L=2,M
203  DO 332 L=M,12
204  DO 334 L=2,M
205  DO 336 L=M,12
206  DO 338 L=2,M
207  DO 340 L=M,12
208  DO 342 L=2,M
209  DO 344 L=M,12
210  DO 346 L=2,M
211  DO 348 L=M,12
212  DO 350 L=2,M
213  DO 352 L=M,12
214  DO 354 L=2,M
215  DO 356 L=M,12
216  DO 358 L=2,M
217  DO 360 L=M,12
218  DO 362 L=2,M
219  DO 364 L=M,12
220  DO 366 L=2,M
221  DO 368 L=M,12
222  DO 370 L=2,M
223  DO 372 L=M,12
224  DO 374 L=2,M
225  DO 376 L=M,12
226  DO 378 L=2,M
227  DO 380 L=M,12
228  DO 382 L=2,M
229  DO 384 L=M,12
230  DO 386 L=2,M
231  DO 388 L=M,12
232  DO 390 L=2,M
233  DO 392 L=M,12
234  DO 394 L=2,M
235  DO 396 L=M,12
236  DO 398 L=2,M
237  DO 400 L=M,12
238  DO 402 L=2,M
239  DO 404 L=M,12
240  DO 406 L=2,M
241  DO 408 L=M,12
242  DO 410 L=2,M
243  DO 412 L=M,12
244  DO 414 L=2,M
245  DO 416 L=M,12
246  DO 418 L=2,M
247  DO 420 L=M,12
248  DO 422 L=2,M
249  DO 424 L=M,12
250  DO 426 L=2,M
251  DO 428 L=M,12
252  DO 430 L=2,M
253  DO 432 L=M,12
254  DO 434 L=2,M
255  DO 436 L=M,12
256  DO 438 L=2,M
257  DO 440 L=M,12
258  DO 442 L=2,M
259  DO 444 L=M,12
260  DO 446 L=2,M
261  DO 448 L=M,12
262  DO 450 L=2,M
263  DO 452 L=M,12
264  DO 454 L=2,M
265  DO 456 L=M,12
266  DO 458 L=2,M
267  DO 460 L=M,12
268  DO 462 L=2,M
269  DO 464 L=M,12
270  DO 466 L=2,M
271  DO 468 L=M,12
272  DO 470 L=2,M
273  DO 472 L=M,12
274  DO 474 L=2,M
275  DO 476 L=M,12
276  DO 478 L=2,M
277  DO 480 L=M,12
278  DO 482 L=2,M
279  DO 484 L=M,12
280  DO 486 L=2,M
281  DO 488 L=M,12
282  DO 490 L=2,M
283  DO 492 L=M,12
284  DO 494 L=2,M
285  DO 496 L=M,12
286  DO 498 L=2,M
287  DO 500 L=M,12
288  DO 502 L=2,M
289  DO 504 L=M,12
290  DO 506 L=2,M
291  DO 508 L=M,12
292  DO 510 L=2,M
293  DO 512 L=M,12
294  DO 514 L=2,M
295  DO 516 L=M,12
296  DO 518 L=2,M
297  DO 520 L=M,12
298  DO 522 L=2,M
299  DO 524 L=M,12
300  DO 526 L=2,M
301  DO 528 L=M,12
302  DO 530 L=2,M
303  DO 532 L=M,12
304  DO 534 L=2,M
305  DO 536 L=M,12
306  DO 538 L=2,M
307  DO 540 L=M,12
308  DO 542 L=2,M
309  DO 544 L=M,12
310  DO 546 L=2,M
311  DO 548 L=M,12
312  DO 550 L=2,M
313  DO 552 L=M,12
314  DO 554 L=2,M
315  DO 556 L=M,12
316  DO 558 L=2,M
317  DO 560 L=M,12
318  DO 562 L=2,M
319  DO 564 L=M,12
320  DO 566 L=2,M
321  DO 568 L=M,12
322  DO 570 L=2,M
323  DO 572 L=M,12
324  DO 574 L=2,M
325  DO 576 L=M,12
326  DO 578 L=2,M
327  DO 580 L=M,12
328  DO 582 L=2,M
329  DO 584 L=M,12
330  DO 586 L=2,M
331  DO 588 L=M,12
332  DO 590 L=2,M
333  DO 592 L=M,12
334  DO 594 L=2,M
335  DO 596 L=M,12
336  DO 598 L=2,M
337  DO 600 L=M,12
338  DO 602 L=2,M
339  DO 604 L=M,12
340  DO 606 L=2,M
341  DO 608 L=M,12
342  DO 610 L=2,M
343  DO 612 L=M,12
344  DO 614 L=2,M
345  DO 616 L=M,12
346  DO 618 L=2,M
347  DO 620 L=M,12
348  DO 622 L=2,M
349  DO 624 L=M,12
350  DO 626 L=2,M
351  DO 628 L=M,12
352  DO 630 L=2,M
353  DO 632 L=M,12
354  DO 634 L=2,M
355  DO 636 L=M,12
356  DO 638 L=2,M
357  DO 640 L=M,12
358  DO 642 L=2,M
359  DO 644 L=M,12
360  DO 646 L=2,M
361  DO 648 L=M,12
362  DO 650 L=2,M
363  DO 652 L=M,12
364  DO 654 L=2,M
365  DO 656 L=M,12
366  DO 658 L=2,M
367  DO 660 L=M,12
368  DO 662 L=2,M
369  DO 664 L=M,12
370  DO 666 L=2,M
371  DO 668 L=M,12
372  DO 670 L=2,M
373  DO 672 L=M,12
374  DO 674 L=2,M
375  DO 676 L=M,12
376  DO 678 L=2,M
377  DO 680 L=M,12
378  DO 682 L=2,M
379  DO 684 L=M,12
380  DO 686 L=2,M
381  DO 688 L=M,12
382  DO 690 L=2,M
383  DO 692 L=M,12
384  DO 694 L=2,M
385  DO 696 L=M,12
386  DO 698 L=2,M
387  DO 700 L=M,12
388  DO 702 L=2,M
389  DO 704 L=M,12
390  DO 706 L=2,M
391  DO 708 L=M,12
392  DO 710 L=2,M
393  DO 712 L=M,12
394  DO 714 L=2,M
395  DO 716 L=M,12
396  DO 718 L=2,M
397  DO 720 L=M,12
398  DO 722 L=2,M
399  DO 724 L=M,12
400  DO 726 L=2,M
401  DO 728 L=M,12
402  DO 730 L=2,M
403  DO 732 L=M,12
404  DO 734 L=2,M
405  DO 736 L=M,12
406  DO 738 L=2,M
407  DO 740 L=M,12
408  DO 742 L=2,M
409  DO 744 L=M,12
410  DO 746 L=2,M
411  DO 748 L=M,12
412  DO 750 L=2,M
413  DO 752 L=M,12
414  DO 754 L=2,M
415  DO 756 L=M,12
416  DO 758 L=2,M
417  DO 760 L=M,12
418  DO 762 L=2,M
419  DO 764 L=M,12
420  DO 766 L=2,M
421  DO 768 L=M,12
422  DO 770 L=2,M
423  DO 772 L=M,12
424  DO 774 L=2,M
425  DO 776 L=M,12
426  DO 778 L=2,M
427  DO 780 L=M,12
428  DO 782 L=2,M
429  DO 784 L=M,12
430  DO 786 L=2,M
431  DO 788 L=M,12
432  DO 790 L=2,M
433  DO 792 L=M,12
434  DO 794 L=2,M
435  DO 796 L=M,12
436  DO 798 L=2,M
437  DO 800 L=M,12
438  DO 802 L=2,M
439  DO 804 L=M,12
440  DO 806 L=2,M
441  DO 808 L=M,12
442  DO 810 L=2,M
443  DO 812 L=M,12
444  DO 814 L=2,M
445  DO 816 L=M,12
446  DO 818 L=2,M
447  DO 820 L=M,12
448  DO 822 L=2,M
449  DO 824 L=M,12
450  DO 826 L=2,M
451  DO 828 L=M,12
452  DO 830 L=2,M
453  DO 832 L=M,12
454  DO 834 L=2,M
455  DO 836 L=M,12
456  DO 838 L=2,M
457  DO 840 L=M,12
458  DO 842 L=2,M
459  DO 844 L=M,12
460  DO 846 L=2,M
461  DO 848 L=M,12
462  DO 850 L=2,M
463  DO 852 L=M,12
464  DO 854 L=2,M
465  DO 856 L=M,12
466  DO 858 L=2,M
467  DO 860 L=M,12
468  DO 862 L=2,M
469  DO 864 L=M,12
470  DO 866 L=2,M
471  DO 868 L=M,12
472  DO 870 L=2,M
473  DO 872 L=M,12
474  DO 874 L=2,M
475  DO 876 L=M,12
476  DO 878 L=2,M
477  DO 880 L=M,12
478  DO 882 L=2,M
479  DO 884 L=M,12
480  DO 886 L=2,M
481  DO 888 L=M,12
482  DO 890 L=2,M
483  DO 892 L=M,12
484  DO 894 L=2,M
485  DO 896 L=M,12
486  DO 898 L=2,M
487  DO 900 L=M,12
488  DO 902 L=2,M
489  DO 904 L=M,12
490  DO 906 L=2,M
491  DO 908 L=M,12
492  DO 910 L=2,M
493  DO 912 L=M,12
494  DO 914 L=2,M
495  DO 916 L=M,12
496  DO 918 L=2,M
497  DO 920 L=M,12
498  DO 922 L=2,M
499  DO 924 L=M,12
500  DO 926 L=2,M
501  DO 928 L=M,12
502  DO 930 L=2,M
503  DO 932 L=M,12
504  DO 934 L=2,M
505  DO 936 L=M,12
506  DO 938 L=2,M
507  DO 940 L=M,12
508  DO 942 L=2,M
509  DO 944 L=M,12
510  DO 946 L=2,M
511  DO 948 L=M,12
512  DO 950 L=2,M
513  DO 952 L=M,12
514  DO 954 L=2,M
515  DO 956 L=M,12
516  DO 958 L=2,M
517  DO 960 L=M,12
518  DO 962 L=2,M
519  DO 964 L=M,12
520  DO 966 L=2,M
521  DO 968 L=M,12
522  DO 970 L=2,M
523  DO 972 L=M,12
524  DO 974 L=2,M
525  DO 976 L=M,12
526  DO 978 L=2,M
527  DO 980 L=M,12
528  DO 982 L=2,M
529  DO 984 L=M,12
530  DO 986 L=2,M
531  DO 988 L=M,12
532  DO 990 L=2,M
533  DO 992 L=M,12
534  DO 994 L=2,M
535  DO 996 L=M,12
536  DO 998 L=2,M
537  DO 1000 L=M,12
538  DO 1002 L=2,M
539  DO 1004 L=M,12
540  DO 1006 L=2,M
541  DO 1008 L=M,12
542  DO 1010 L=2,M
543  DO 1012 L=M,12
544  DO 1014 L=2,M
545  DO 1016 L=M,12
546  DO 1018 L=2,M
547  DO 1020 L=M,12
548  DO 1022 L=2,M
549  DO 1024 L=M,12
550  DO 1026 L=2,M
551  DO 1028 L=M,12
552  DO 1030 L=2,M
553  DO 1032 L=M,12
554  DO 1034 L=2,M
555  DO 1036 L=M,12
556  DO 1038 L=2,M
557  DO 1040 L=M,12
558  DO 1042 L=2,M
559  DO 1044 L=M,12
560  DO 1046 L=2,M
561  DO 1048 L=M,12
562  DO 1050 L=2,M
563  DO 1052 L=M,12
564  DO 1054 L=2,M
565  DO 1056 L=M,12
566  DO 1058 L=2,M
567  DO 1060 L=M,12
568  DO 1062 L=2,M
569  DO 1064 L=M,12
570  DO 1066 L=2,M
571  DO 1068 L=M,12
572  DO 1070 L=2,M
573  DO 1072 L=M,12
574  DO 1074 L=2,M
575  DO 1076 L=M,12
576  DO 1078 L=2,M
577  DO 1080 L=M,12
578  DO 1082 L=2,M
579  DO 1084 L=M,12
580  DO 1086 L=2,M
581  DO 1088 L=M,12
582  DO 1090 L=2,M
583  DO 1092 L=M,12
584  DO 1094 L=2,M
585  DO 1096 L=M,12
586  DO 1098 L=2,M
587  DO 1100 L=M,12
588  DO 1102 L=2,M
589  DO 1104 L=M,12
590  DO 1106 L=2,M
591  DO 1108 L=M,12
592  DO 1110 L=2,M
593  DO 1112 L=M,12
594  DO 1114 L=2,M
595  DO 1116 L=M,12
596  DO 1118 L=2,M
597  DO 1120 L=M,12
598  DO 1122 L=2,M
599  DO 1124 L=M,12
600  DO 1126 L=2,M
601  DO 1128 L=M,12
602  DO 1130 L=2,M
603  DO 1132 L=M,12
604  DO 1134 L=2,M
605  DO 1136 L=M,12
606  DO 1138 L=2,M
607  DO 1140 L=M,12
608  DO 1142 L=2,M
609  DO 1144 L=M,12
610  DO 1146 L=2,M
611  DO 1148 L=M,12
612  DO 1150 L=2,M
613  DO 1152 L=M,12
614  DO 1154 L=2,M
615  DO 1156 L=M,12
616  DO 1158 L=2,M
617  DO 1160 L=M,12
618  DO 1162 L=2,M
619  DO 1164 L=M,12
620  DO 1166 L=2,M
621  DO 1168 L=M,12
622  DO 1170 L=2,M
623  DO 1172 L=M,12
624  DO 1174 L=2,M
625  DO 1176 L=M,12
626  DO 1178 L=2,M
627  DO 1180 L=M,12
628  DO 1182 L=2,M
629  DO 1184 L=M,12
630  DO 1186 L=2,M
631  DO 1188 L=M,12
632  DO 1190 L=2,M
633  DO 1192 L=M,12
634  DO 1194 L=2,M
635  DO 1196 L=M,12
636  DO 1198 L=2,M
637  DO 1200 L=M,12
638  DO 1202 L=2,M
639  DO 1204 L=M,12
640  DO 1206 L=2,M
641  DO 1208 L=M,12
642  DO 1210 L=2,M
643  DO 1212 L=M,12
644  DO 1214 L=2,M
645  DO 1216 L=M,12
646  DO 1218 L=2,M
647  DO 1220 L=M,12
648  DO 1222 L=2,M
649  DO 1224 L=M,12
650  DO 1226 L=2,M
651  DO 1228 L=M,12
652  DO 1230 L=2,M
653  DO 1232 L=M,12
654  DO 1234 L=2,M
655  DO 1236 L=M,12
656  DO 1238 L=2,M
657  DO 1240 L=M,12
658  DO 1242 L=2,M
659  DO 1244 L=M,12
660  DO 1246 L=2,M
661  DO 1248 L=M,12
662  DO 1250 L=2,M
663  DO 1252 L=M,12
664  DO 1254 L=2,M
665  DO 1256 L=M,12
666  DO 1258 L=2,M
667  DO 1260 L=M,12
668  DO 1262 L=2,M
669  DO 1264 L=M,12
670  DO 1266 L=2,M
671  DO 1268 L=M,12
672  DO 1270 L=2,M
673  DO 1272 L=M,12
674  DO 1274 L=2,M
675  DO 1276 L=M,12
676  DO 1278 L=2,M
677  DO 1280 L=M,12
678  DO 1282 L=2,M
679  DO 1284 L=M,12
680  DO 1286 L=2,M
681  DO 1288 L=M,12
682  DO 1290 L=2,M
683  DO 1292 L=M,12
684  DO 1294 L=2,M
685  DO 1296 L=M,12
686  DO 1298 L=2,M
687  DO 1300 L=M,12
688  DO 1302 L=2,M
689  DO 1304 L=M,12
690  DO 1306 L=2,M
691  DO 1308 L=M,12
692  DO 1310 L=2,M
693  DO 1312 L=M,12
694  DO 1314 L=2,M
695  DO 1316 L=M,12
696  DO 1318 L=2,M
697  DO 1320 L=M,12
698  DO 1322 L=2,M
699  DO 1324 L=M,12
700  DO 1326 L=2,M
701  DO 1328 L=M,12
702  DO 1330 L=2,M
703  DO 1332 L=M,12
704  DO 1334 L=2,M
705  DO 1336 L=M,12
706  DO 1338 L=2,M
707  DO 1340 L=M,12
708  DO 1342 L=2,M
709  DO 1344 L=M,12
710  DO 1346 L=2,M
711  DO 1348 L=M,12
712  DO 1350 L=2,M
713  DO 1352 L=M,12
714  DO 1354 L=2,M
715  DO 1356 L=M,12
716  DO 1358 L=2,M
717  DO 1360 L=M,12
718  DO 1362 L=2,M
719  DO 1364 L=M,12
720  DO 1366 L=2,M
721  DO 1368 L=M,12
722  DO 1370 L=2,M
723  DO 1372 L=M,12
724  DO 1374 L=2,M
725  DO 1376 L=M,12
726  DO 1378 L=2,M
727  DO 1380 L=M,12
728  DO 1382 L=2,M
729  DO 1384 L=M,12
730  DO 1386 L=2,M
731  DO 1388 L=M,12
732  DO 1390 L=2,M
733  DO 1392 L=M,12
734  DO 1394 L=2,M
735  DO 1396 L=M,12
736  DO 1398 L=2,M
737  DO 1400 L=M,12
738  DO 1402 L=2,M
739  DO 1404 L=M,12
740  DO 1406 L=2,M
741  DO 1408 L=M,12
742  DO 1410 L=2,M
743  DO 1412 L=M,12
744  DO 1414 L=2,M
745  DO 1416 L=M,12
746  DO 1418 L=2,M
747  DO 1420 L=M,12
748  DO 1422 L=2,M
749  DO 1424 L=M,12
750  DO 1426 L=2,M
751  DO 1428 L=M,12
752  DO 1430 L=2,M
753  DO 1432 L=M,12
754  DO 1434 L=2,M
755  DO 1436 L=M,12
756  DO 1438 L=2,M
757  DO 1440 L=M,12
758  DO 1442 L=2,M
759  DO 1444 L=M,12
760  DO 1446 L=2,M
761  DO 1448 L=M,12
762  DO 1450 L=2,M
763  DO 1452 L=M,12
764  DO 1454 L=2,M
765  DO 1456 L=M,12
766  DO 1458 L=2,M
767  DO 1460 L=M,12
768  DO 1462 L=2,M
769  DO 1464 L=M,12
770  DO 1466 L=2,M
771  DO 1468 L=M,12
772  DO 1470 L=2,M
773  DO 1472 L=M,12
774  DO 1474 L=2,M
775  DO 1476 L=M,12
776  DO 1478 L=2,M
777  DO 1480 L=M,12
778  DO 1482 L=2,M
779  DO 1484 L=M,12
780  DO 1486 L=2,M
781  DO 1488 L=M,12
782  DO 1490 L=2,M
783  DO 1492 L=M,12
784  DO 1494 L=2,M
785  DO 1496 L=M,12
786  DO 1498 L=2,M
787  DO 1500 L=M,12
788  DO 1502 L=2,M
789  DO 1504 L=M,12
790  DO 1506 L=2,M
791  DO 1508 L=M,12
792  DO 1510 L=2,M
793  DO 1512 L=M,12
794  DO 1514 L=2,M
795  DO 1516 L=M,12
796  DO 1518 L=2,M
797  DO 1520 L=M,12
798  DO 1522 L=2,M
799  DO 1524 L=M,12
800  DO 1526 L=2,M
801  DO 1528 L=M,12
802  DO 1530 L=2,M
803  DO 1532 L=M,12
804  DO 1534 L=2,M
805  DO 1536 L=M,12
806  DO 1538 L=2,M
807  DO 1540 L=M,12
808  DO 1542 L=2,M
809  DO 1544 L=M,12
810  DO 1546 L=2,M
811  DO 1548 L=M,12
812  DO 1550 L=2,M
813  DO 1552 L=M,12
814  DO 1554 L=2,M
815  DO 1556 L=M,12
816  DO 1558 L=2,M
817  DO 1560 L=M,12
818  DO 1562 L=2,M
819  DO 1564 L=M,12
820  DO 1566 L=2,M
821  DO 1568 L=M,12
822  DO 1570 L=2,M
823  DO 1572 L=M,12
824  DO 1574 L=2,M
825  DO 1576 L=M,12
826  DO 1578 L=2,M
827  DO 1580 L=M,12
828  DO 1582 L=2,M
829  DO 1584 L=M,12
830  DO 1586 L=2,M
831  DO 1588 L=M,12
832  DO 1590 L=2,M
833  DO 1592 L=M,12
834  DO 1594 L=2,M
835  DO 1596 L=M,12
836  DO 1598 L=2,M
837  DO 1600 L=M,12
838  DO 1602 L=2,M
839  DO 1604 L=M,12
840  DO 1606 L=2,M
841  DO 1608 L=M,12
842  DO 1610 L=2,M
843  DO 1612 L=M,12
844  DO 1614 L=2,M
845  DO 1616 L=M,12
846  DO 1618 L=2,M
847  DO 1620 L=M,12
848  DO 1622 L=2,M
849  DO 1624 L=M,12
850  DO 1626 L=2,M
851  DO 1628 L=M,12
852  DO 1630 L=2,M
853  DO 1632 L=M,12
854  DO 1634 L=2,M
855  DO 1636 L=M,12
856  DO 1638 L=2,M
857  DO 1640 L=M,12
858  DO 1642 L=2,M
859  DO 1644 L=M,12
860  DO 1646 L=2,M
861  DO 1648 L=M,12
862  DO 1650 L=2,M
863  DO 1652 L=M,12
864  DO 1654 L=2,M
865  DO 1656 L=M,12
866  DO 1658 L=2,M
867  DO 1660 L=M,12
868  DO 1662 L=2,M
869  DO 1664 L=M,12
870  DO 1666 L=2,M
871  DO 1668 L=M,12
872  DO 1670 L=2,M
873  DO 1672 L=M,12
874  DO
```

```

181 C 00 130 L=20M
182 SPCLIAL CASE- J=C
183 00 80 I=20N2LEAP
184 11=1 + LEAP1
185 12=112 LEAP1
186 13 =120LEAP1
187 V=A(1-1)
188 A(1-1) = T +A(12-1)
189 A(12-1) = T-A(12-1)
190 T =A(1)
191 A(12) = T+A(12)
192 V = -A(12)
193 T1 = A(12-1)
194 A(12-1) = A(11-1) - T
195 A(12) = A(11) - T1
196 A(11-1) = A(11-1) + T
197 8* A(11) = A(11) + T1
198 IF(L-2) 120,120,90
199 9 KLAST=N2-LEAP
200 JJ=NPL
201 DO 110 J=4,LEAP1,2
202 MPJ=NT-JJ
203 UR=S(MPJ)
204 U1=S(JJ)
205 ILAST=J+KLAST
206 00 100 I=J,ILAST,LEAP
207 11=1+LEAP1
208 12=11LEAP1
209 13=120LEAP1
210 V=A(12-1)*UR-A(12)*U1
211 11=A(12-1)*U1+A(12)*UR
212 A(12-1)=A(12-1)-T
213 A(12) =A(12) - T1
214 A(11-1) =A(11-1)+T1
215 A(11) =A(11)+T1
216 V=A(11-1)*U1-A(11)*U1
217 11=A(11-1)*UR-A(11)*U1
218 A(11-1)=A(11-1)-T
219 A(11) =A(11) -T1
220 A(11-1)=A(11-1)+T1
221 100 A(11) =A(11) +T1
222 C END OF 1 LOOP
223 110 JJ=JJ+NPL
224 C END OF J LOOP
225 120 LEAP1=2+LEAP1
226 LEAP = 2+LEAP
227 130 NPL=NPL/2
228 C END OF L LOOP
229 140 IF(115)145,201
230 00106 FOURIER ANALYSIS. REPLACE A BY CONJUGATE.
231 145 00 150 I=1,M
232 150 A(2+1) =A(2+1)
233 160 60 10 I
234 170 RTURN
235 C ABL TABLE OF S(J)=SIN(20PI/J/MP),J=1,2,.....NT-1,NT=NP/4
236 170 NP=M
237 170 M=M
238 170 M1=M/4
239 170

```

FORT 276
 FORT 277
 FORT 278
 FORT 279
 FORT 280
 FORT 281
 FORT 282
 FORT 283
 FORT 284
 FORT 285
 FORT 286
 FORT 287
 FORT 288
 FORT 289
 FORT 290
 FORT 291
 FORT 292
 FORT 293
 FORT 294
 FORT 295
 FORT 296
 FORT 297
 FORT 298
 FORT 299
 FORT 300
 FORT 301

```

177 11-N-2
178 IF (AT) 2-0, -0.205
179 205 THETA = 2053981634
180 C THETA = PI/2 * (L+1) FOR L=1
181 210 JSTEP = NI
182 C JSTEP = 2 * (NI - L + 1) FOR L=1
183 JDI = NI/2
184 C JDI = NI/2
185 JDI = NI/2
186 S(JDI) = SIN(THETA)
187 IF (NI-2) 260, 220, 220
188 220 DO 250 L=2, NI
189 THETA = THETA/2.
190 JSTEP = JSTEP
191 JDI = JDI/2
192 S(JDI) = SIN(THETA)
193 JDI = JDI
194 S(JDI) = COS(THETA)
195 JLAST = NI - JSTEP
196 IF (JLAST - JSTEP) 250, 210, 210
197 210 DO 240 J = JSTEP, JLAST, JSTEP
198 JC = NI - J
199 JDI = JDI
200 S(JDI) = S(JDI) * S(JDI) + S(JDI) * S(JDI)
201 250 CONTINUE
202 250 IF (IES) 201, 20
203 END
  
```

1818